

https://dspace.org/

The evolutionary origin(s) of the trunk in Proboscidea (Mammalia, Afrotheria) based on Osteology

Nxumalo, Mpilo

2022
https://hdl.handle.net/10539/33868

Downloaded from a DSpace repository. https://dspace.org/

UNIVERSITY OF THE WITWATERSRAND, JOHANNESBURG

The Evolutionary Origin(s) of the Trunk in Proboscidea (Mammalia, Afrotheria) based on Osteology

Submitted to the Evolutionary Studies Institute, University of the Witwatersrand,

in partial fulfilment of the requirements for the

Degree Master of Science

(Palaeontology)

By Mpilo Nxumalo

Student no. 884171

January 2022

http://orcid.org/0000-0002-3739-9655

Supervisors: Dr. Julien Benoit and Prof. Paul R. Manger

Evolutionary Studies Institute, University of the Witwatersrand, Private Bag 3,

WITS 2050, Johannesburg, South Africa.

Contents

Abstract	1
Introduction	2
Reconstruction, Evidence and Evolution of the Proboscis	3
The Evolutionary History and Diversification of Proboscidea	9
The Evidence for the Evolution of the Proboscis in Proboscidea	15
Research Problem	21
Hypothesis	21
Aims and Objectives	21
Material and Methods	22
Results	31
I- Descriptions	31
II- Statistics	58
Discussion	64
Conclusion	68
Acknowledgements	69
References	70

Abstract

To date, no quantitative assessment of the evolution of the trunk in elephant ancestors has been undertaken. This study aims to quantify the dimensions of the infraorbital canal (volume and surface area of the infraorbital foramen) and retraction of the naris, to test how these metrics correlate with the dimensions of the nose/trunk in some selected modern mammals and apply these assessments to the fossil record to determine the evolutionary origin(s) of the trunk in Proboscidea. The gross morphology of the infraorbital canal in these species is described in detail for the first time. The results indicate that there is a significant and strong correlation between the surface area of the infraorbital foramen and the dimensions of the snout. The dimensions of the infraorbital canal increase with the size of the facial appendage. There is no correlation between the degree of narial retraction and dimension of the snout in extant taxa. There is a strong taxonomic and phylogenetic signal in the morphology of the infraorbital canal. The application to fossils suggests that *Numidotherium* possessed a trunk shorter than that of tapirs, and *Deinotherium* a more tapir-like trunk length. Gomphotheres, *Anancus* and *E. rackei* possessed snout lengths shorter than proposed in the literature. The trunk did not originate as a single event at the root of Proboscidea but is a result of a long evolution that spanned the proboscidean phylogenetic tree for at least 60 My, between the last common ancestor of Proboscidea and that of Sirenia.

Introduction

Carl Illiger was the first to name the Order Proboscidea (Mammalia, Afrotheria), which contains extant elephants and their extinct relatives (Illiger, 1811). Molecular data suggest that the Afrotheria originated in the African Cretaceous, followed by an Afro-Arabian endemic evolution (from ~105 to 25 my ago) (Adaci *et al*., 2007; and Alberdi *et al*., 2011). The proboscideans are named after their single-most diagnostic feature, the trunk (Dierenfeld & Milewski, 2013; and Shoshani, 1998). The elephants are the only living proboscideans, from the 164 confirmed species that lived in the past, and that they originated in the late Paleogene of the Afro-Arabian landscape (Abraha *et al*., 2007; Fisher, 2018; and Gheerbrant & Tassy, 2009). Although the range of extant species is limited to Africa and Asia, extinct species were widely distributed on most continents (except Antarctica and Australia), inhabiting a variety of habitats, from deserts to mountains (Fisher, 2018; and Osborne, 1942).

The proboscis, or trunk, is a flexible facial appendage that is formed by the fusion of nostrils and nasal passages with the upper lip musculature (Dierenfeld & Milewski, 2013; Shoshani, 1998; and Shoshani & Tassy, 2005). This is supported by the observation of early fetal development in elephants, where the upper labial surface and nose are clearly separated (Shoshani, 1998). Different from the true trunk, Wall (1980: pp968) defined the mobile upper-lip as "an enlarged movable lip which is adapted for seizing or grasping food but does not drastically change the position of the nostrils". The elephant trunk is extremely sensitive and functionally used to detect subtle tactile, thermal, and pressure changes in the environment (Shoshani, 1998; and Shoshani & Tassy, 2005). It is also used for breathing, sound production, touching and navigation, olfaction, and manipulation of objects (Galton *et al.*, 2006; Shoshani, 1998; and Shoshani & Tassy, 2005).

Based on morphology and behavioral function, beyond the order Proboscidea, the only extant mammals observed to possess a true proboscis are the four species within the superfamily Tapiridae (Order Perissodactyla) (Dierenfield & Milowski, 2013; Galton *et al.*, 2006; Giannini & Moyano, 2018; and Wall, 1980). The Tapiridae meets the minimum requirements of this definitionin that they possess an extension formed by the narial joint and upper lip musculature, which is both flexible and tubular, and used partly for feeding and olfaction (Dierenfield & Milowski, 2013). The tapirs' trunk differs from elephants', in that the trunk's anterior occlusion beyond the incisors is minimal and the nasal bones are relatively less reduced and retracted (Dierenfield & Milowski, 2013).

Saiga tatarica (Clifford & Witmer, 2004a; and Frey & Hofmann, 1996), *Alces alces* (Clifford & Witmer, 2004b; and Linnaeus, 1758), elephant-shrews (Macroscelidea: *Rhynchocyon*, *Elephantulus, Galegeeska, Petrosaltator, Petrodromus* and *Macroscelides* spp.) (Kingdon, 1997), elephant seals (*Mirounga* spp.) (Galimberti *et al.*, 2007; and Bryden & Ling, 1992), proboscis monkeys (*Nasalis larvatus*) (Yeager, 1989) and dik-diks (*Rhynchotragus* and *Madoqua* spp.) (Frey & Hofmann, 1996; and Kingdon, 1997) possess facial appendages that are referred to as a "proboscis", but do not meet the minimum requirements of the proposed definition (Dierenfield & Milowski, 2013). None of these mammals use their trunk for grasping (Dierenfield & Milowski, 2013). Instead, they possess a prorhiscis (Dierenfield & Milowski, 2013; and Giannini & Moyano, 2018). Beyond Mammalia, no fish or reptile possesses a true proboscis or a facial appendage that meets the above-mentioned minimum requirements for a true trunk (Clifford & Witmer, 2004a; Dierenfield & Milowski, 2013; and Witmer, 1999).

Reconstruction, Evidence and Evolution of the Proboscis

The elephant trunk is composed of soft-tissue, and it is not readily preserved in the fossil record. Paleontologists make use of osteological proxies, which are believed to be associated with the possession of a trunk in extant taxa, in order to reconstruct its potential presence in the fossil record. Based on cranial modifications that are associated with the presence of a trunk, there are many extinct taxa that have been hypothesized to possess a trunk and are reconstructed with a proboscis-like facial appendage (Galton *et al.,* 2006). According to Galton *et al.* (2006), the first published inference of a proboscis in extinct taxa was the historical study carried out by Cuvier (1796: pp309)on the *Megatherium* (Xenarthra: Megatheriidae) from South America.

Shortly after, each discovery of non-proboscidean extinct mammalian taxa with similar cranial modifications (i.e. the degree of narial retraction), but with varying cranial gross morphologies, were assigned a proboscis (Galton *et al.,* 2006). Wall (1980) studied in detail the cranial modifications of the nasal region, that are believed to be associated with the presence of a trunk or a prehensile upper lip. A detailed comparative study of *Cadurcodon* (Rhinocerotoidea, Amynodontidae) and *Tapirus pinchaque*, revealed compelling evidence that Oligocene amynodonts bore a trunk (Wall, 1980).

A review of other extinct mammalian taxa, hypothesized to possess a proboscis (*Palaeomastodon*, *Astrapotherium*, and *Macrauchenia*) suggested that the characters which are important when reconstructing and inferring the presence of the trunk are: retraction of the external nares, enlargement of the nasal opening and the presence of large muscle attachment sites, or entheses (Wall, 1980). Osborn (1898) noted these cranial modifications as evidence for the presence of the trunk or prehensile upper lip in amynodonts. It was suggested by Troxell (1921) that *Metamynodon* bore a prehensile upper lip based on the caliber of the infraorbital canal, morphology of the nasal

opening, and roughening of the supraorbital ridge. Gromova (1954) suggested that some of the advanced amynodonts likely bore a proboscis; however, she did not state which cranial modifications were associated with the proposed proboscis.

The amynodont genus that has been found to possess most of the cranial modifications associated with a proboscis is *Cadurcodon.* The skull of AMNH 26029 is the best example for these cranial modifications (Wall, 1980). Wall (1980) conducted a detailed comparison between this skull and that of *Tapirus pinchiqua,* and identified twelve cranial features that are common between the two taxa and are associated with the presence of the proboscis (Table 1) (Wall, 1980).

Palorchestidae, a late Oligocene family of eastern Australian marsupial megafauna, are well known for their odd 'tapir-like' cranial morphology (Adams *et al*., 2019). A detailed description of *Propalorchestes* shows a heavily retracted nasal morphology (Sharp & Trusler, 2016). The presence of this characteristic has been used to support the hypothesis that they could have possessed a proboscis (Adams *et al*., 2019; and Sharp & Trusler, 2016). They possessed a mosaic of morphological characters not seen in other mammals, including hyper retraction of the osseous naris, specialised forelimbs resembling a 'marsupial-tapir', and overall nasal bone morphology that superficially resembles those of tapirs (Adams *et al*., 2019); however, the hypothesis of the proboscis-bearing Palorchestidae has been challenged, in favor of a sensitive prehensile lip (Adams *et al*., 2019; and Sharp & Trusler, 2016).

Like *Propalorchetes*, *Macrauchenia patachonica* possesses extremely retracted nasal bones and opening of the osseous naris (Blanco *et al*., 2021). *Macrauchenia patachonica* belongs to the Macraucheniidae, and the members of this family are characterised by their degree of narial retraction (Blanco *et al*., 2021). The morphology of the vomer along with the retracted nares were used as evidence for the presence of a trunk (Burmeister, 1864; and Scott, 1910). The wide muscle

attachment surfaces were interpreted as evidence for a prolonged trunk, much longer than the tapir trunk, but not quite elephantine (Lydekker, 1903). Other authors contested this view and argued that Macraucheniidae did not bear a trunk, but a prehensile *Alces*-like lip (Moyano & Giannini, 2018).

Other evidence such as the dimensions of the infraorbital foramen have been used to infer the presence of the trunk, in addition to the modification of the nasal region (Shoshani, 1998). The infraorbital ramus of the maxillary branch (V2) of the trigeminal nerve innervates the follicles of the sensory hairs and skin of the elephant trunk (Crumpton & Thompson, 2013; Galton *et al.*, 2006; Muchlinski, 2008; Nabavizadeh, 2015; Nabavizadeh & Reidenberg, 2019; Osborn, 1936, 1942; Sampson *et al*., 1999; and Wall, 1980). It passes through the infraorbital canal, which opens caudally within the orbit (maxillary foramen) and rostrally on the lateral aspect of the maxilla (infraorbital foramen) (Benoit *et al.*, 2019; Crumpton & Thompson, 2013; and Muchlinski, 2008) (figure 1).

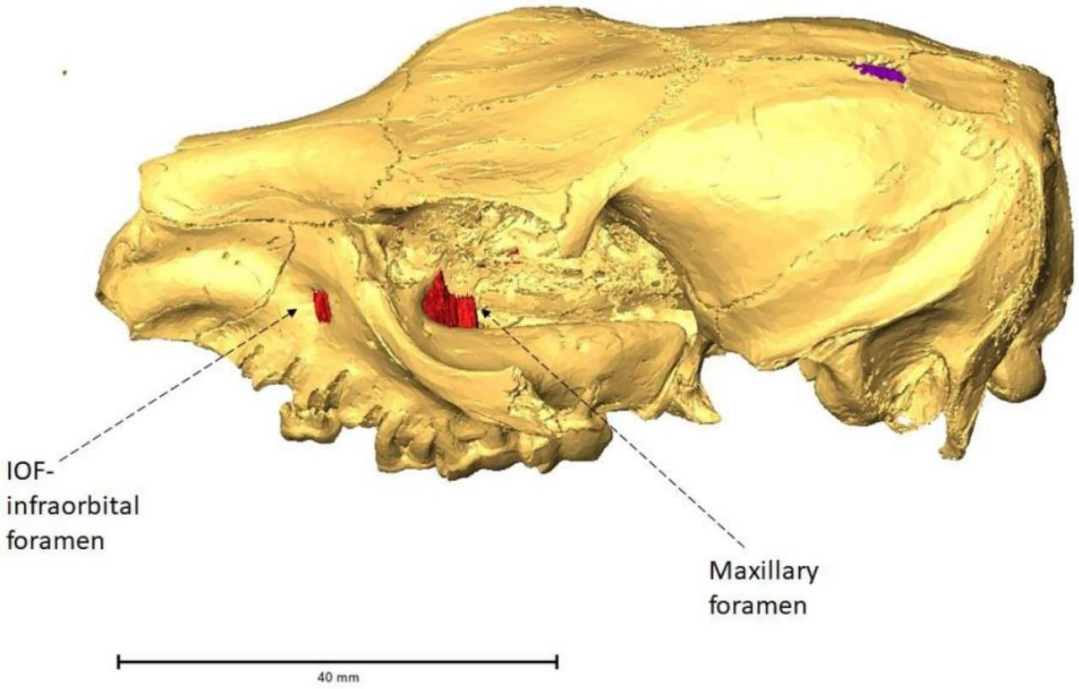


Figure 1. Procavia capensis *skull in left dorso-lateral view, showing the length of the infraorbital canal (in red).*

Table 1. The cranial modification characters associated with the presence of the trunk (Wall, 1980).

Character state (number)	Character or feature
1	Enlargement of the nasal opening and its caudal retraction to the level of the orbit
2	Process of the premaxilla and its nasal contact is lost or absent. A portion of the maxilla is incorporated along the border of the external nares
3	Nasal bone length reduced
4	The turbinal bone and cribriform plate are migrated posteriorly to a level medial to the Orbit
5	The lateral concavity on the maxilla is medially developed to the level of the orbit to accommodate the displacement of the nasal diverticulum
6	Lacrimal knobs for muscle attachment
7	The preorbital elements of the skull are reduced in overall length
8	Orbit migrated anteriorly relative to the cheek teeth
9	Infraorbital canal and foramen dimensions are increased in size
10	Premaxillae fused and vertically thickened
11	Enlargement and presence of the frontal sinus
12	Occipital region increased in width, due the presence of well developed, and strong neck Muscles

Outside Mammalia, it has been noted that *Diplodocus* possesses a single, relatively enlarged narial orifice that is retracted to the level of the orbits (Galton *et al.*, 2006). Based on the morphology of this character, it has been suggested that diplodocus possessed a proboscis, like an elephant (Galton *et al.*, 2006). Hypotheses of proboscis-bearing hadrosaurs (Ornithopoda: Hadrosauridae) have

been proposed in a series of papers by Wilfarth (1938, 1939, 1940, 1948, 1949). Wilfarth argued that the beak of the duck-billed dinosaurs is used to attach strong proboscis muscles (Wilfarth, 1939, 1940, 1948). Sternberg (1939), noted the redundancy of evolving a proboscis on top of a beak, and compellingly disproved this hypothesis.

Contrary to the condition in extant elephants, the relatively small size of the maxillary branch of the trigeminal nerve in *Diplodocus* (based on analyses of the endocranial cast) suggests that there is no paleo-neuroanatomical evidence to support the presence of an elephantine trunk (Galton *et al.*, 2006). Living mammals that have a trunk possess well-developed intrinsic narial muscles (Clifford & Witmer, 2002b), and as a result, they possess an enlarged maxillary branch of the trigeminal nerve (Galton *et al.*, 2006). *Loxodonta africana* and *Elephas maximus* possess a significantly enlarged maxillary branch of the trigeminal nerve (Shoshani, 1998).

In pinnipeds, the infraorbital foramen is enlarged to accommodate the enlarged infraorbital nerve (Adam & Berta, 2002). Wall (1980) also noted that *Cadurcodon* possesses a relatively enlarged diameter of the infraorbital canal, to accommodate the enlarged infraorbital nerve. *Diplodocus* possesses an infraorbital canal that has a relatively small diameter, suggesting the absence of paleo-neuroanatomical evidence for the presence of an elephant-like proboscis (Galton *et al.*, 2006).

The Evolutionary History and Diversification of Proboscidea

Before tackling the question of what is currently known about the evolution of the proboscidean trunk, it is important to detail the major phases in the evolutionary history of the Proboscidea. Early proboscideans, the 'Plesielephantiformes' originated in the Afro-Arabian Palaeogene, (Abraha *et al*., 2007; Gheerbrant & Tassy, 2009; and Harzhauser *et al*., 2002). This suborder incorporates primitive, bilophodont proboscideans such as phosphatheres, barytherioids,

numidotheres, moeritheres, and daouitheres (Amaghzaz *et al*., 2002; and Sanders *et al*., 2001a). The 'Plesielephantiformes' are a paraphyletic assemblage, formed by a group of stem proboscideans at the base of the Proboscidea clade (figure 2) (Amaghzaz *et al*., 2005).

They share the plesiomorphic bilophodont dental condition of the primitive proboscideans (Todd, 2006). 'Plesielephantiformes' differ from Deinotheriidae and Elephantiformes in the size of the tusks (relatively smaller on this suborder), and dimensions of the inferred proboscis (short, tapir-like) (Sanders *et al.,* 2001a). Deinotheres possess lophodont dentition, however, they descended from a bunodont ancestor (Harris, 1978; and Kappelman *et al*., 2004).

The lifestyle of the 'plesielephantiforms' has been a centre of controversy for a century now, with different lines of evidence indicating terrestrial, semiaquatic and aquatic lifestyles (Domning & McKenna, 1986; and Osborn, 1909). Evidence from palaeontology, morphology and embryology led authors to hypothesize that elephants and sirenians share a common amphibious ancestor (Liu *et al*., 2008). Measurements of oxygen isotopes on the tooth enamel of the genera *Barytherium* and *Moeritherium* show an isotopic pattern that is different from terrestrial mammals, but more similar to that of aquatic and semiaquatic mammals (Liu *et al*., 2008).

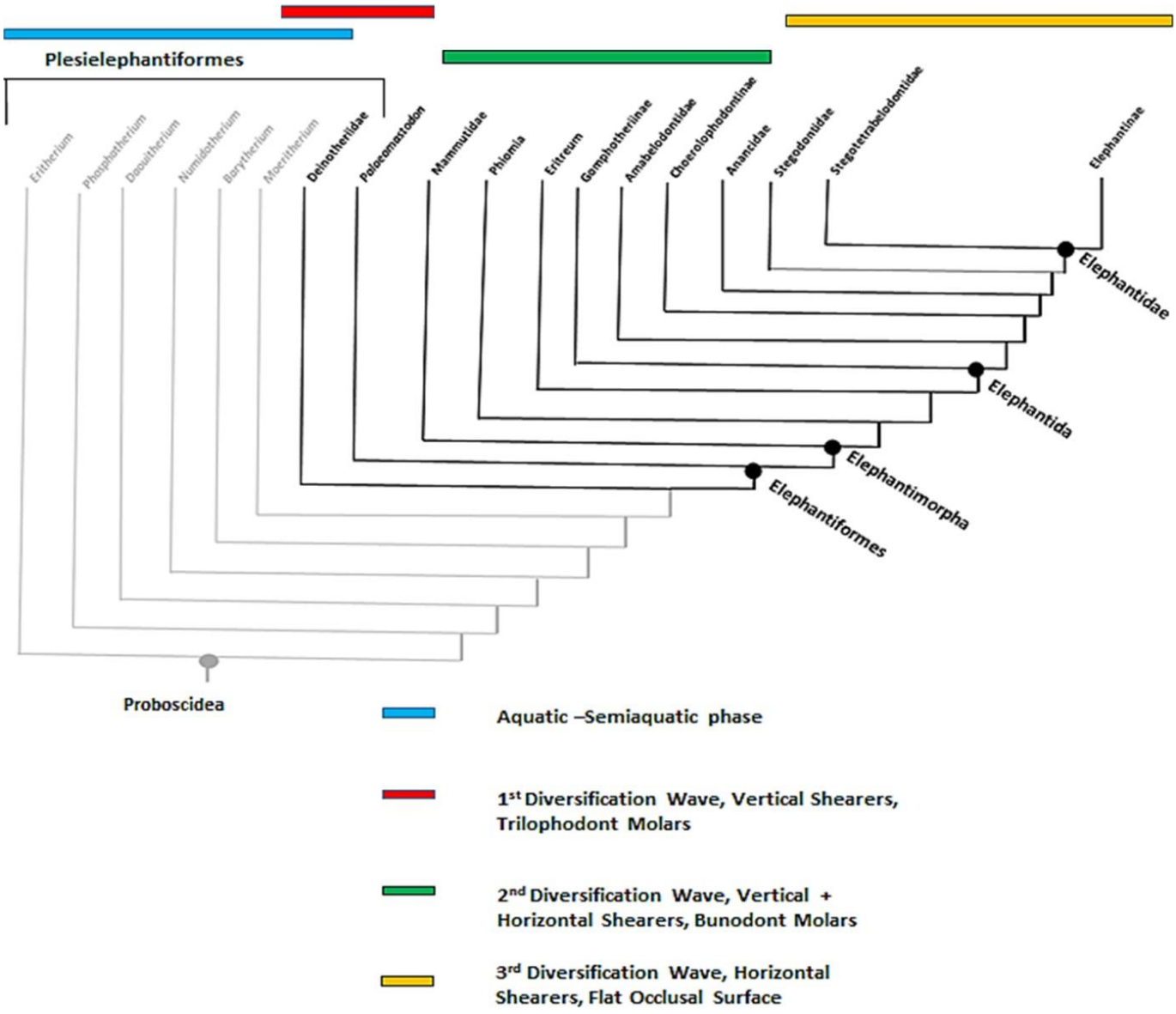


Figure 2: The Phylogeny of Proboscidea, along with the proposed amphibious phase and the three waves of diversification based on ecomorphological evidence, developed from Todd, (2006); Liu et al*., (2008); and Fisher, (2018).*

The carbon-13 measurements obtained from both these genera indicate that their diet was a mixture of fresh-water vegetation from fresh-water swamps, and C3 terrestrial plants (Alberdi *et al*., 2011; and Liu *et al*., 2008). These results support the hypothesized Oligocene amphibious phase (figure2), and aquatic ancestry of Proboscidea (Berenbrink *et al.*, 2013; and Liu *et al.*, 2008). *Moeritherium* possesses a mosaic of features in the skull that have been observed in both aquatic and semiaquatic

mammals; its auditory region is adapted to terrestrial hearing, not underwater hearing; however, its skull is relatively telescoped, with anteriorly placed orbits, seen mostly in marine mammals (Court, 1994; Liu *et al*., 2008; and Matsumoto, 1923). The postcranial skeleton of *Moeritherium* shows evidence of hind limb reduction similar to that observed in the semiaquatic Desmostylia (i.e. small pelvic hip socket) (Simons, 1968). Elephants share many common features with sirenians, such as double-apex hearts and their lungs are not surrounded by a pleural cavity; which both groups are hypothesizes to have inherited from a common aquatic ancestor (Sukumar, 2003).

The sedimentology of the Fayum region of Egypt, where *Moeritherium* was found, indicates that these fossils were deposited in a periodically flooded lagoon, lake or pond near the Ocean; shark and marine fish remains were recovered, with the majority of the remains constituting terrestrial vertebrates (Liu *et al*., 2008). Berenbrink *et al.* (2013) studied the evolution of the diving capacity on various afrotherian mammals using myoglobin net surface change. The results from this study support an amphibious ancestry for Proboscidea, and suggests that the 'Plesielephantiformes' possessed muscle oxygen storage capacity that is relatively higher than that of other early paenungulates (Berenbrink *et al.*, 2013*).*

The muscle oxygen storage capacity of late Eocene to early Oligocene proboscideans was likely comparable to that of extant sirenians (i.e. estimated diving capacity of *Moeritherium* ~ 10 min), followed by a secondary decrease in diving ability in elephantiforms (i.e. diving capacity of *Elephas maximus* ~ 2.5 min) (Berenbrink *et al.*, 2013). At the beginning of the Cenozoic world (65 – 50 Mya) the warm and wet African environment had very dense forests (Guillermo & Spencer, 2010). An environment with dense vegetation favours small-bodied animals, as opposed to large ground-dwelling savannah animals (Guillermo & Spencer, 2010). This is when proboscideans originated, with forms such as *Eritherium* and

Phosphatherium in the late Paleocene to early Eocene (Amaghzaz *et al*., 2005). They were adapted to living in swampy, wet forested environments (Liu *et al*., 2008).

In the early Eocene, the climate was even warmer, tropical forests were widespread all the way to polar latitudes, with an evenly spread annual rainfall (Guillermo & Spencer, 2010). Christine Janis hypothesized that the more phased distribution of yearly rainfall during the peak warming triggered the spacing of forests, and thus promoted the undergrowth and evolution of grasses (Janis, 1989). From the middle to late Eocene, the global climate became cooler and arid, resulting in the retreat of tropical forests and spread of grasses (Markov *et al*, 2001). It has been hypothesized that the evolution of features such as body mass and brain mass in elephantids and 'plesielephantiforms' is better explained by environmental and climatic changes in Africa (Benoit *et al.*, 2019; Burckle *et al.*, 1995; and Vrba, 1993).

The evolution of the Proboscidea is hypothesized to have followed environmental changes, which led to a series of adaptive shifts in the dentition and skull, as members of the Order evolved various dietary specialisations (Fisher, 2018; and Shoshani, 1998). Todd, (2006) argues that even though this view has been prevalent in the literature, there are other selective pressures, which are equally important in driving the evolution of Proboscidea, such as competition and biotic interaction. Niche partitioning in proboscideans was driven by ecomorphological innovations (Alberdi *et al*., 2011). Competition and biotic interaction may have led to resource partitioning; for example, *Loxodonta* is proposed to have migrated into open savanna niches with the demise of *Elephas* in Africa around 500,000 ya (Alberdi *et al*., 2011; and Todd, 2006).

Three periods of diversification and radiation are recognized for the Order Proboscidea, based on masticatory functional morphology (figure 2):

The first period occurred in the late Eocene, from 41 to 21 Ma, and is characterised by *Barytherium*, *Moeritherium*, *Phiomia,* and *Palaeomastodon* (Fairfield, 1934; Fisher, 2018; Gohlich, 1999; Harris, 1978; Shoshani, 1998; and Todd, 2006). Proboscideans from this period of diversification are mostly trilophodont, possessing molars with high cusps (i.e Deinotheriidae, *Phiomia* and *Palaeomastodon),* which are used in a vertical shearing motion during chewing (*Moeritherium* and *Barytherium* have bilophodont molars) (Alberdi *et al*., 2011; and Todd, 2006).

Based on ecomorphological evidence, members from the families Moeritheriidae, Barytheriidae and Deinotheriidae are also included in this period (Todd, 2006). The transition from the first to the second radiation is marked by major trends such as an increase in body size, skull size and shape, tusk size, physiological changes, and changes in cheek dentition (Fisher, 2018; and Shoshani, 1998). All the taxa in the first radiation had the typical mammalian vertical tooth displacement mechanism (Shoshani, 1998), whereas the proboscideans in the second radiation evolved the typical horizontal, conveyor-belt type of tooth replacement that characterises proboscideans (Abraha *et al*., 2007). Proboscidean masticatory functional diversity changed at a constant rate during this period, with very low species diversity (Alberdi *et al*., 2011).

The second diversification period contains the trilophodont gomphotheres, and occurred from 21 to 11 Ma (Fisher, 2018; Shoshani, 1998; and Todd, 2006). The most important event of this period is the biogeographic expansion of Proboscidea beyond Africa (*Gomphotherium* datum event), and they reached the Americas by 16 Ma (Alberdi *et al*., 2011). This expansion event led to a dramatic explosion in proboscidean eco-morphology and functional diversity, and the origin of several lineages (Alberdi *et al*., 2011). The proboscideans of this period are characterised by bunodont molars (with isolated conical cusps), two pairs of tusks, and a chewing motion that is a combination of predominantly horizontal (lateral and forward), and vertical motions (Alberdi

et al., 2011; and Todd, 2006). The taxa of the second and third radiations are characterised by horizontal tooth replacement (Shoshani, 1998). Due to the modification in the skull morphology, the mandible became too short to house all the molars and premolars simultaneously (Nabavizadeh, 2015; Nabavizadeh & Reidenberg, 2019; and Shoshani, 1998).

The last period of radiation and diversification occurred from 7 to 1 Ma, and it includes Elephantidae (Fisher, 2018; Gohlich, 1999; Shoshani, 1998; and Todd, 2006). During this period, the first major proboscidean extinction event is recorded; driven by palaeoclimatic dynamics, and a high ecomorphological specialisation (Alberdi *et al*., 2011). The proboscideans of this period are characterised by a strictly proal chewing motion, and hypsodont molars (Todd, 2006). Based on masticatory functional morphology, the elephants of this period are further subdivided into two groups: the first are the horizontal shearing browsers with cusp-like occlusal surfaces (i.e.) *Primelephas* and *Stegotetrabelodon,* and the second are the horizontal shearing grazers and they were hypsodont, i.e., the Elephantidae (Alberdi *et al*., 2011; and Todd, 2006).

The Evidence for the Evolution of the Proboscis in Proboscidea

Early proboscideans from the late Palaeocene to early Oligocene, such as *Phosphatherium*, have a relatively small nasal opening that is positioned rostral on the snout (Shoshani, 1998). This is a primitive condition, which many authors have used to argue for the absence of a trunk or the presence of a fleshy, mobile upper lip (Shoshani & Tassy, 2005; and Sukumar, 2003). Most authors agree that the slightly more phylogenetically crownward *Numidotherium koholense* possessed a short, tapir-like proboscis, based on the retracted external nares and the elevated skull (Shoshani, 1998; Shoshani & Tassy, 2005; and Sukumar, 2003). Even though these authors have

qualitatively used the degree of the narial retraction in their arguments and restorations, none have tested if there is a real correlation between the trunk and the degree of narial retraction.

Moving crown-ward on the phylogenetic tree (figure 2), Larramendi inferred the presence or absence of the trunk in various proboscideans, on restorations based on femoral measurements and estimated body sizes (Larramendi, 2016). *Moeritherium* possesses a long neck with an elongated mandible, but lacks the cranial modifications (or degree of modification) associated with the presence of a short trunk (Larramendi, 2016). According to the reconstructions of Larramendi, (2016), *Moeritherium* seemingly did not possess a trunk, nor even the mobile upper lip similar to rhinos, as proposed by other authors (i.e. Shoshani, 1996).

The dimensions of the infraorbital foramen are correlated to the number of nerve fibres passing through the infraorbital canal in mammals (Muchlinski 2008). As the proboscis developed during proboscidean evolution, it is thus inferred that the size of the infraorbital foramen on fossilised skulls would reflect the increasing innervation of the "growing" trunk (Andrews, 1904; and Osborn, 1936, 1942). To the best of our knowledge, no quantitative approach to trace the evolution of the dimensions of the proboscidean infraorbital foramen has been undertaken, and only qualitative accounts are available.

It is noteworthy that even the basal-most "Plesielephantiformes", such as *Eritherium*, *Phosphatherium,* and *Numidotherium* (Amaghzaz *et al*., 2005; Ameur *et al.*, 1984; and Gheerbrant 2009), already present with a relatively large infraorbital foramen, surrounded by a deep infraorbital fossa (or canine fossa) for the attachment of a presumably well-developed *levator alae nasi* muscle (Boas, 1908; and Shoshani & Eisenberg, 1982). This strongly suggests that a mobile and prehensile upper lip was already present in the basal-most proboscideans and is likely a plesiomorphic feature of the Tethytheria (Amaghzaz *et al*., 2005).

Deinotheriidae and Elephantiformes, including the basal elephantiform *Palaeomastodon*, possess a very large infraorbital foramen, comparable to that of modern elephants (Andrews, 1904; Osborn, 1936, 1942; and Sanders *et al*., 2010), although some variations exist and remain to be fully explored, like in *Gomphotherium angustidens*, which exhibits a condition where the infraorbital canal is divided into a small dorsal foramen and a relatively larger ventral one (Tassy, 2013). In general, the infraorbital canal is long and runs horizontally in basal "plesielephantiforms" but becomes relatively short and more obliquely oriented in deinotheres and elephantiforms as the rostrum shortens and the external nares are retracted (Andrews, 1904; Osborn, 1936, 1942; and Sanders *et al*., 2010).

The proboscis, molars, and tusks combined weigh hundreds of kilograms (Larramendi, 2016; and Shoshani & Eisenberg, 1982) contributing 5 to 10% of total body mass in extant elephants. The proboscideans have evolved a highly pneumatised skull with deep insertions for the nuchal ligaments, seemingly to compensate for the increased cranial mass (Andrews, 1904; Bezuidenhout *et al*., 1995; Osborn, 1936, 1942; Sanders *et al*., 2010; and Shoshani & Tassy, 1996). *Eritherium*, *Phosphatherium*, and *Moeritherium* show few signs of cranial pneumatisation, whereas *Numidotherium* and *Barytherium* do reveal aspects of cranial pneumatisation (Amaghzaz *et al*., 2005; Ameur *et al*., 1984; Delmer, 2005b; Gheerbrant, 2009; and Gheerbrant & Tassy, 2009). This makes it difficult to determine the exact origin of a pneumatised skull among "plesielephantiforms". It is nevertheless likely that *Moeritherium* secondarily lost its cranial pneumaticity as an adaptation to a semi-aquatic lifestyle (Matsumoto, 1923; and Tassy, 1985). The deinotheres, *Palaeomastodon*, and more derived elephantiformes all share the presence of cranial pneumaticity and deep nuchal fossae for ligamentous attachment (Andrews, 1904; Osborn, 1936, 1942; Sanders *et al.*, 2010; and Shoshani & Tassy, 1996).

Due to the evolution of the proboscis, the proboscidean skull changed in overall gross morphology to accommodate attachments of the heavy labial and nasal musculature needed to operate the massive trunk, i.e. the nares became increasingly large and retracted, the snout shortened and the premaxilla became wider (Andrews, 1904; Gheerbrant & Tassy, 2009; Osborn, 1936, 1942; and Shoshani 1998). The earliest proboscidean to display an enlarged narial opening is *Numidotherium koholense*, whereas the first hints of narial retraction appear with *Barytherium* and *Moeritherium* (Ameur *et al*., 1984; Andrews, 1906; Delmer, 2005, 2005c; and Sanders *et al.*, 2010). These anatomical changes are consistent with a gradual increase in size of the pre-existing mobile upper lip.

Larremendi (2016) argues that *Deinotherium* had a short neck, columnar limbs, and a long femur; therefore, it must have possessed a long proboscis to aid during feeding (Larramendi, 2016). Since their discovery 50 years ago, there has been a lot of debate and controversy about the facial morphology of deinotheres (Markov *et al*., 2001). Abel (1922) reconstructed deinotheres with a more elephantine trunk, along with downturned lower tusks, based on the presence of a large nasal opening. Harris (1975), Markorv *et al.* (2001), Svistun (1974), Tassy (1998), and Tarabukin (1974), all argued that this reconstruction is improbable both for evolutionary and anatomical reasons.

They opposed this reconstruction despite the presence of the large nasal opening, which has been used by previous authors to support the presence of the trunk (Markorv *et al.*, 2001). The skull does not have enough surface area for muscle insertion of an elephantine-sized trunk, and the orientation of the premaxilla would have hindered its movement (Markov *et al.,* 2001). Markorv *et al.* (2001) attempted to reconstruct the facial morphology, and then elucidated the feeding behaviour of *Deinotherium*. They concluded that the gross cranial morphology of *Deinotherium* suggests that they possessed a giant tapir-like trunk.

Proboscideans from the 2nd wave (Oligocene to Miocene) are marked by enlarged and heavily retracted nares (Shoshani, 1998). These advanced features are observed as early as the Miocene "gomphotheres", and are well established on derived taxa such as mammoths (Shoshani, 1998).

Phiomia and *Palaeomastodon* are usually reconstructed as bearing a trunk that is slightly longer than the tapir-like condition, but not as long as the elephantine trunk (Sukumar, 2003). On the restorations of *Phiomia* and *Palaeomastodon* from Sukumar (2003), the osteological proxies used were not specified. Wall (1980) noted that *Palaeomastodon* possesses cranial modifications that are associated with the presence of the trunk, including retracted external nares, enlarged nasal opening, and large muscle attachment scars.

Andrews (1904) and subsequent authors (e.g. Nabavizadeh, 2015; and Nabavizadeh & Reidenberg, 2019) hypothesized that the onset of a very long mandibular symphysis in basal elephantiforms (i.e. *Palaeomastodon*, Mammutida, Gomphotheriinae, Choerolophodontinae, Amebelodontinae and other "gomphotheres") and deinotherids accompanied the evolution of the proboscis. The proboscis would occlude with the symphysis to enhance trophic activities and food processing, and as such, the growth of the trunk would parallel the lengthening of the symphysis throughout phylogeny (Nabavizadeh, 2015). This initial lengthening is coupled with the formation of tusk-like upper and shovel-shaped lower incisors (Andrews, 1904; Hautier *et al*., 2008; and Nabavizadeh, 2015).

The maximum length of the mandibular symphysis is reached in Choerolophodontinae, and Amebelodontinae indicating that a trunk comparable to that in modern elephants was present as early as the middle Miocene, and is followed by the convergent, secondary reduction of the symphysis in the late Miocene and Pliocene in the Mammutida and Stegodontidae (modern elephant ancestors) whilst the proboscis remained stable (Andrews, 1904; Bezuidenhout, 2010; Nabavizadeh, 2015; Osborn, 1936, 1942; and Tassy, 2013).

The convergent loss of lower tusks may be correlated to the decrease of global temperature and humidity in the upper Miocene and Pliocene, as the presence of four tusks would enhance heat loss (Guillermo & Spencer, 2010). Based on the retraction of the narial opening, length of the mandibular symphysis, enlargement of the infraorbital foramen, and other cranial adaptations, it is most likely

that basal “plesielephantiforms" had a prehensile upper lip (Nabavizadeh, 2015). The facial and narial musculature eventually evolved into a large and prehensile proboscis in the last common ancestor of the Deinotheriidae and Elephantiformes in the late Eocene (Andrews, 1904; Nabavizadeh, 2015; and Osborn, 1936, 1942).

The presence of a prehensile upper lip would account for the relatively large cerebellum of *Moeritherium*, which makes up about one-third of the total length of the endocast in dorsal view (Benoit *et al.*, 2019). The endocast of all known Elephantiformes displays an enlarged cerebellum comparable to that in modern elephants (Benoit, 2016; and Benoit *et al.*, 2019). In the rare occasion when it is preserved and depicted, the cast of the trigeminal nerve is correspondingly large on the endocranial cast of elephantiforms (Andrews, 1906; Dechaseaux, 1958; Giovinazzo & Palombo, 2005; and Kupsky *et al.*, 2006). Though the cerebellar morphology of deinotherids is unknown, the size of the *foramen rotundum* indicates that the trigeminal nerve was relatively large (Harris, 1975).

Finally, there are special cases where we have direct evidence of a proboscis and do not need to rely on proxies (i.e., the mummified remains of mastodons and mammoths) (Fisher, 2018). In the absence of direct anatomical evidence, we can use information from ichnology and trace remains to supplement the morphological fossil record (Cawthra *et al*., 2021). Along the coastline of the South African Cape, thirty-five Pleistocene proboscidean track remains have been identified (Cawthra *et al*., 2021). Elongated grove impressions found along track marks from these sites have been interpreted as elephant proboscis drag marks (Cawthra *et al*., 2021).

These drag impressions were found in association with a tusk and at least five other occurrences of elephant skeletal material all dated to no later than the Pleistocene (likely *Loxodonta* sp.) (Cawthra *et al*., 2021). No one so far has attempted to use such trunk drag impressions to reconstruct the dimensions of the trunk in the fossil record; however, the very existence of drag marks suggests that

the proboscis was long enough in these Pleistocene proboscideans to reach the ground.

Most of the osteological proxies used by authors to argue for the presence or absence of the trunk on this literature review can be easily measured (i.e. degree of narial retraction, surface area of the infraorbital foramen and volume of the infraorbital canal); however, to date the correlation of the trunk to these proxies have not been examined in a statistical framework.

Research Problem

To date, no quantitative assessment of the evolution of the trunk in elephant ancestors has been undertaken. We do not know exactly when the trunk evolved, how it grew (assuming it started small), and we do not have a quantifiable metric or systematic approach for determining whether a trunk was present or not in fossil species, and for determining how large such a trunk may have been. This project aims to develop a better understanding of the evolution of the trunk in elephants, which has implications regarding our understanding of the evolutionary success of elephants, their feeding and drinking habits, and intra- and interspecific behaviours (e.g. tactile and scent recognition). This project will thus shed new light on a hitherto understudied research question.

Hypotheses

1. The evolutionary origin(s) of the proboscis in Proboscidea occurred gradually during the course of their evolution.
2. The presence and dimensions of a proboscis can be reconstructed using simple measurements on dry and fossil skulls.

Aims and Objectives

1. To quantify the dimensions of the infraorbital canal (i.e. volume and surface area of the infraorbital foramen) and retraction of the nares on the dry skulls of a selected sample of modern "ungulates" and afrotherians.
2. To test how these metrics correlate with the dimensions of the nose/trunk in the corresponding

live animals (as measured in lateral view).

3. Apply these assessments to fossil proboscideans, from the basal-most 'Plesielephantiformes' to more derived Elephantidae.

Material and Methods

CT scan samples:

This project is based on observations and measurements made on an existing dataset of 126 CT-scanned dry skulls representing 126 modern species of Mammalia (113 Artiodactyla, 8 Perissodactyla and 5 species of Paenungulata). The CT scans of dry skulls of mammals that are proposed to possess a trunk or "trunk-like" structures (the saiga antelope, Asian and American tapirs, elephant shrew and African elephants) are compared to the skulls of outgroup taxa with no trunk. These medical quality CT scans were made from the collections of the American Natural Museum (ANMH), Ditsong National Museum of Natural History (AZ and TM), Natural History Museum of Basel (NMB), Evolutionary Studies Institute of the University of the Witwatersrand (BP), School of Anatomical Science of the University of the Witwatersrand (MS and ZA), Wits Life Science Museum (WLSM), Yale Peabody Museum of Natural History (YPM), and Zoological Museum of the University of Zurich (ZM). The list of the specimens (and their CT scanning parameters) is available in the appendix (supplementary Table 1 and 2), and in Benoit *et al.,* (2020). The elephant shrew (AMNH 161535) was Laser Scanned by Leif Tapanila (published 06/16/2020), at Idaho Virtualization Lab (Idaho State University) available on morphosource; (www.morphosource.org/concern/media/000119087?locale=en).

Segmentation and Measurements of the CT data:

All the measurements on the CT scans were undertaken using the software AVIZO 9 (FEI VSG, Hillsboro OR, USA) at the virtual imaging lab of the Evolutionary Studies Institute, University of the Witwatersrand. The volume of both the left and right canals (if available) was measured on the

same software, and the average between the two was used for statistical analyses. If only one side was preserved, only one canal was used. The measured volume includes all the branches of the infraorbital canal, from the maxillary foramen to the rostral alveolar branch.

The retraction of the naris (e.g. 2D measurement, figure 3), skull length (i.e. 2D measurements, figure 4), and the surface area of the infraorbital foramen (i.e. 3D measurements of the diameter, of both the long-Y and short-X axis, figure 5) were measured on the same software. The retraction of the osseous naris on the skull was quantified as the distance between the anterior margin of the skull and the posterior-most margin of the narial opening in lateral view (figure 3). The length of the skull was defined as the distance between the anterior-most margin of the premaxilla to the tip of the condyle (figure 4). The surface area was calculated using the formula $A = \pi(a.b)$, where a is half the height of the infraorbital foramen (long axis-Y) and b is half the width of the infraorbital foramen (short axis-X).

These measurements co-vary with body size, so this effect is accounted for by taking the ratio of the infraorbital canal volume to log body mass, surface area of the infraorbital foramen over the head length, and the ratio of snout length to head length (body masses are available in the literature; Benett *et al*., 2012; Benoit *et al*., 2020 and, Holling & Lambert, 1998). The internal gross morphology of the infraorbital canal (branching patterns) across these mammalian taxa was documented and described.

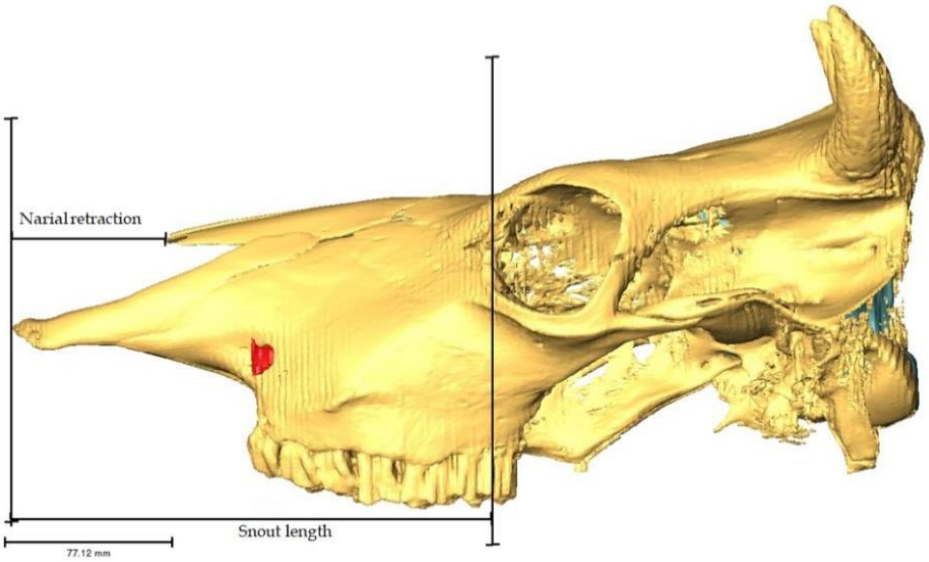


Figure 3. Skull of Bos taurus *in lateral view, showing the measurement of the narial retraction.*

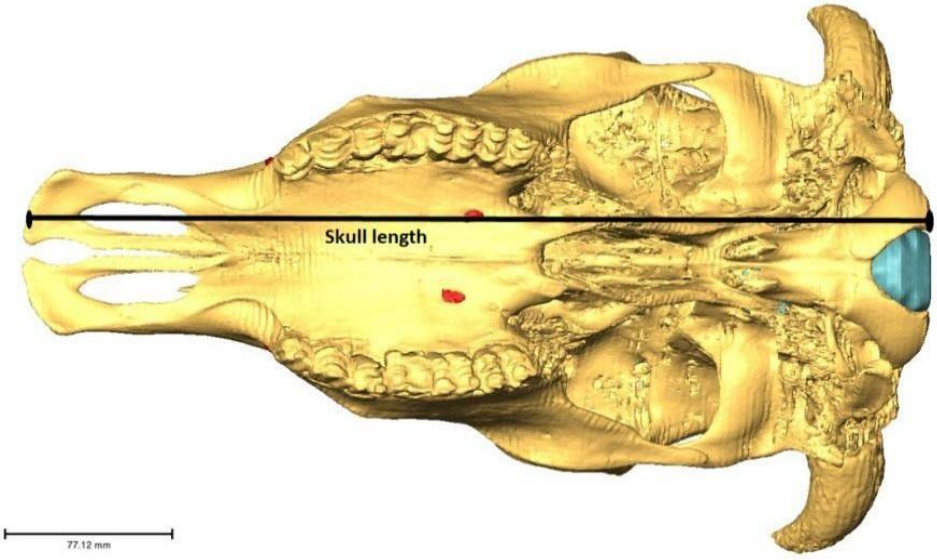


Figure 4. Skull of Bos taurus in ventral view, showing the measurement of the skull.

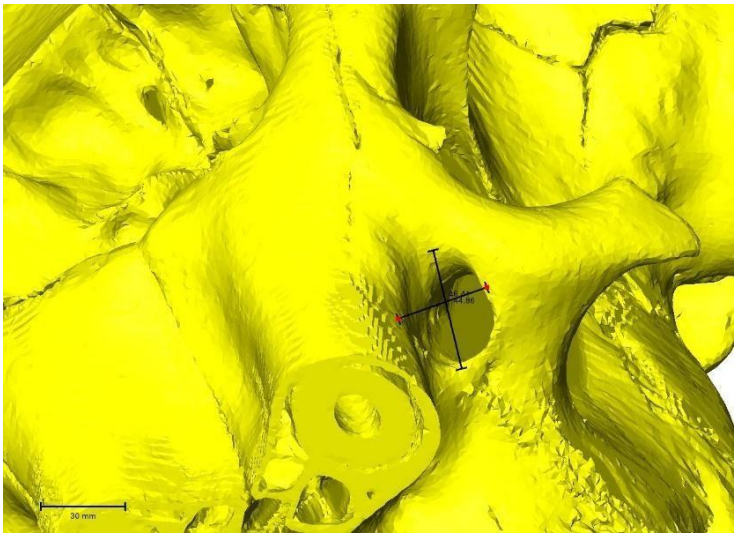


Figure 5. Diameter of the infraorbital foramen in Loxodonta africana*, in oblique anterior view.*

Measurements on pictures:

After taking measurements of the dimensions of the infraorbital canal and naris on dry skulls, measurements of the snout and lower jaw length (head length) were taken on living species using the software Image J (figure 6). The measurements on living species were taken in order to test the correlation of the snout to the proposed osteological proxies (i.e. calibre of the infraorbital canal). Pictures of zoo animals in lateral view were taken using a camera equipped with a spirit level. The images were taken in the years 2018 and 2019 at the Zoologischer Garten (Germany), Zoopare of Beauval (France), Ménagerie du Jardin des Plantes (France), Lory Park and Owl Sanctuary, Johannesburg Zoo (South Africa), National Zoological Garden (South Africa), Montecasino Bird Garden (South Africa), and Chester Zoo (United Kingdom). K. H. Vogel provided the images of the saiga, and this dataset represents about 10,000 pictures documenting the lateral view of 129 species and is available at https://osf.io/4vpnj/?view_only=3dc98 7012f cd44a 6a64a d7d8949ec0 1f (https://doi.org/10.17605 /OSF.IO/4VPNJ (Benoit *et al.*, 2020). The linear distance between the eyeball and the distal-most extremity of the

snout (or of the trunk when applicable) was measured in order to quantify the length of the nose (or trunk) (figure 6).

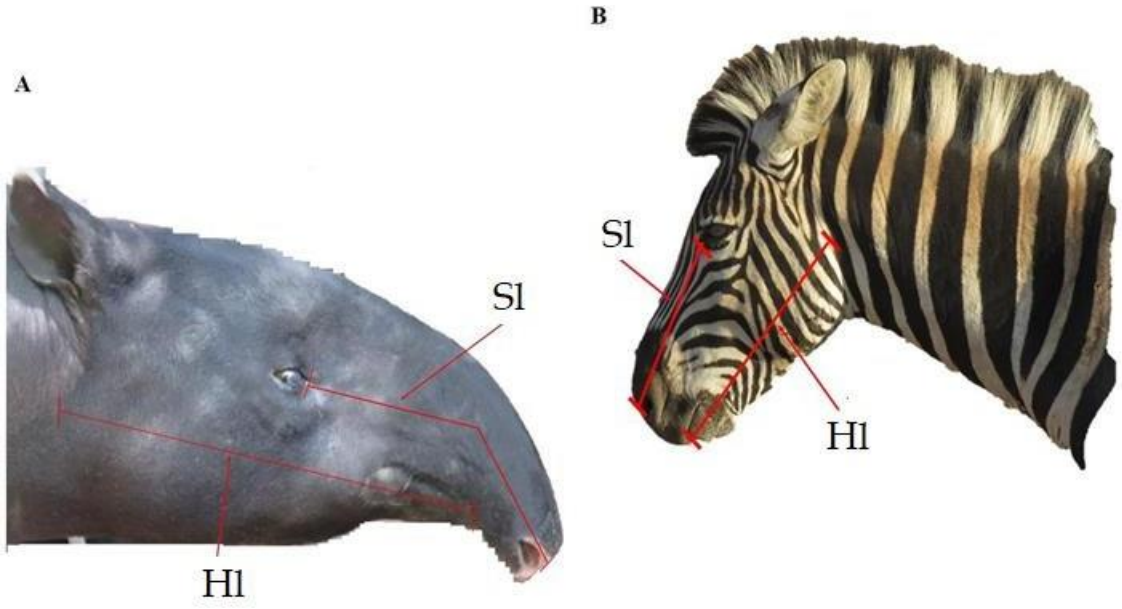


Figure 6.The heads of A, Tapirus indicus *and B,* Equus zebra*, in both lateral view, showing the measurements of the snout (Sl) and lower jaw (Hl) lengths on the images.*

Regression models

The aim of this study is to test if there is a significant correlation between the dimensions of the trunk and the osteological proxies listed above using linear regressions. Simple linear regression tests were conducted using the software PAST (see Hammer, 1999-2021). Three regression models were generated and tested on the sample (n = 43) used for the current study. These models include:

(1) Snout length/Head length (photos) vs Surface area of Infraorbital foramen/Skull length (dry skull); (2) Snout length/Head length (photos) vs Narial retraction; and (3) Snout length/Head length (photos) vs Average Volume Infraorbital canal/log (body mass). If one or more of these osteological measurements prove to be strongly correlated to the dimensions of the trunk (which

is the expected result based on the available literature), the regression formula will then be applied to the following extinct proboscidean taxa.

Application to fossils

Dr J. Benoit provided the CT scan of the basal-most *Numidotherium koholense (*UOK5 from the early Eocene of Algeria, 48 million years old, scanned at 81.66 μm voxel size, at the AST-RX platform of the MNHN in Paris). The Pleistocene *Mammut americanum* (ANSP VP 13307) was scanned using surface scanning, converted into image stack using the Scan Surface to Volume function of Aviso, at Greenfield 3-D Imaging Lab of the Academy of Natural Sciences (Drexel University), and uploaded by Kyle Luchenbill (01/09/2919) (acquired from morphosource.org: https://www.morphosource.org/concern/media/000066352?locale=en).

The volume of the canals and surface area of the cross-section of the infraorbital foramen, and retraction of the naris of *Numidotherium* and *Mammut* were measured using Avizo 9 (FEI VSG, Hillsboro OR, USA) (*Mammut* is represented by partial maxilla; its narial retraction can be measured from images in the literature). The body mass of *Numidotherium* used here is 250 -300 kg (Larramendi, 2016), and *Numidotherium* skull length is 37.0 cm (Ameur *et al*., 1984). The body mass of *Mammut americanum* is 5761 kg (Larramendi, 2016). The skull length of *Mammut americanum* is 97.7 cm (Branstrator & Woodman, 2008). Dr J. Benoit also provided measurements of the infraorbital foramen in fossil proboscidean taxa, from the Nairobi National Museum, Kenya (see table 2):

Table 2. The measurements of the infraorbital foramen (IOF) from the museum of Nairobi, Kenya.

Specimen no.	ID	IOF height (cm)	IOF width (cm)	Surface area(cm^2)
KNM-LU975	*Anancus kenyansis*	5	3.2	12.57
KNM-WS12874	*Gomphotheriidae* indet	1.9	1.9	2.84
KNM-KP30204	*Loxodonta* sp.	7	8	43.98

KNM-ER5711	*Elephas recki*	5	12	47.12
KNM-ER1087	*Deinotherium bozasi*	6.5	4	20.42
KNM-WS12660	*Gomphotheriidae* indet	3	5.5	12.96

The skull lengths of these fossil taxa were calculated from the literature: *Anancus kenyansis* = 70 cm (Brunet *et al*., 2009)*; Elephas recki* = 112 cm (Larramendi, 2016)*; Deinotherium bozasi* = 115cm (Harris, 1975). For Gomphotheriidae, the species is indeterminate. As such, an average skull length was calculated and used for the gomphothere specimens*: G. tassyi* = 76 cm (Jaroon *et al.*, 2017); *G. productum* = 106.25 cm (Larramendi, 2016); *G. steinheimense* = 93.75 cm (Larramendi, 2016); *Notiomastodon, N. platensis* MECN82 = 81.25 cm (Larramendi, 2016)*; Stegomastodon, S.mirificus* NMNH 10707 = 87.5 cm (Larramendi, 2016); G. hondurensis = 57.5 cm (Guillermo & Spencer, 2010); *Cuvieronius* = 90 cm (Guillermo & Spencer, 2010)*;* and the average skull length = 90 cm.

Sampling:

This data is heterogeneously sampled, with a bias towards ruminants, especially bovids which are over-represented. As this will yield biased results towards ruminants, taxonomic re-sampling was undertaken, to diminish the confounding effects of phylogeny and create a more homogenous dataset for statistical analyses. It was sampled so that the species within the three Orders Afrotheria, Perissodactyla and Artiodactyla are more evenly represented (n = 43). In addition, an in-group sub-sample containing all the taxa that possess a trunk or proboscis-like snouts in the study (n = 8; 2 *Loxodonta*, 2 tapirs, 1 elephant shrew, 2 saiga and 1 dik-dik) were isolated for some of the analyses. This dataset does not include proboscis monkeys, elephant seals or other carnivores because ungulates are the closest ecological relatives of proboscideans, and afrotherians are the closest phylogenetic relatives of proboscideans.

Results

I – Descriptions

The nomenclature used for the description of the maxillary canal branches is that of Benoit *et al.* (2016). The infraorbital canal is never perfectly cylindrical, but is divided into the canal for the infraorbital nerve *per se* (which leads to the infraorbital foramen), the rostral or incisivomaxillary alveolar canal (the longest and anterior-most branch, abbreviated RAC) which is oriented towards the canine root, and the middle (MAC) and caudal (CAC) alveolar ramus which are both oriented towards cheek teeth (Wilber, 2008, 2011; Evans & Lahunta, 2012; Rodella *et al.*, 2012; German *et al.*, 2015; and Benoit *et al*., 2016). The infraorbital foramen is more-or-less elliptical, with varying degrees of lateral and dorso-ventral compressions amongst the taxa.

Afrotheria

Orycteropus afer:

The two aardvarks sampled here possesses a short and conical canal, with a long and well-defined RAC (figure 7). The RAC is twice as long as the infraorbital canal and gives off three to four smaller branches that diverge ventrally and medially towards the tooth row. The CAC and MAC are not present or clearly defined.

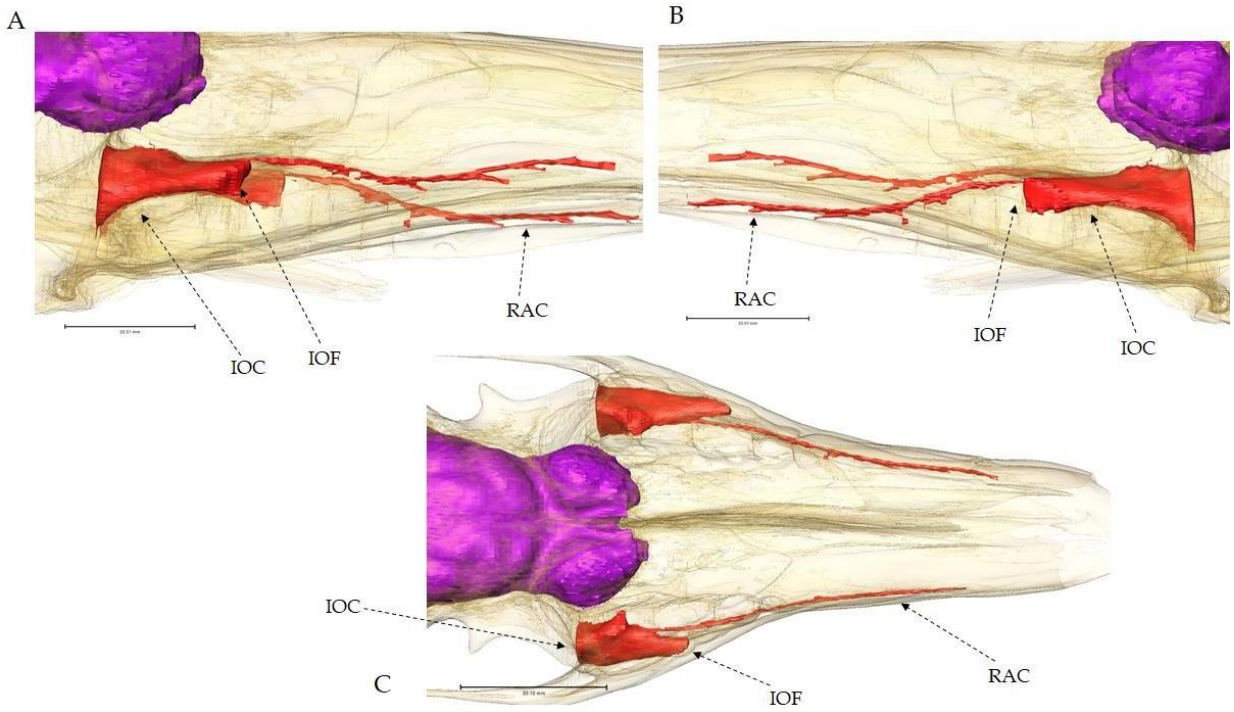


Figure 7. The canal in Orycteropus afer*: A; right lateral view, B; left lateral view, and C; dorsal view (all skulls are transparent) (scale: 20 mm). IOC; infraorbital canal, IOF; infraorbital foramen, RAC; rostral alveolar canal. The purple structure is the brain.*

Procavia capensis

The canal of *Procavia* is conical caudally and becomes more tubular and relatively elongated rostrally. Specimen N291 possesses a MAC and RAC that diverge from the middle of the main canal, at the same level (figure 8 A). The MAC diverges laterally towards the check teeth, and the RAC branches anterior-ventrally towards the root of the upper tusk-like incisor. There are four *Procavia capensis* specimens in this study; specimen UNM462 has a gross morphology of the canal similar to that of UMN76: i.e. MAC is absent, but possesses a RAC that bifurcates to two or three branches of equal size, towards the root of the tusk-like incisor (figure 8 C). Specimen UNM305 is similar to UNM276; i.e. possesses a MAC and along with a simple RAC (figure 8 A and B).

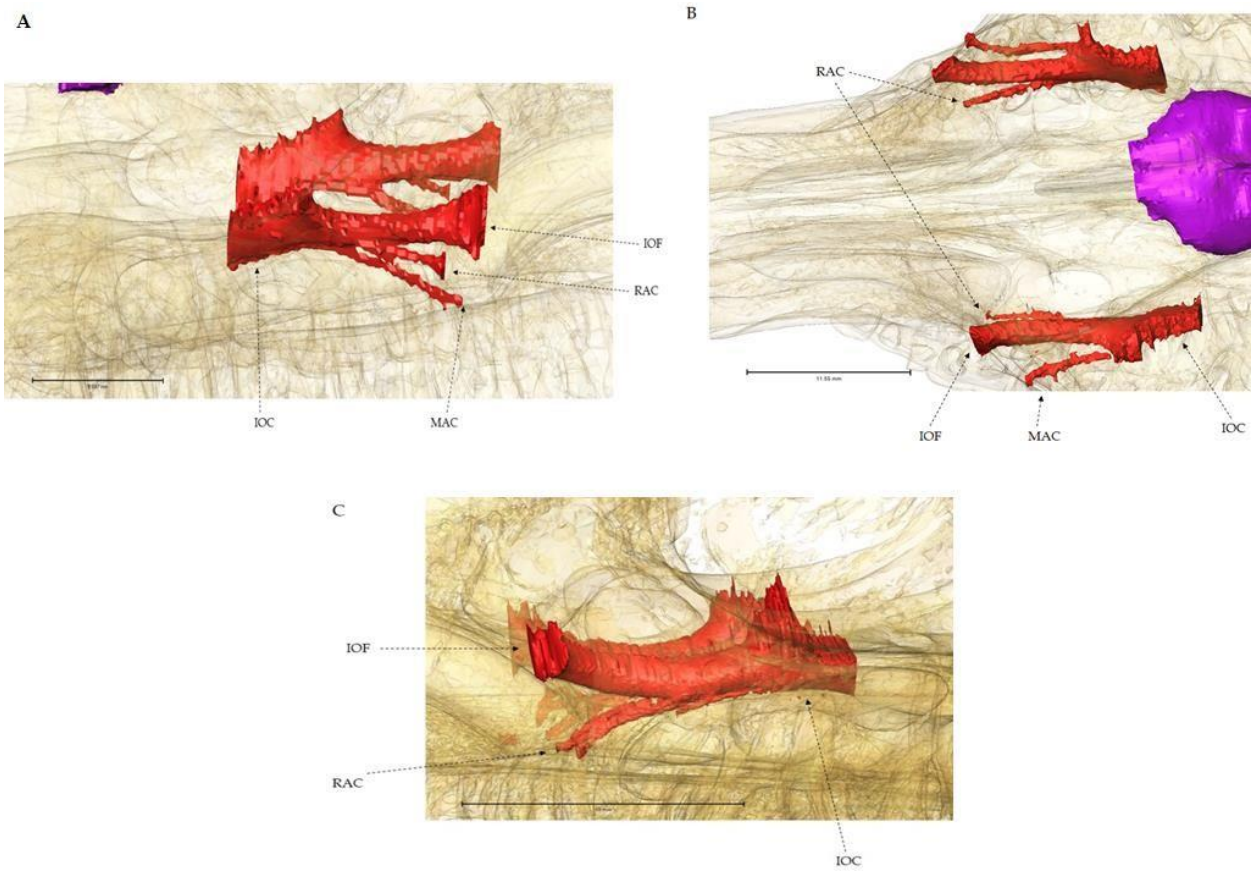


Figure 8. The infraorbital canal in Procavia capensis*; A; UNM291 in right lateral view (scale: 10 mm, B; UNM291 in dorsal view, C; UNM76 in left lateral view. IOC; infraorbital canal, IOF; infraorbital foramen, MAC; middle alveolar canal, RAC; rostral alveolar canal. The purple structure is the brain.*

Macroscelides proboscideus:

The elephant shrew possesses an infraorbital canal that is relatively short, conical and voluminous (3.2819 cubic centimeters). It also possesses an elongated, simple RAC without visible side branches (figure 9); however, there is a small and short branch caudal to the RAC, which appears to run parallel to the rostral alveolar canal. This condition is symmetrical as it is present on both the left and right canals.

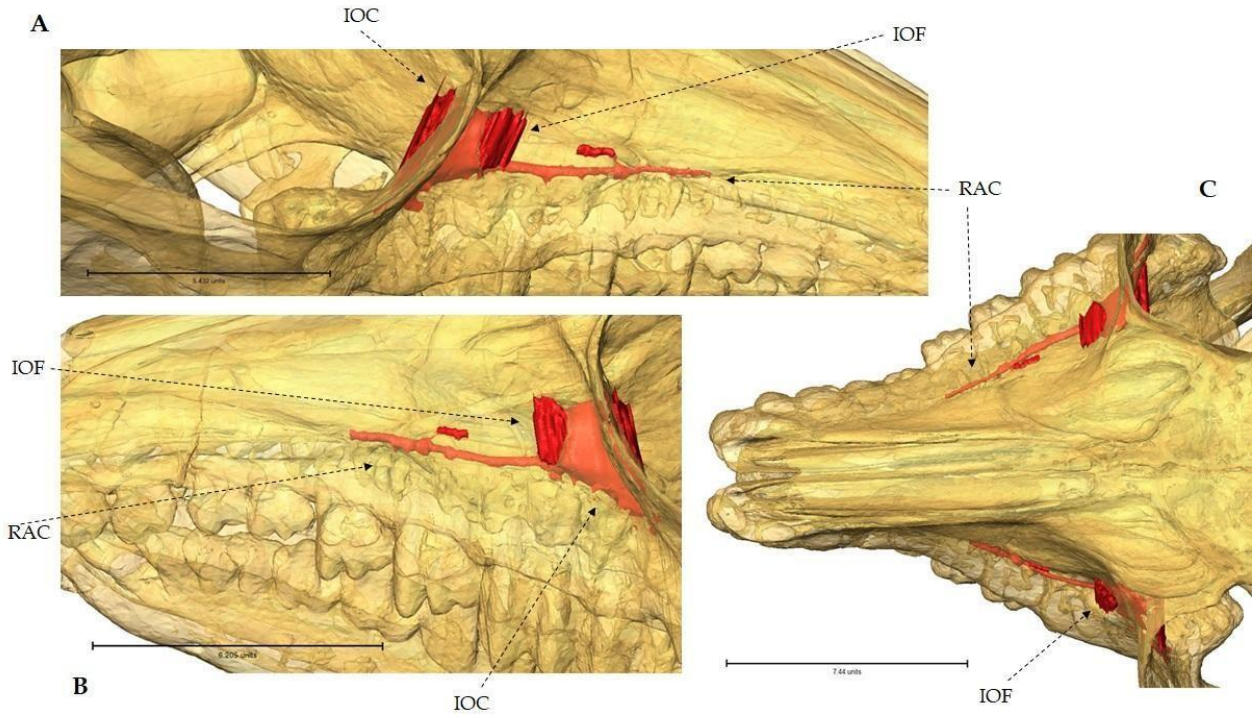


Figure 9. The infraorbital canal in Macroscilides proboscideus; A; right lateral view (scale: 5 mm), B; left lateral view (scale: 6mm), C; dorsal view, all skulls transparent (scale: 7 mm). IOC; infraorbital canal, IOF; infraorbital foramen; RAC; rostral alveolar canal.

Proboscidea

The proboscideans possess a relatively voluminous, short and cylindrical infraorbital canal with reduced side branches. The 'Plesielephantiform' proboscidean *Numidotherium koholense* possesses a relatively long and tubular canal (figure 10). *Mammut americanum* possesses a short and cylindrical canal, with a relatively more circular infraorbital foramen (figure 11), similar to that of *Loxodonta africana* (figure 10) and the *Loxodonta africana* with no specimen number (figure 11). Both the *Loxodonta africana* specimens possess a MAC that branches off ventro- medially towards the cheek teeth, with no clear RAC. Similar to *Macroscelides proboscideus*, *Loxodonta africana* possesses a small branch, which is oriented caudo-dorsal to the main canal; however, it differs from that of Macroscelides *proboscideus* in that it is positioned caudal to the

main canal, instead of the RAC. The specimen on figure 13 does not seem to possess this caudo-dorsalbranch.

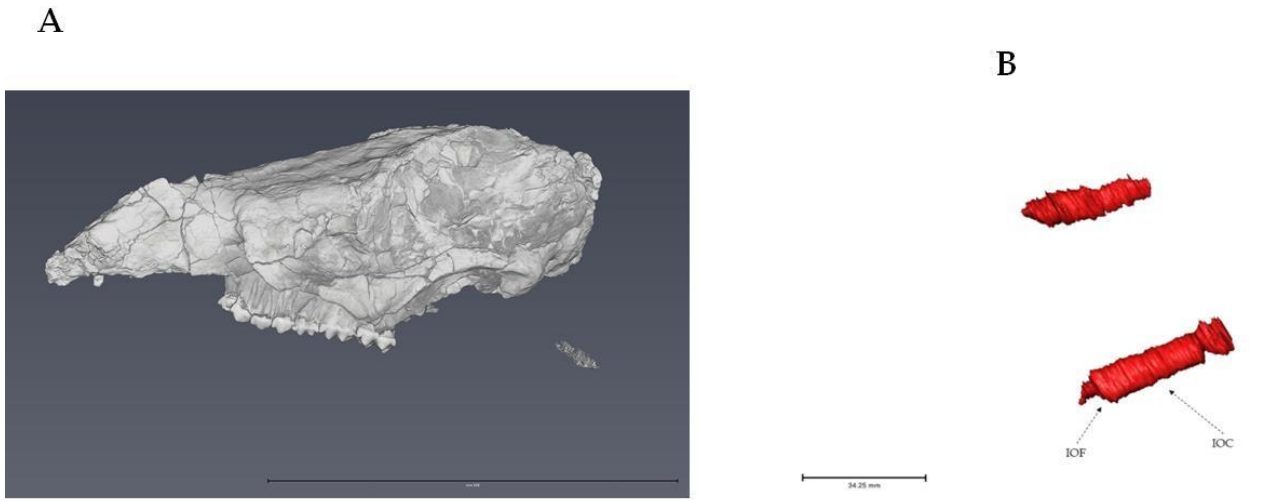


Figure 10. The infraorbital canals in Numidotherium koholense*; A, opaque skull in in right lateral view, scale bar is 350 mm; B, infraorbital canal in left lateral view missing the transparent, Scale bar is 35 mm. IOC; infraorbital canal; IOF; infraorbital foramen.*

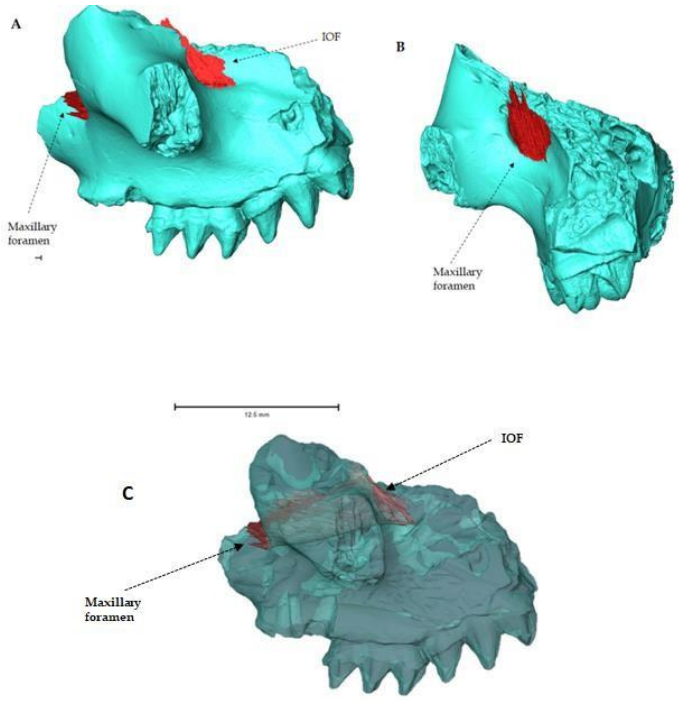


Figure 11. The infraorbital canal (in red) in Mammut americanum*. A; right lateral view, B; caudal view; C, right lateral view, transparent skull. IOF; infraorbital foramen. Scale bar is 13 mm.*

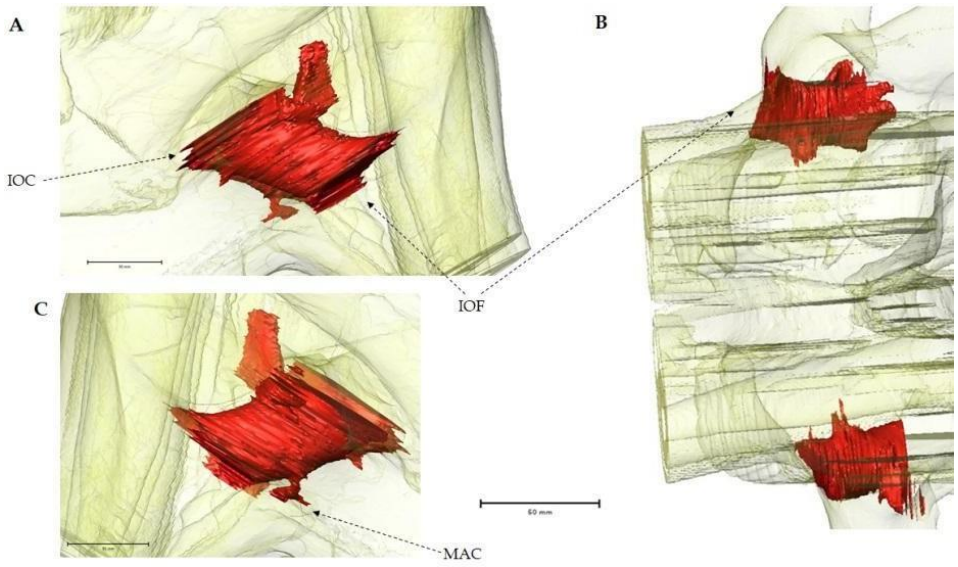


Figure 12. Infraorbital canal in Loxodonta africana*. A; right lateral view (scale: 30 mm), B; dorsal view, C; left lateral view (scale: 40 mm). IOC; infraorbital canal, IOF; infraorbital foramen; MAC; middle alveolar canal. Scale bar is 30 mm A, 77 mm B, 40 mm C.*

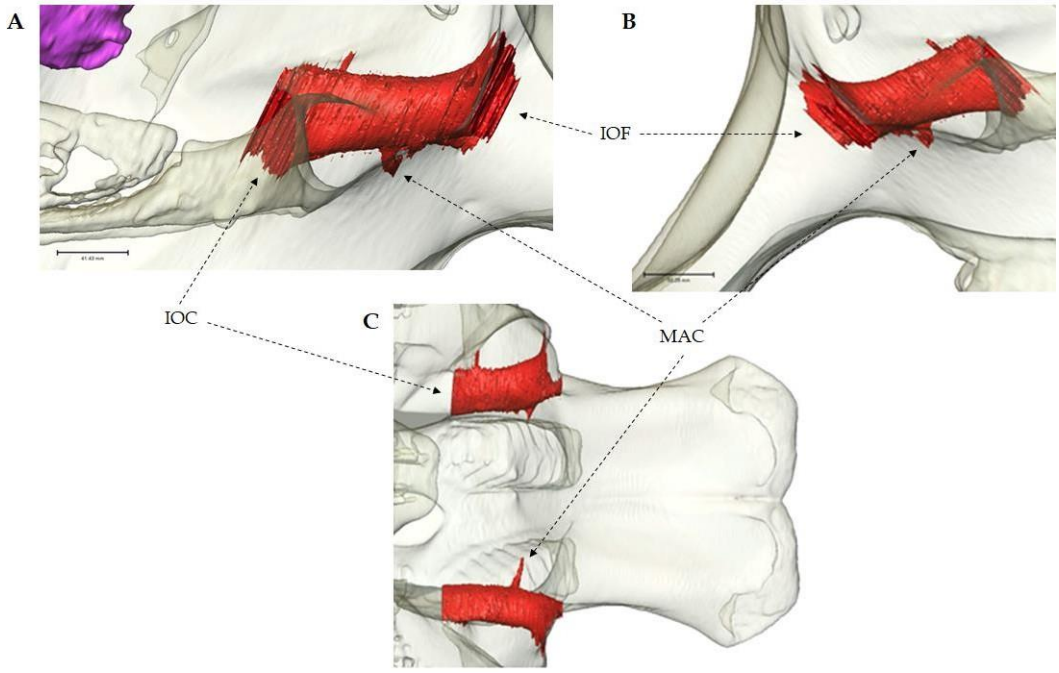


Figure 13. The infraorbital canal in Loxodonta africana*, no-specimen number. A; right lateral view (scale: 41 mm), B; left view, C; left dorsall view. IOC; infraorbital canal, IOF; infraorbital canal; MAC; middle alveolar canal. Scale bar is40 mm A, 50 mm B, 77 mm C. The purple structure in A is the brain.*

Artiodactyla

Tylopoda

Tylopods possess an infraorbital canal with a gross morphology that is mostly tubular, medio-laterally compressed in the middle, and much thicker rostrally in lateral view, unlike the condition observed in most ungulate taxa. *Camelus bactrianus* (figure 14 A and B) possesses a dorsoventrally thicker infraorbital canal than that of *Camelus dromedarius* (figure 14 C and D)*;* however, its RAC is relatively shorter. The RAC of *Camelus dromedarius* is almost equal to that of the main canal in length, but much thinner in thickness compared to that of *Camelus bactrianus.* Both taxa seemingly do not possess a visible MAC nor CAC.

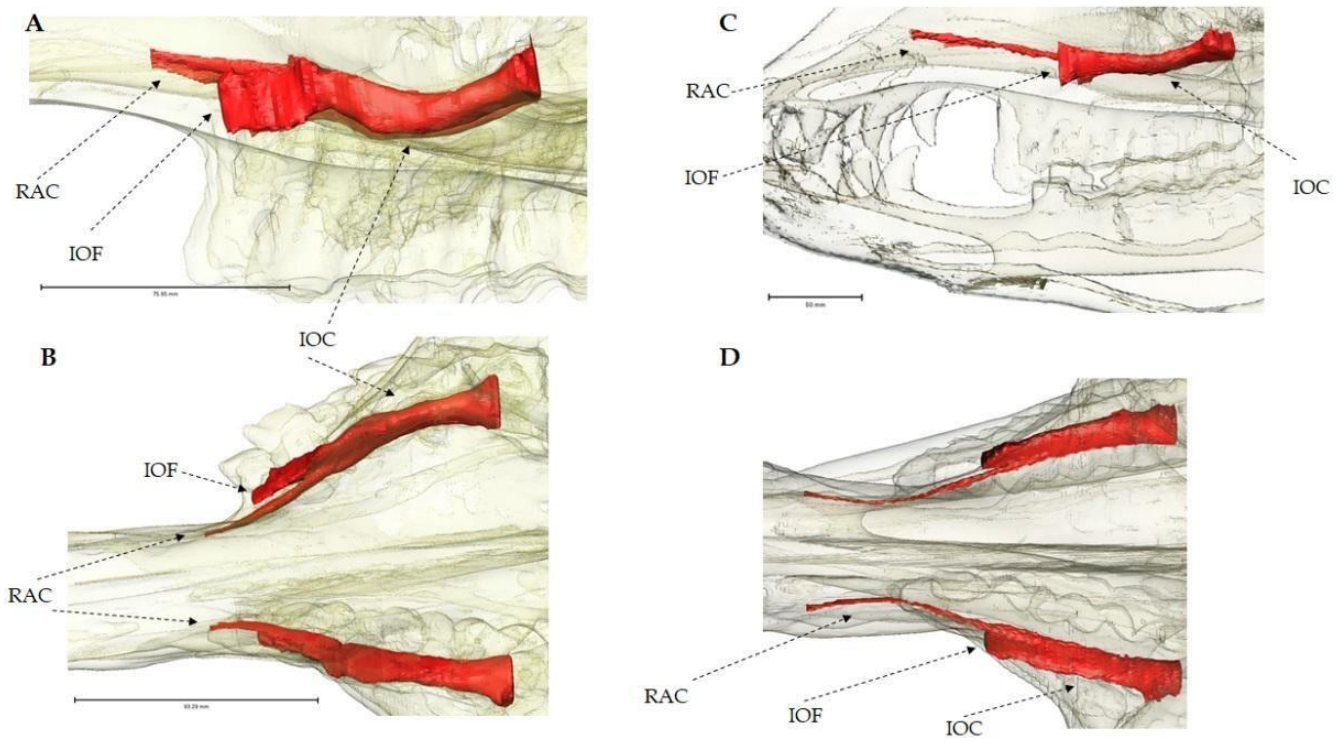


Figure 14. Infraorbital canal in; A; Camelus bactrianus *in left lateral view (scale: 75.95 mm), B; dorsal view(scale: 93.29 mm), C;* Camelus dromedarius *left lateral view (scale: 50 mm), D; dorsal view, all skulls transparent. IOC; infraorbital canal, IOF; infraorbital canal; RAC; rostral alveolar canal.*

Suoidea

The gross morphology of the infraorbital canal in the suids is generally thicker when compared to other artiodactyls such as bovids (figures 15 - 18). *Potamochoerus porcus* (figure 15), has an outline that is jagged in lateral view, and is laterally compressed. The rest of the suid specimens possess a more cylindrical canal. It is conical caudally (except *Phacochoerus africana*, figure 17), and then elongates and tapers rostrally in dorsal view. All the suid specimens possess a well-defined, elongated RAC, with the exception of *Phacochoerus africanus* (figure 17), which possesses a short, dorsoventrally thickened RAC. Both the MAC and CAC are seemingly absent in suids except in *Potamochoerus porcus* (figure 15) which possesses a visible MAC. The RAC terminates at the root of the tusk-like canines, on the taxa with an elongated canal (figure 18). The taxa who possess a canal with a smooth outline seem to have fewer branches (i.e. figure 16), compared to the irregularly shaped types (figure 15).

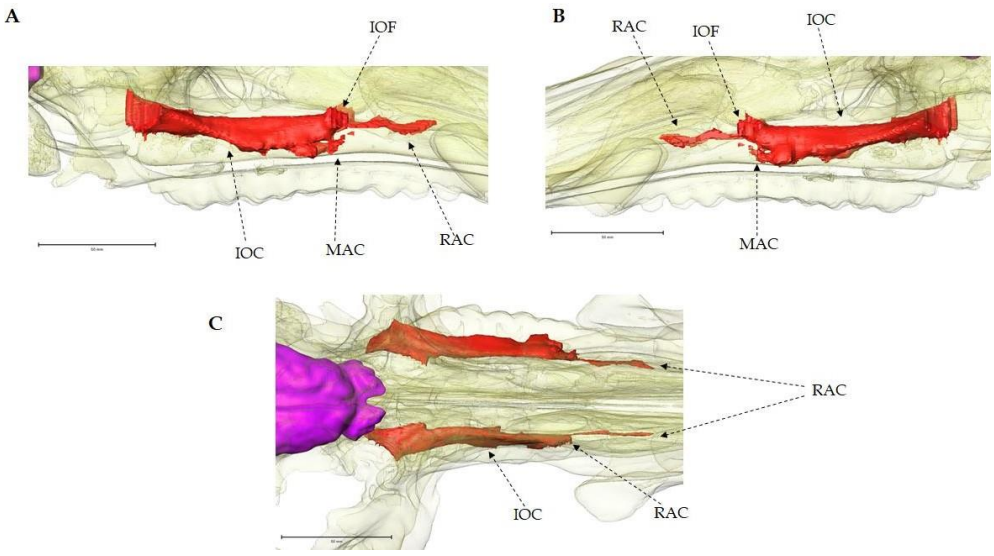


Figure 15. Infraorbital canal in Potamochoerus porcus; *A; right lateral view (scale: 50 mm), B; left lateral view (scale:50 mm), C; dorsal view (scale: 50 mm), all skulls transparent. IOC; infraorbital canal, IOF; infraorbital canal; MAC; middle alveolar canal, RAC; rostral alveolar canal. The purple structure on figure C is the brain.*

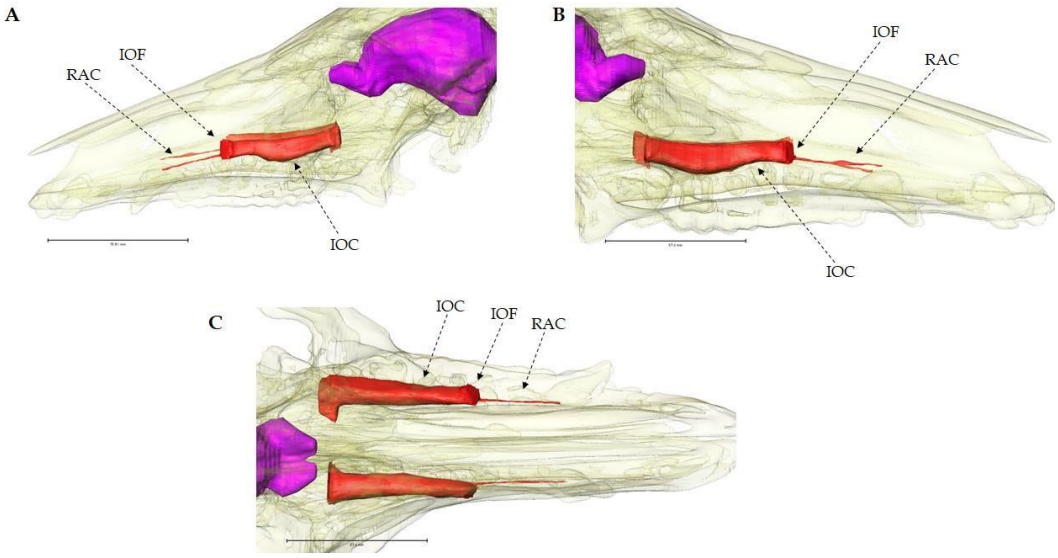


Figure 16. The infraorbital canal in Sus scrofa domesticus*; A; left lateral view (scale: 75.81 mm, B; right lateral view (scale: 57.4 mm), C; dorsal view (scale: 57.4 mm), all skulls transparent. IOC; infraorbital canal, IOF; infraorbital canal; RAC; rostral alveolar canal. The purple structure is the brain.*

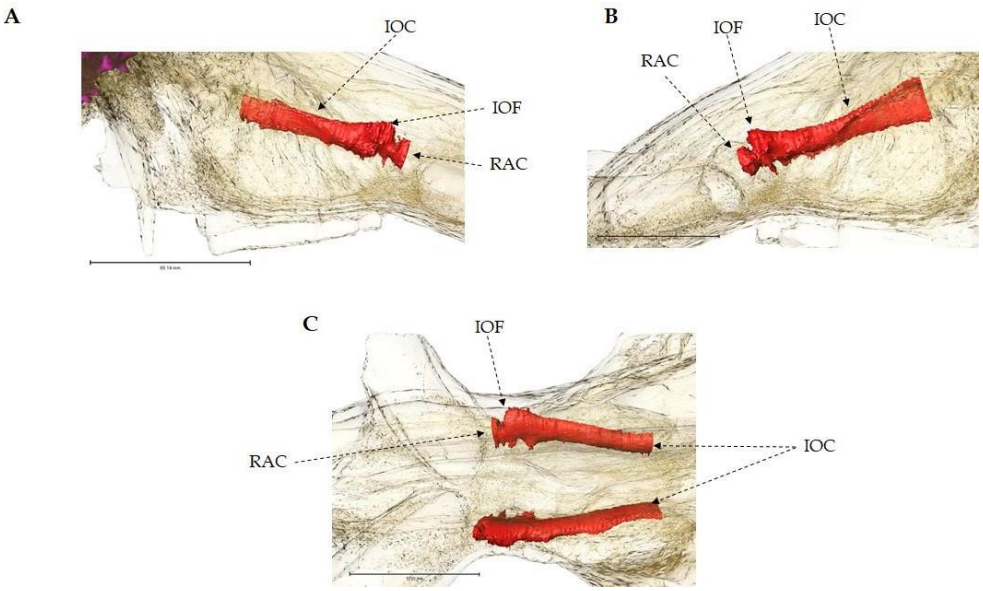


Figure 17. The infraorbital canal in Phacochoerus africanus*; A; right lateral view (scale: 65.14 mm), B; left lateral view (scale: 65.14 mm), C; dorsal view (scale: 57.02 mm), all skulls transparent. IOC; infraorbital canal, IOF; infraorbital canal; RAC; rostral alveolar canal.*

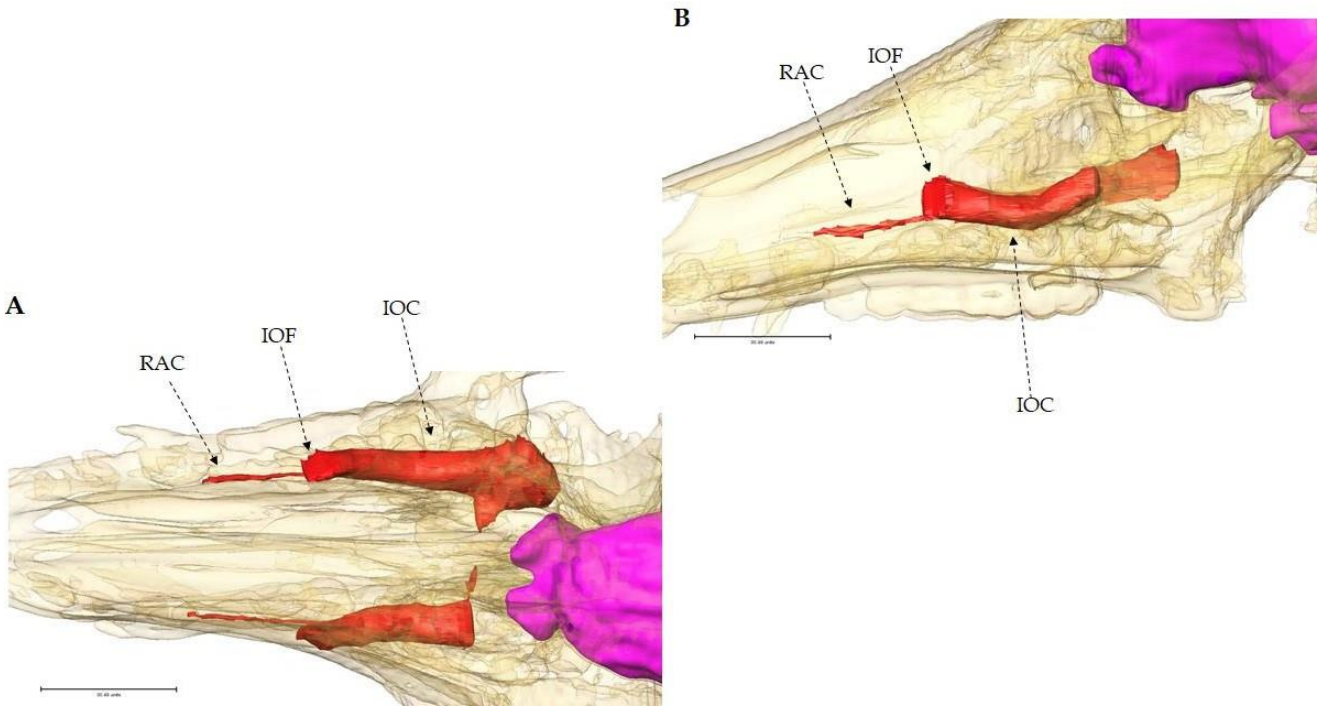


Figure 18. The infraorbital canal in Sus scrofa *(wild boar); A; right dorsal view (scale: 30.4 mm), B; left lateral view (scale: 30 mm), all skulls transparent. IOC; infraorbital canal, IOF; infraorbital foramen; RAC; rostral alveolar canal. The purple structure in both figures is the brain.*

Hippopotamidae

Hippopotamus amphibius possesses a very complex, relatively large infraorbital canal, which is narrow caudally and thickens rostrally, when viewed laterally (figure 19). The canal is medio-laterally compressed when viewed dorsally, and contains multiple recesses on its lateral external surface. The RAC is complex, being divided into two main branches, each ramifying into multiple smaller branches. The dorsal-most branches are relatively small and go above the root of the tusk-like incisor. The ventral-most branches are larger and go below the root, along the palate (figure 19). The condition in *Hexaprotodon* is similar to that of *H. amphibius*, however, relatively simpler as it bears fewer branches (figure 20). The RAC in *Hexaprotodon* bifurcates into two branches

only (with no further subdivisions), but with a similar orientation to those of *H. amphibius.* The MAC and CAC seem absent in both taxa.

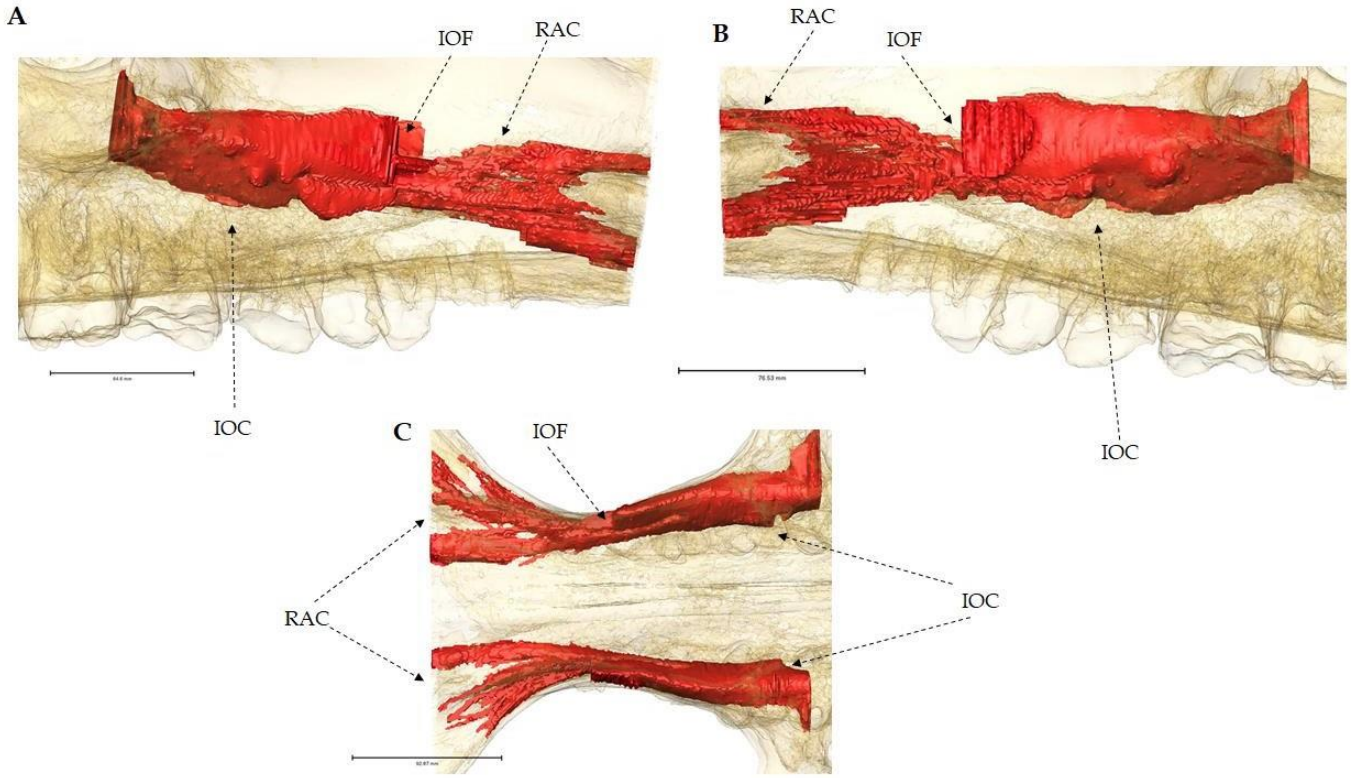


Figure 19. The infraorbital canal in Hippopotamus amphibius*; A; right lateral view (scale: 65 mm), B; left lateral view (scale: 76.5 mm), C; dorsal view (scale: 93 mm), all transparent. IOC; Infraorbital canal, IOF; Infraorbital canal; RAC; rostral alveolar canal.*

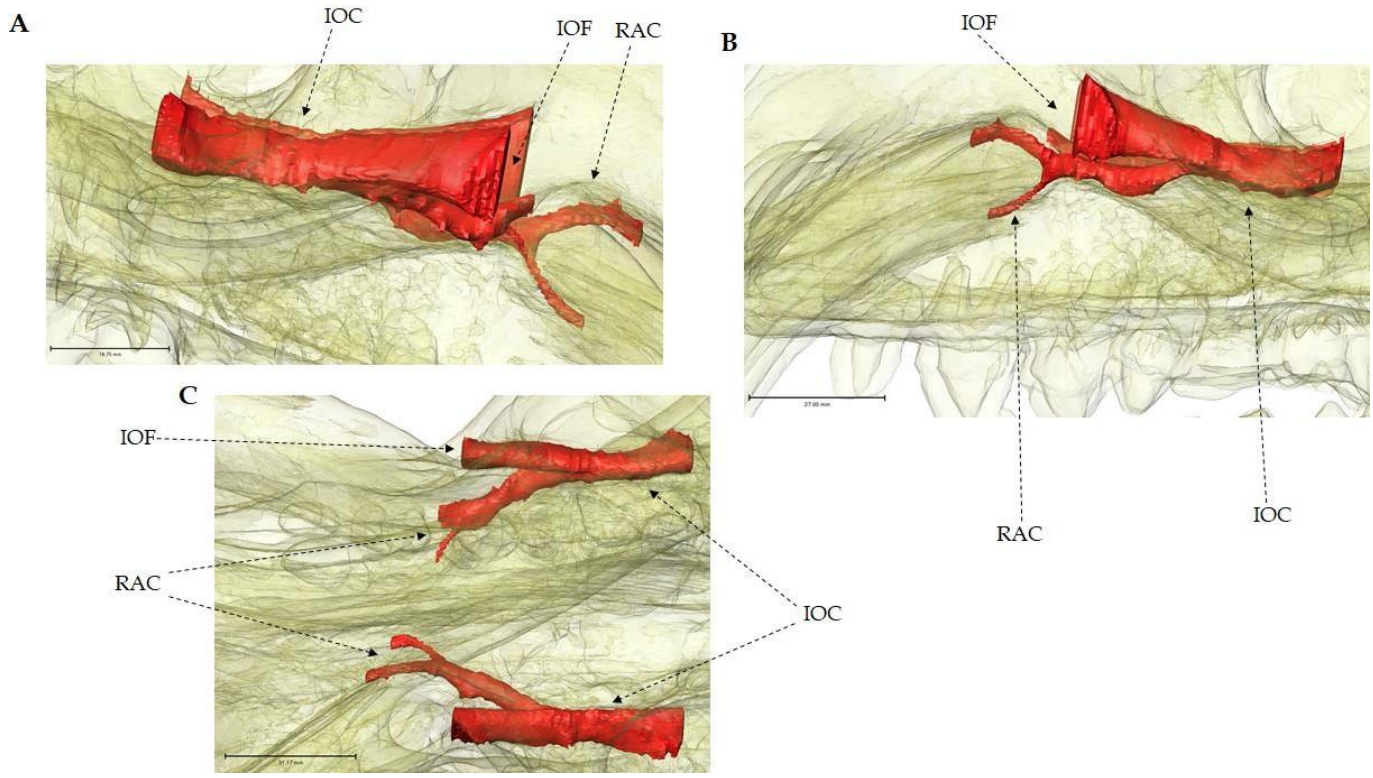


*Figure 20. The infraorbital canal in (*Hexaprotodon liberiensis; *A; right lateral view (scale: 26.63 mm), B; left lateral view (scale: 28 mm), C; dorsal view (scale: 31.17 mm), all transparent. IOC; infraorbital canal, IOF; infraorbital canal; Rac; rostral alveolar canal.*

Moschidae and Tragulidae

Though the Moschids and Tragulidae are not closely related, they share a simple infraorbital canal morphology, with no side branches. Both canals are thin, elongated and tubular; however, the canal in Tragulidae is medio-laterally compressed so that the infraorbital canal is more elliptical than that of the Moschidae (figures 21 and 22). The MAC and CAC are absent in both taxa.

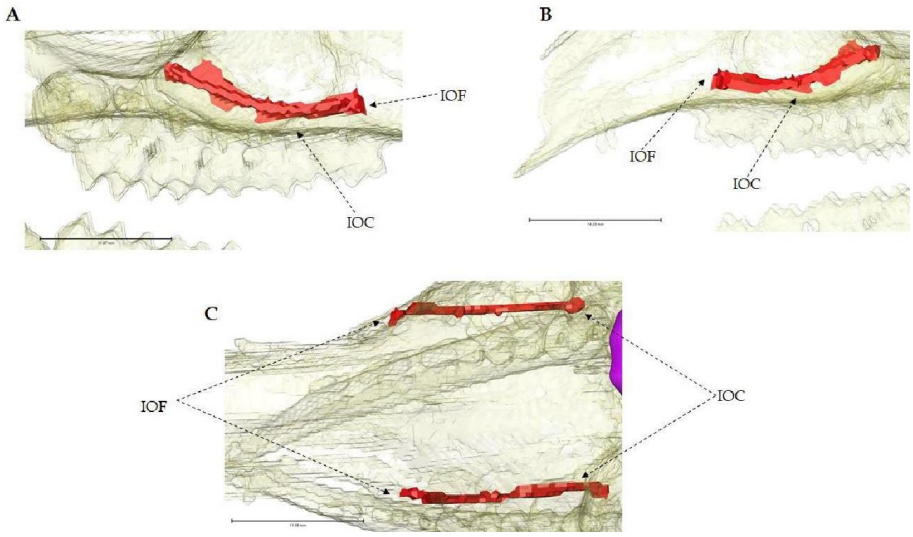


Figure 21. The infraorbital canal in Tragulus javanicus*; A; right lateral view (scale: 11.87 mm), B; left lateral view (scale: 14.23 mm), C; dorsal view (scale: 11.58 mm), all transparent. IOC; infraorbital canal, IOF; infraorbital foramen.*

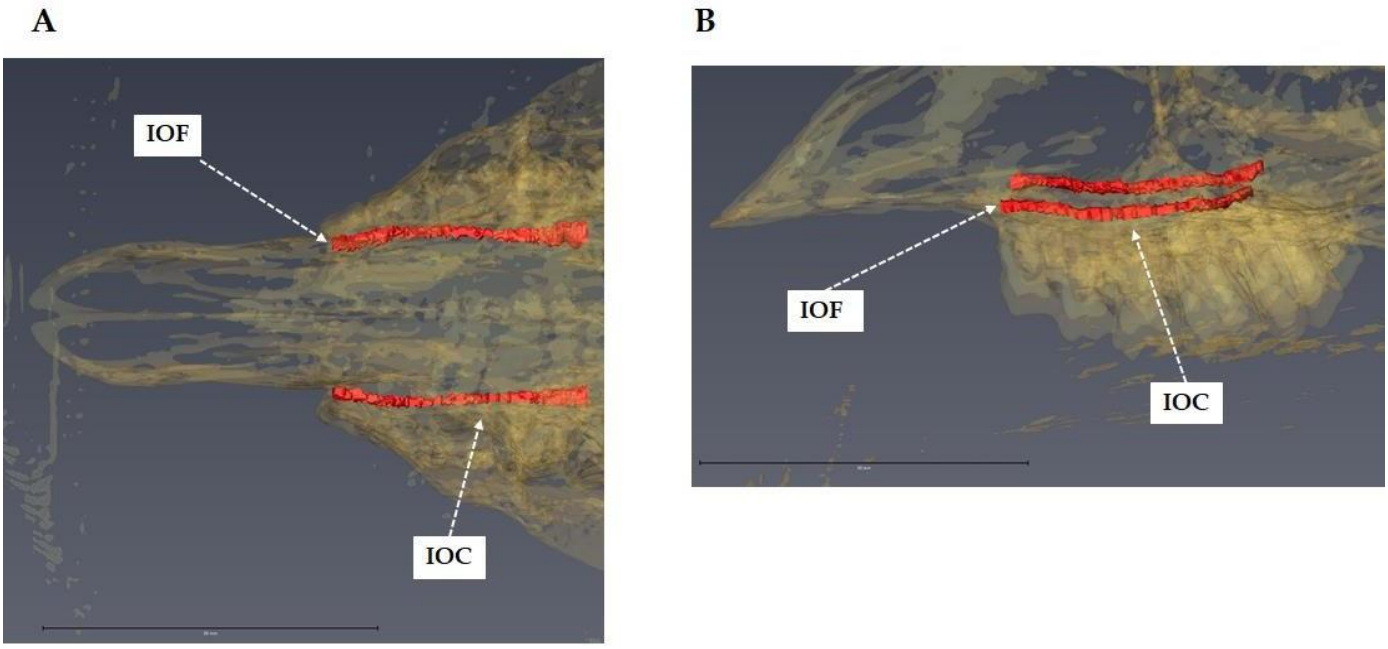


Figure 22. The infraorbital canal in Moschus A; dorsal view (scale: 30 mm), B; left dorso-lateral (scale: 30 mm), all transparent. IOC; infraorbital canal, IOF; infraorbital foramen. All skulls are transparent.

Giraffidae

Unlike other ruminants such as bovids, giraffids have a relatively thicker infraorbital canal , with more branches (especially *Okapia johnstoni*, figure 24). The infraorbital canal in the giraffe is

thicker caudally, and then elongates and tapers rostrally (figure 23). The infraorbital canal in *Okapia* bears more branches than in the giraffe. The left canal bifurcates in two separate canals rostrally, of equal thickness and length, and both terminate externally at the level of the infraorbital foramen (IOF 1 & 2, figure 24). The right infraorbital canal divides into three branches rostrally, with IOC 1 and 2 being thicker, and IOC 3 being relatively thin. They also terminate externally on the surface of the maxilla, at the level of the infraorbital foramen. Both taxa do not seem to possess the MAC and CAC branches.

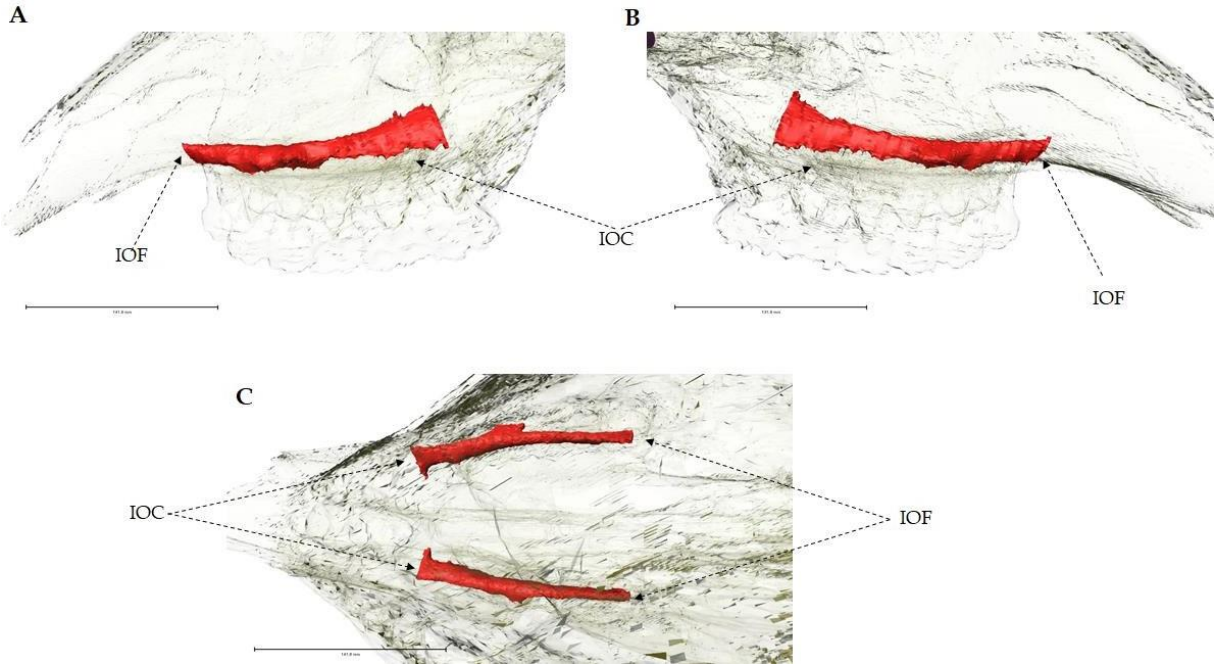


Figure 23. The infraorbital canal Giraffa camelopardalis*. A; left lateral view (scale: 141.8 mm), B; right lateral view (scale: 131.8 mm), C; left dorsal view (scale: 141.8 mm), all transparent. IOC; infraorbital canal, IOF; infraorbital foramen*.

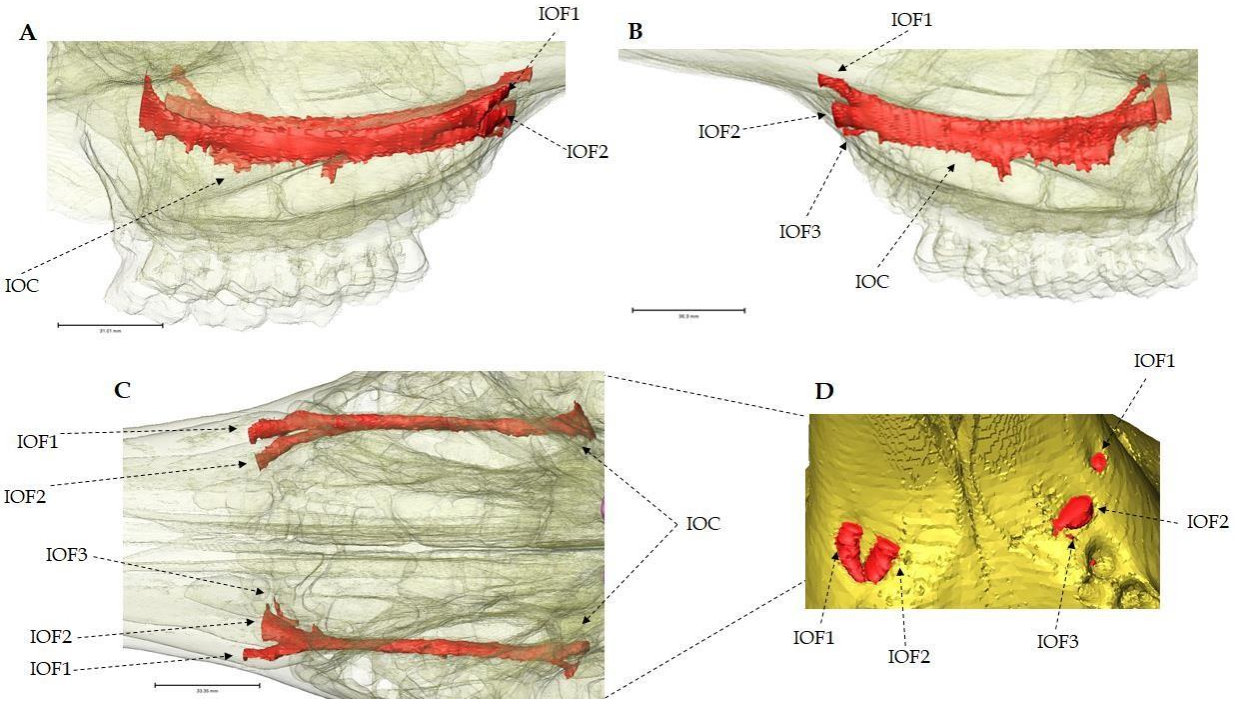


Figure 24. The infraorbital canal in Okapia johnstoni*; A; right lateral view (scale: 31.01 mm), B; left lateral view (scale: 36.3 mm), C; left dorsal view (scale: 33.55 mm), D; oblique ventro-lateral view of the infraorbital canal. Skulls, A to C are transparent, D is opaque. IOC; infraorbital canal, IOF; infraorbital foramen.*

Bovidae (non-proboscis bearing)

The bovids possess a simple, thin, tubular and relatively long infraorbital canal (figure 25 to 27). They bear fewer branches compared to other artiodactyls, except for a simple RAC, when present (figure 27A). The only bovid that seem to have a relatively complex infraorbital canal morphology, with multiple branches is *Raphicerus campestris* (figure 28). Its infraorbital canal morphology is similar to that of the saiga. *Raphicerus campestris* also has a well-defined, right CAC.

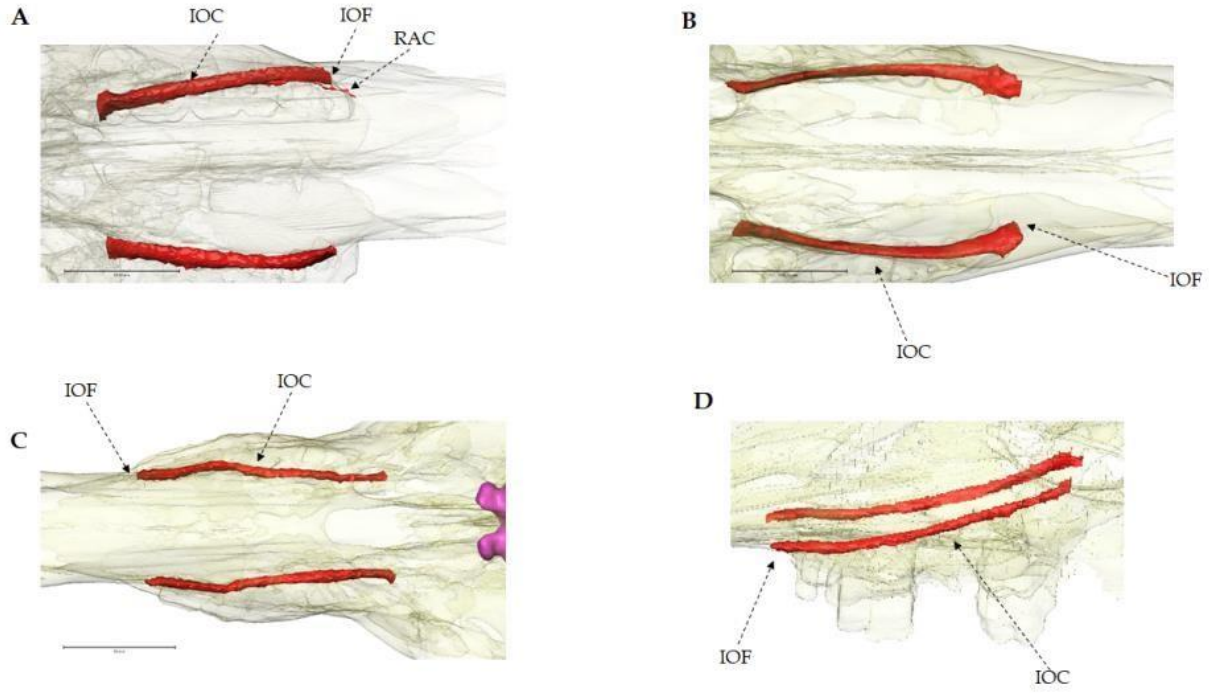


Figure 25. The infraorbital canal in bovids without a proboscis; A; Syncerus caffer*, dorsal view (scale: 55.55 mm), B;* Tragelaphus strepsiceros*, dorsal view (scale: 60 mm), C;* Connochaetes taurinus*, dorsal view (scale: 34. 19 mm), D;* Redunca fulvorufula*,* left dorso-lateral view, all transparent. IOC; infraorbital canal, IOF; infraorbital foramen; RAC; rostral alveolar canal. The purple structure in C is the brain.

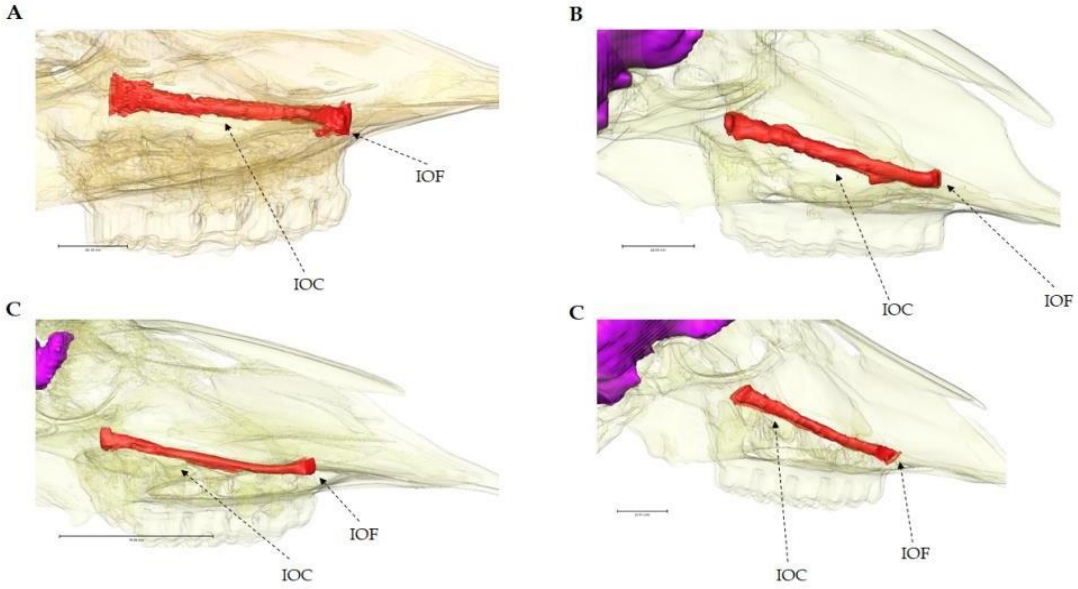


Figure 26. The infraorbital canal in bovids without a proboscis; A; Bos taurus*, right lateral view (scale: 23.15 mm), B;* Capra aegagrus*, right lateral view (scale: 22.93 mm), C;* Kobus ellipsiprymnus*, right lateral view (scale: 78.88 mm), D;* Kobus leche*, right lateral view (scale: 23.01 mm) all skulls transparent. IOC; infraorbital canal, IOF; infraorbital foramen. The purple structure in B to D is the brain.*

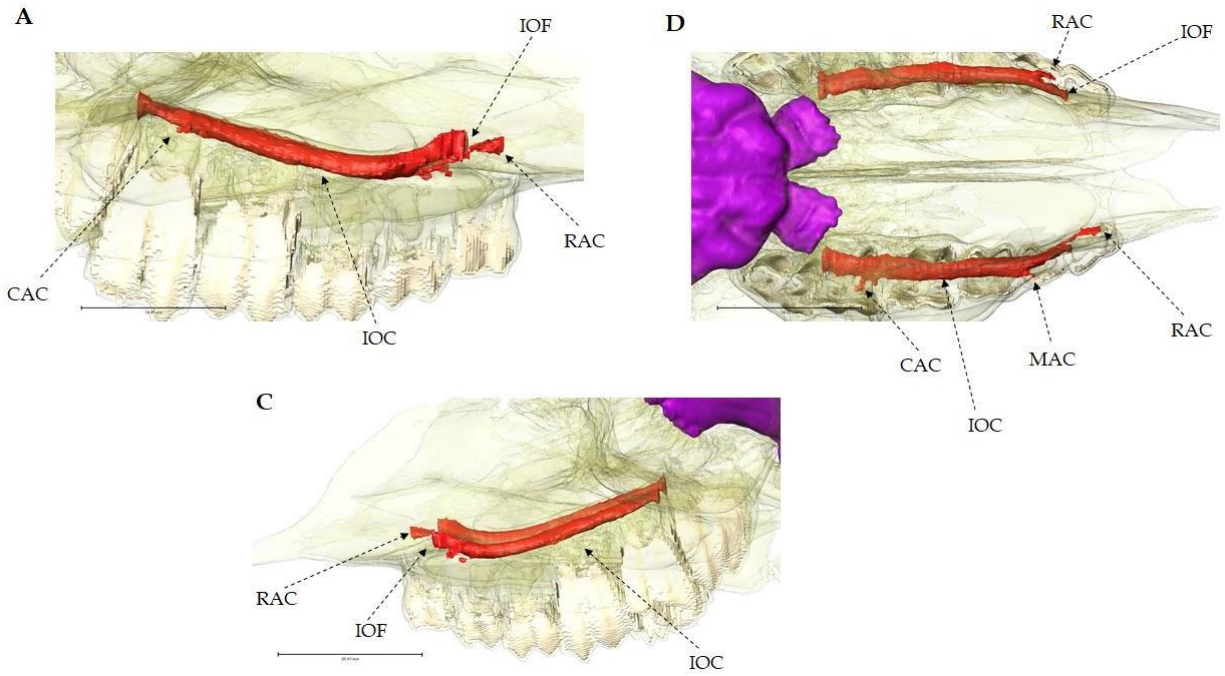


Figure 27. The infraorbital canal in Raphicerus campestris*; A; right lateral view (scale: 14.41 mm), B; dorsal view (scale: 19.03 mm), C; left lateral view (scale: 20.47 mm), all transparent. IOC; infraorbital canal, IOF; infraorbital foramen; MAC, middle alveolar canal, RAC; rostral alveolar canal. The purple structure in C and D is the brain.*

Bovid taxa who possess proboscis-like snouts

All bovids possess a narrow, elongated and tubular canal; however, the proboscis-bearing bovids bear a slightly more complex canal, with multiple MAC and RAC branches. *Saiga tatarica* (figure 34 and 35) possesses only one clearly visible MAC, which branches at the cheek teeth level and terminates externally at the level of the infraorbital foramen. This condition is only observed on the right canal in specimen YPM 85301 (figure 34), and on the left canal in YPM 1510 (figure 35).The CACs in both specimens are not well defined.

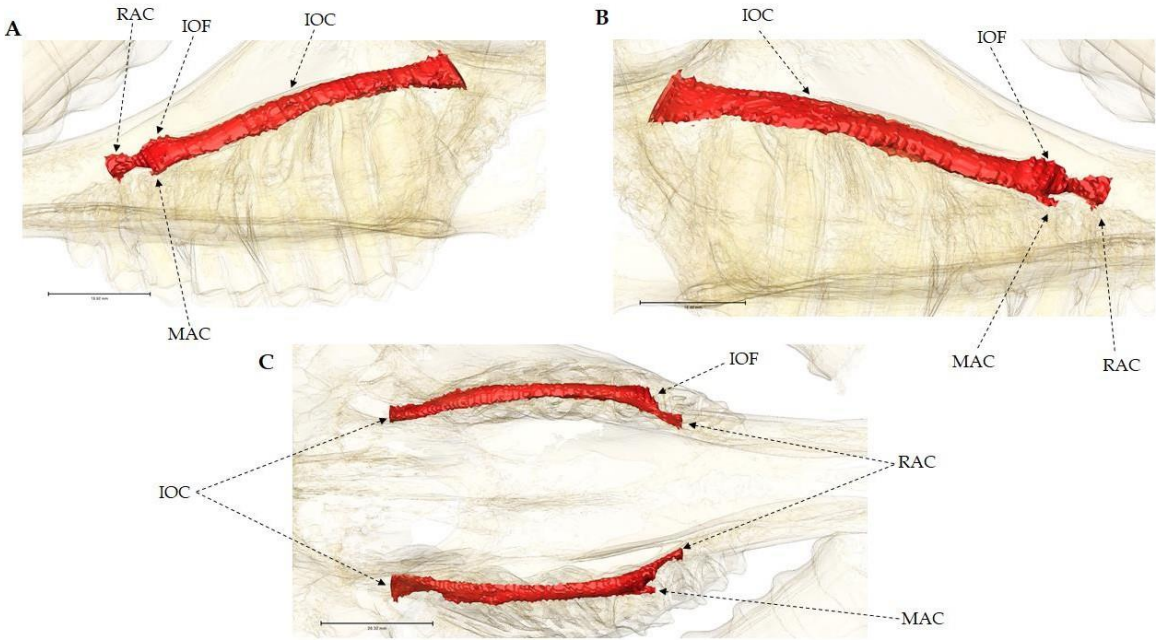


Figure 34. The infraorbital canal in Saiga tatarica (YPM 85301)*; A; left lateral view (scale: 19.92 mm), B; right lateral view (scale: 16.42 mm), C; dorsal view (scale: 22.32 mm) all skulls transparent. IOC; infraorbital canal, IOF; infraorbital foramen; MAC; middle alveolar canal, RAC; rostral alveolar canal.*

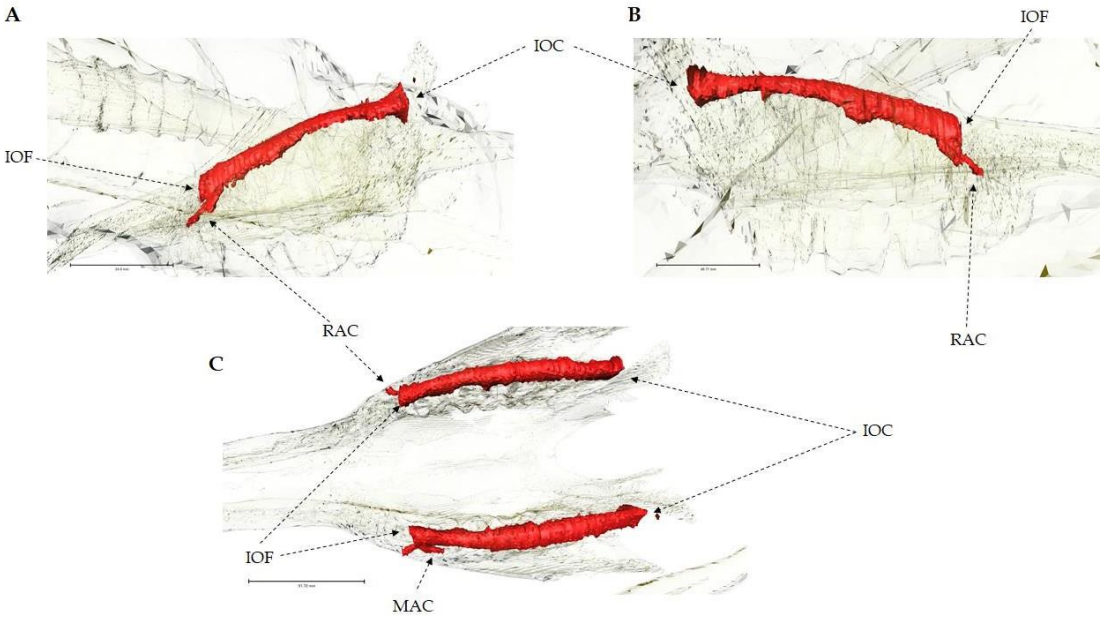


Figure 35. The infraorbital canal in Saiga tatarica *(YPM 1510); A; right lateral view (scale: 30.49 mm), B; left lateral view (scale: 30.49 mm), all skulls transparent. IOC; infraorbital canal, IOF; infraorbital canal; RAC; rostral alveolar canal.*

Madoqua kirkii possesses an infraorbital canal with a gross morphology that is similar to that of the saiga; however, its MAC and RAC branches are relatively well defined. Its infraorbital canal morphology ranges from a canal with fewer branches (the left canal only bears a single side branch, figure 37), to one with well-defined MAC branches, in both canals (figure 36). These branches also terminate externally, at the level of the infraorbital foramen. The two canals are symmetrical in specimen YPM 3985 (figure 36), whereas in specimen YPM 5462, the condition is asymmetrical, with the right canal having more branches (figure 37). The CAC in both specimens is not clearly visible or present.

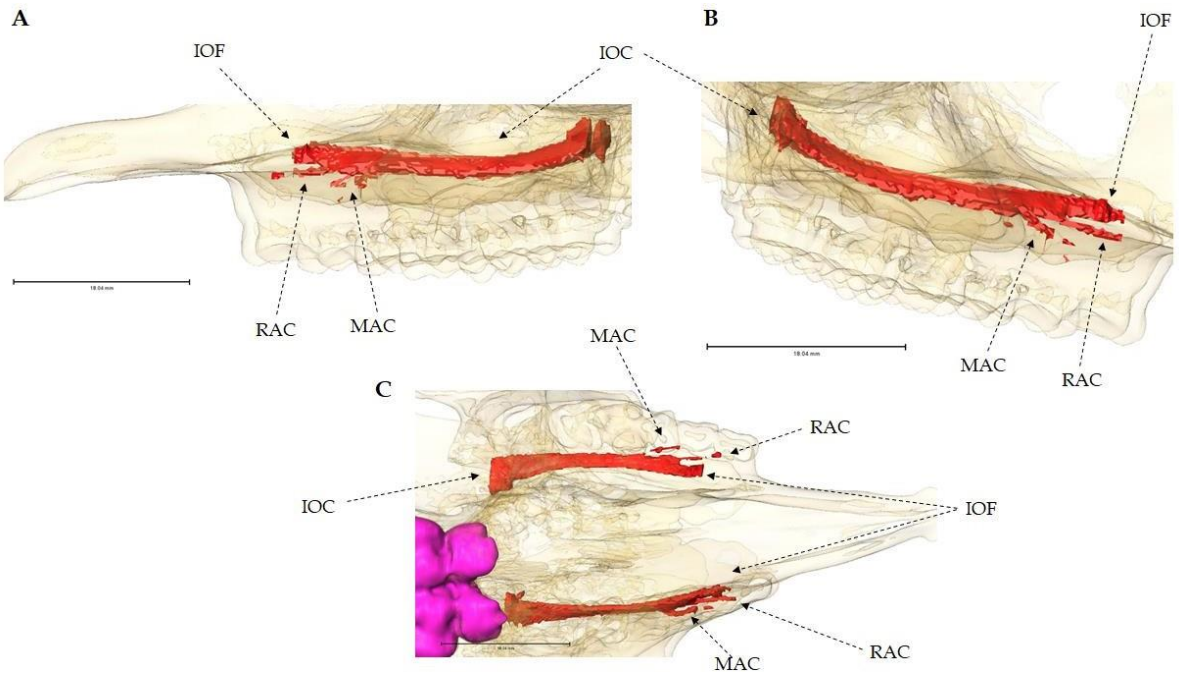


Figure 36. The infraorbital canal in Madoqua kirkii *(YPM 3985); A; left lateral view (scale: 18.04 mm), B; right lateral view (scale: 18.04 mm), C; dorsal view (scale: 18.04 mm), all transparent. IOC; infraorbital canal, IOF; infraorbital foramen; MAC; middle alveolar canal, RAC; rostral alveolar canal. The purple structure in C is the brain.*

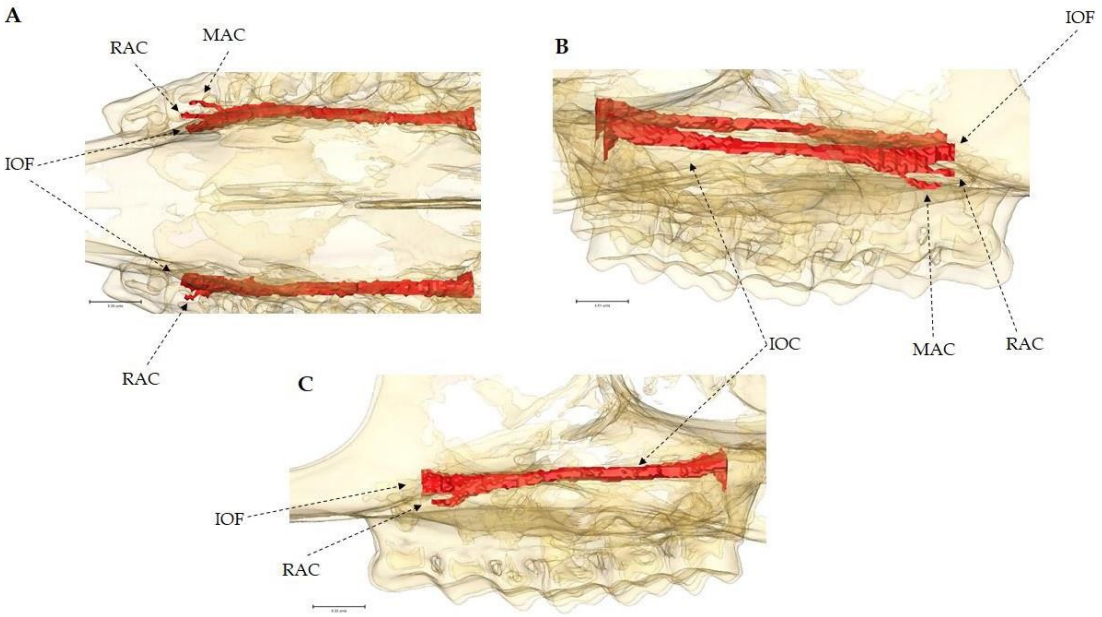


Figure 37. The infraorbital canal in Madoqua kirkii *(YPM 5462); A; dorsal view (scale: 5.33 mm), B; right lateral view (scale: 4.61 mm), C; left lateral view (scale: 5.33 mm), all transparent. IOC; infraorbital canal, IOF; Infraorbital foramen; MAC; middle alveolar canal, RAC; rostral alveolar canal.*

Cervidae

The gross morphology of the infraorbital canal in the cervids is similar to that of non-proboscis bearing bovids. Its overall shape is tubular and elongated. However, more cervid specimens were observed to possess a RAC than in none proboscis-bearing bovids. *Alces* (figure 28) possesses a visible MAC, while *Dama*, *Hippocamelus* and *Mazama* (Figures 29 to 32) all bear a well-defined RAC. In *Hippocamelus* the RAC terminates externally on the surface of the maxilla, at the level of the infraorbital foramen, instead of internally within a tooth socket as is usual for mammals (Benoit *et al.*, 2016). Similar to the majority of the bovids, the CAC is seemingly absent in all these taxa.

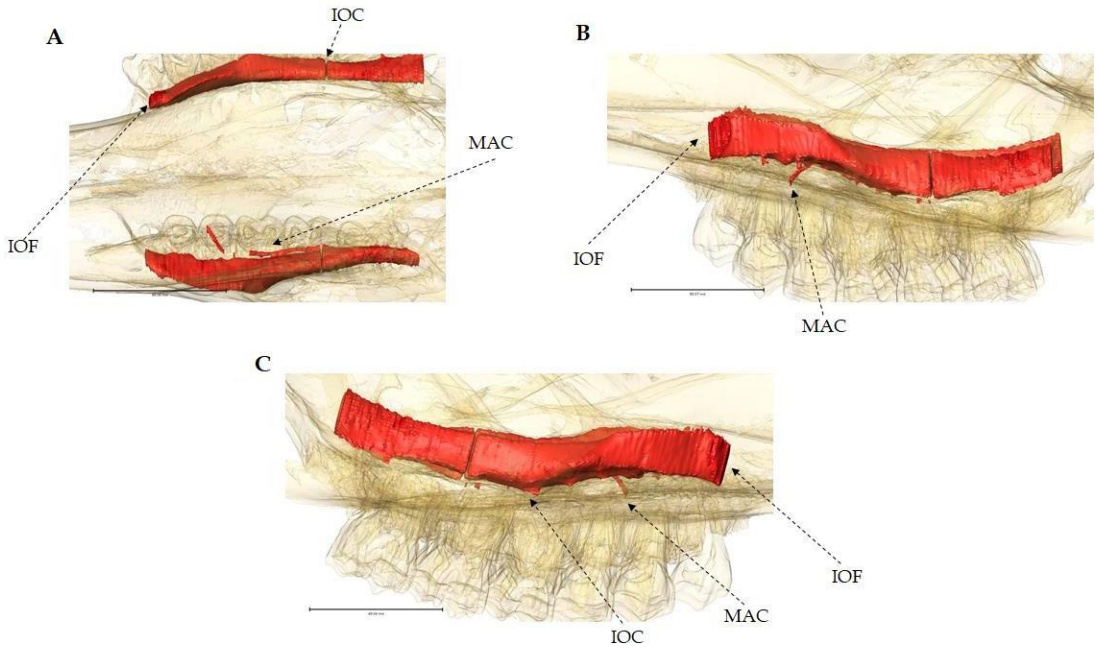


Figure 28. The infraorbital canal in Alces alces*; A; dorsal view (scale: 69.09 mm), B; left lateral view (scale: 55.57 mm), C; right lateral view (scale: 49.24 mm), all transparent. IOC; infraorbital canal, IOF; infraorbital foramen; MAC, middle alveolar canal, RAC; rostral alveolar canal.*

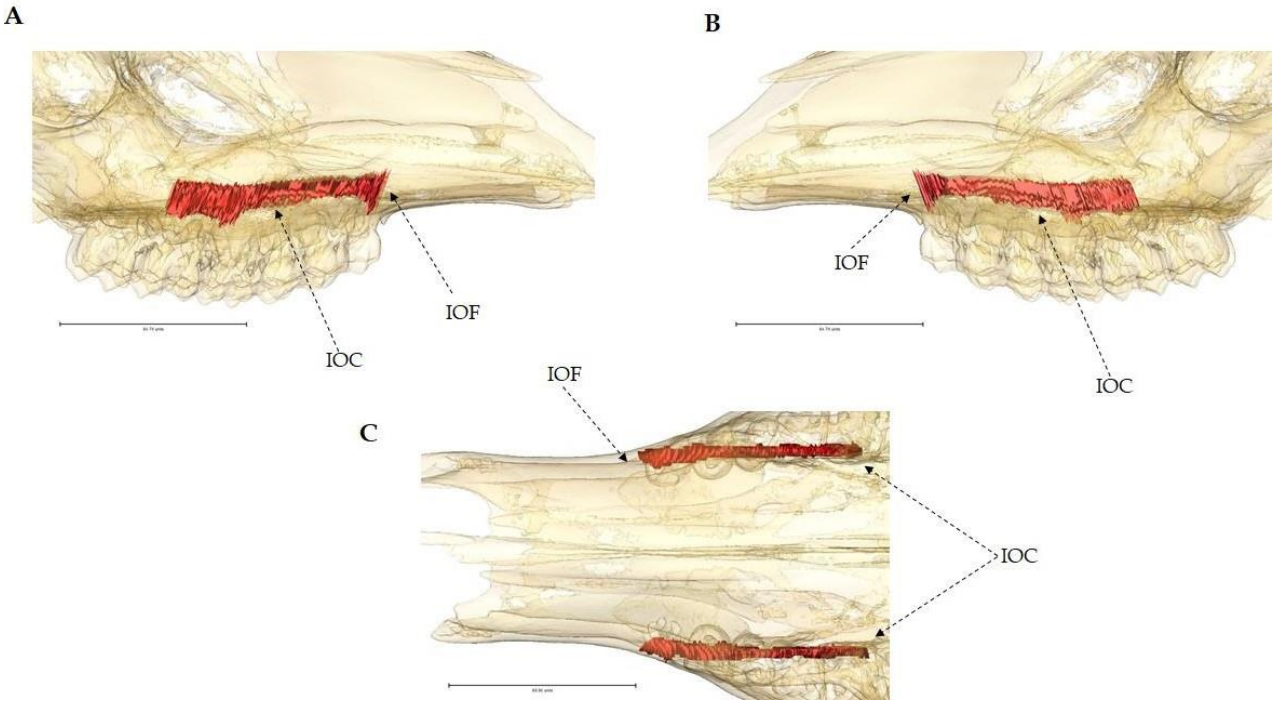


Figure 29. The infraorbital canal in Cervus elaphus*; A; right lateral view (scale: 64.74 mm), B; left lateral view (scale: 64.74 mm), C; left dorsal view (scale: 69.96 mm), all transparent. IOC; infraorbital canal, IOF; infraorbital foramen.*

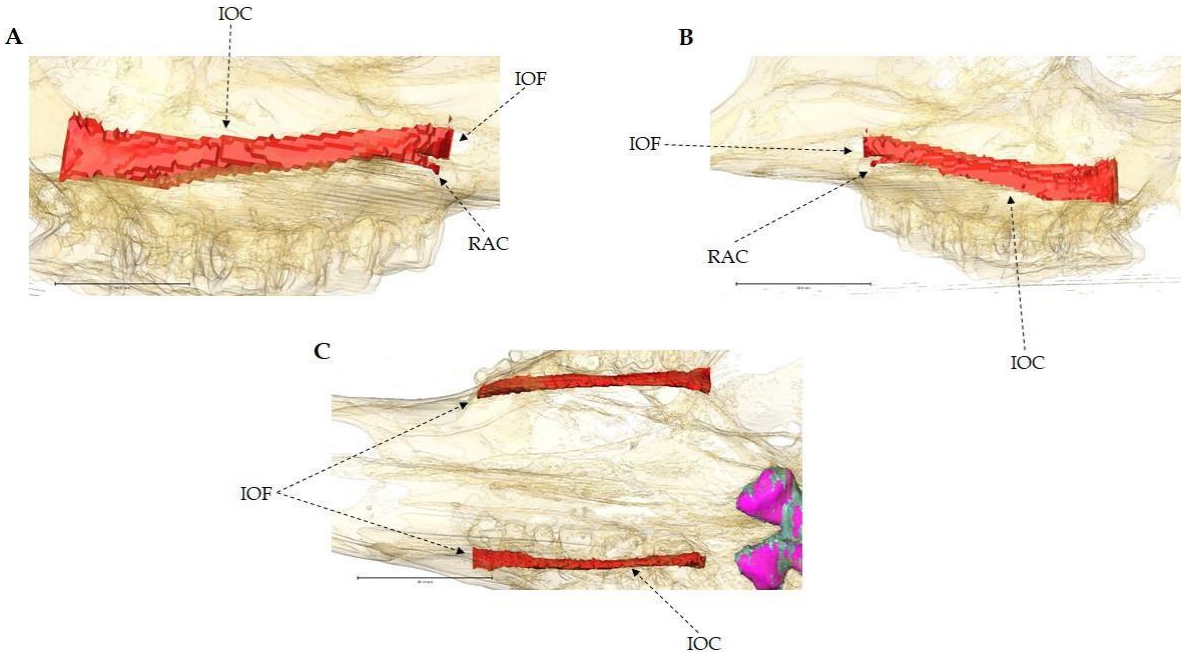


Figure 30. The infraorbital canal in Dama dama*; A; right lateral view (scale: 23.51 mm), B; left lateral view (scale: 35.9 mm), C; dorsal view (scale: 38.14 mm), all transparent. IOC; infraorbital canal, IOF; infraorbital foramen; RAC; rostral alveolar canal. The purple structure in C is the brain.*

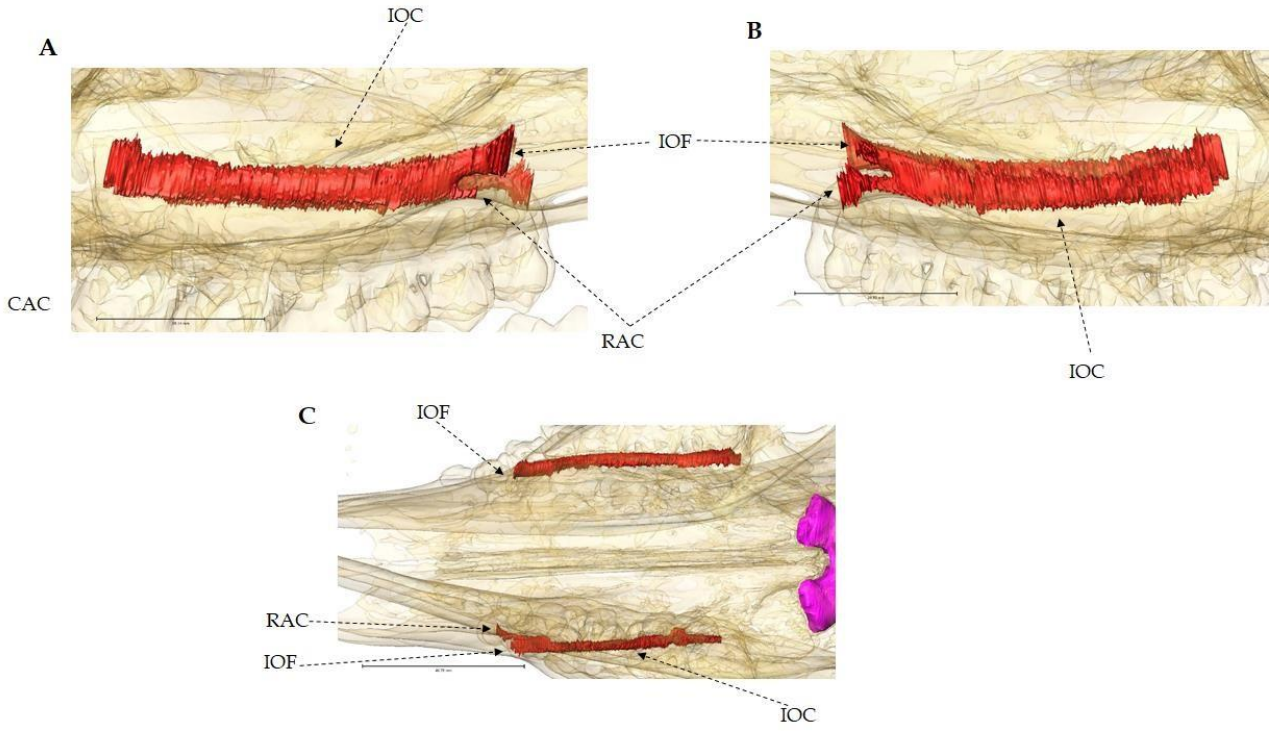


Figure 31. The infraorbital canal in Hippocamelus sp.*; A; left lateral view (scale: 28.83 mm), B; right lateral view (scale: 28.14 mm), C; dorsal view (scale: 46.78 mm), all transparent. IOC; infraorbital canal, IOF; infraorbital foramen; rostral alveolar canal. The purple structure in C is the brain.*

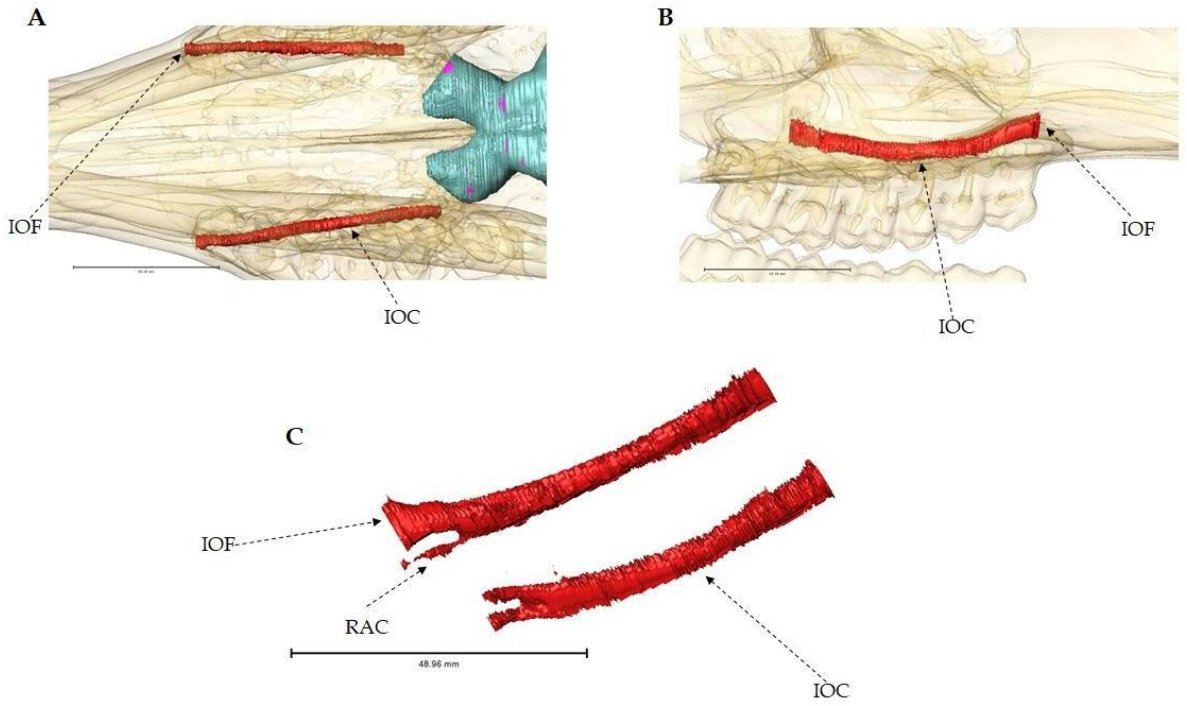


Figure 32. The infraorbital canal; A; Muntjac*, dorsal view (scale: 29.18 mm), B; right lateral view (scale: 29.18 mm), C;* Mazama americana*, left dorso-lateral view (scale: 49.96 mm), A and B are transparent. IOC; infraorbital canal, IOF; infraorbital foramen, Rac; rostral alveolar canal. The blue structure in A is the brain.*

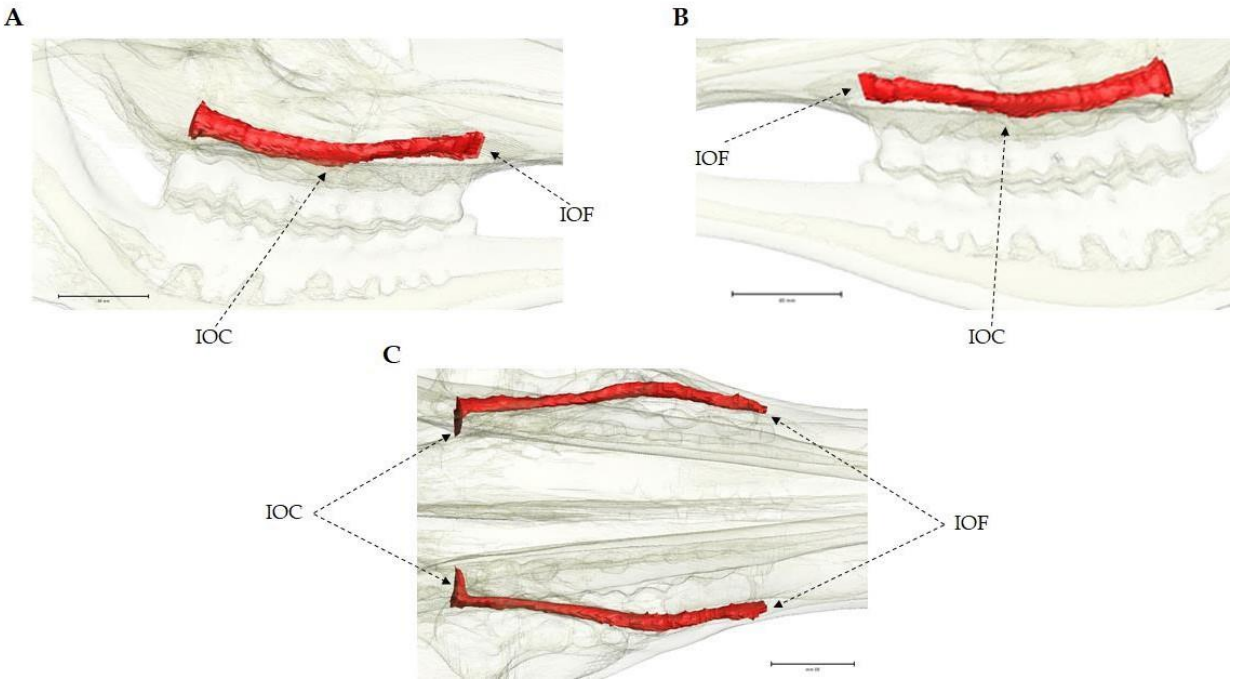


Figure 33. The infraorbital canal in Cervus elaphus*; A; right lateral view (scale: 35 mm), B; left lateral view (scale: 30 mm), C; dorsal view (scale: 30 mm), all transparent. IOC; infraorbital canal, IOF; infraorbital foramen.*

Perissodactyla

Equidae

The infraorbital canal morphology of the equids is similar to that of ruminants, but differs in the way its slopes – the slope is very shallow caudally and steepens rostrally. The canal is concave-down bent resulting in an upside-down U-shape gross morphology. This condition is much more visible in zebras, and almost absent in *Equus asinus* (figure 38). The infraorbital canal in *E. asinus* appears U-shaped when viewed dorsally, and this condition is absent in other Equidae. In equids, the infraorbital foramen is positioned more dorsally, unlike most ruminants where it is positioned more ventrally. All the Equidae taxa appear to bear a simple RAC (figures 38, 40 and 41). *E. caballus* possesses the longest RAC when compared to the other *Equus* taxa (figure 40). *E. quagga* does not possess a RAC (figure 39). None of the Equidae taxa appears to possess the MAC and CAC branches.

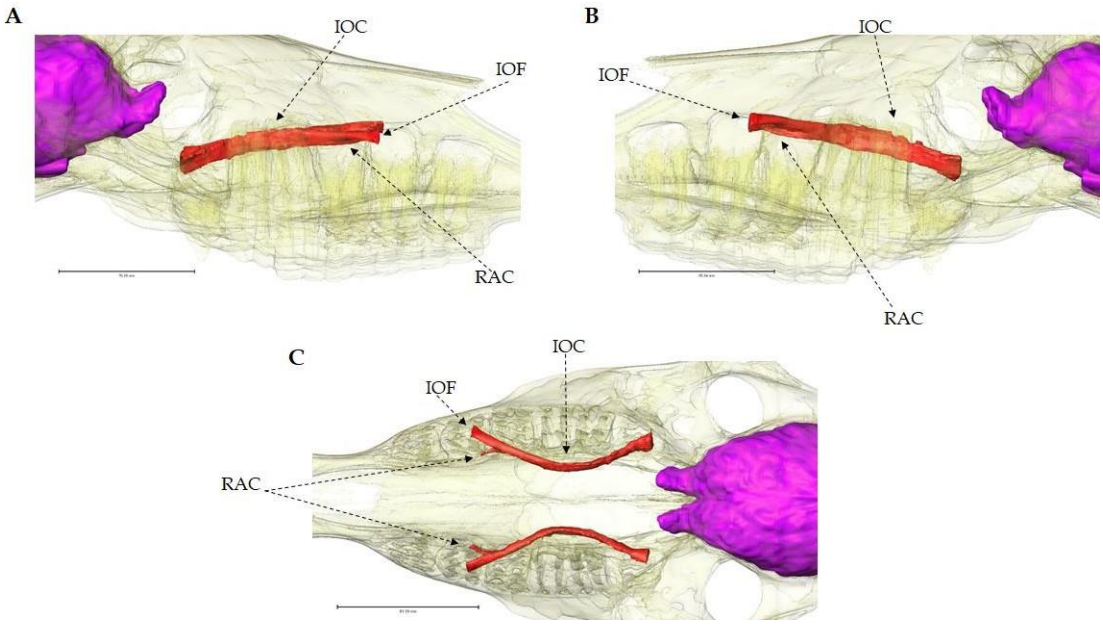


Figure 38. The infraorbital canal Equus asinus*; A; right lateral view (scale: 70.26 mm), B; left lateral view (scale: 65.34 mm), C; dorsal view (scale: 81.23 mm), all transparent. IOC; infraorbital canal, IOF; infraorbital foramen; RAC; rostral alveolar canal. The purple structure in the figures is the brain.*

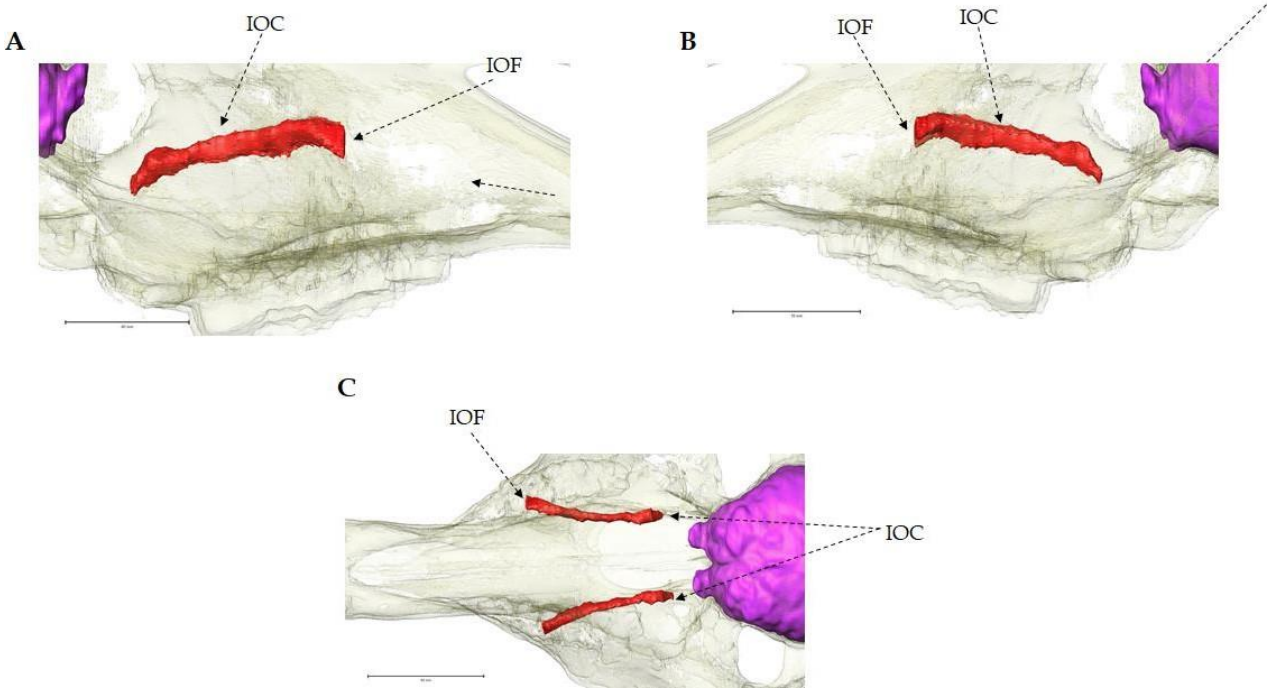


Figure 39. The infraorbital canal Equus quagga*; A; right lateral view (scale: 60 mm), B; left lateral view (scale: 70 mm), C; left dorsal view (scale: 90 mm), all transparent. IOC; infraorbital canal, IOF; infraorbital foramen. The purplestructure in all the figures is the brain.*

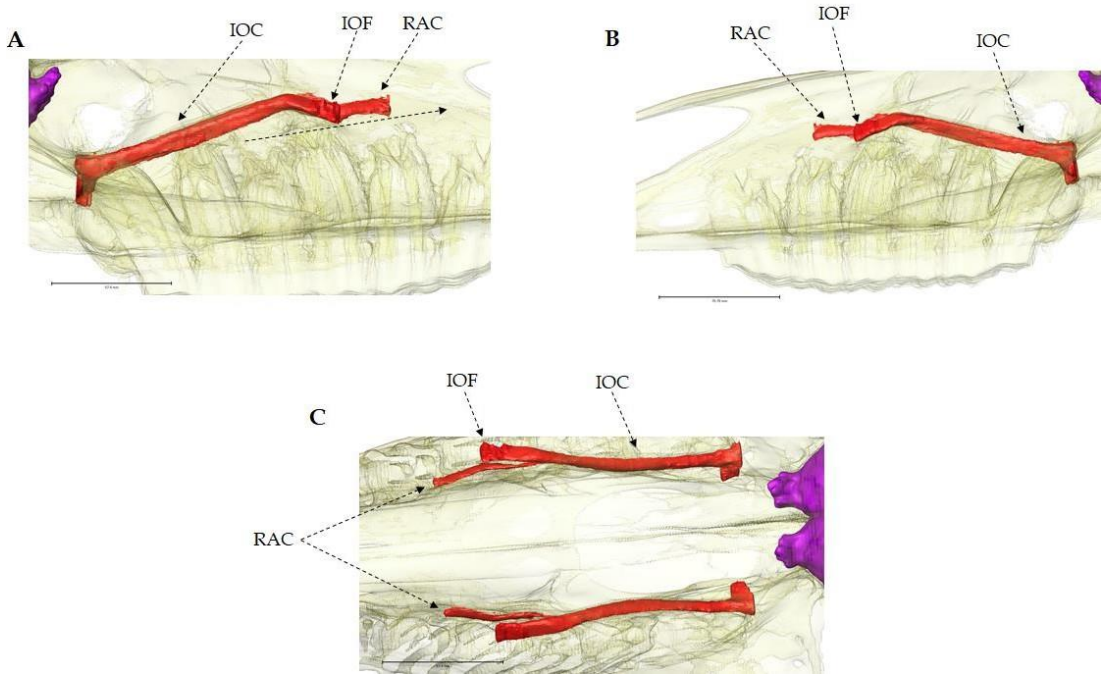


Figure 40. The infraorbital canal in Equus caballus*; A; right lateral view (scale: 57.56 mm), B; left lateral view (scale: 70.75 mm), C; dorsal view (scale: 57.6 mm), all transparent. IOC; infraorbital canal, IOF; infraorbital foramen; RAC; rostral alveolar canal. The purple structure in all the figures is the brain.*

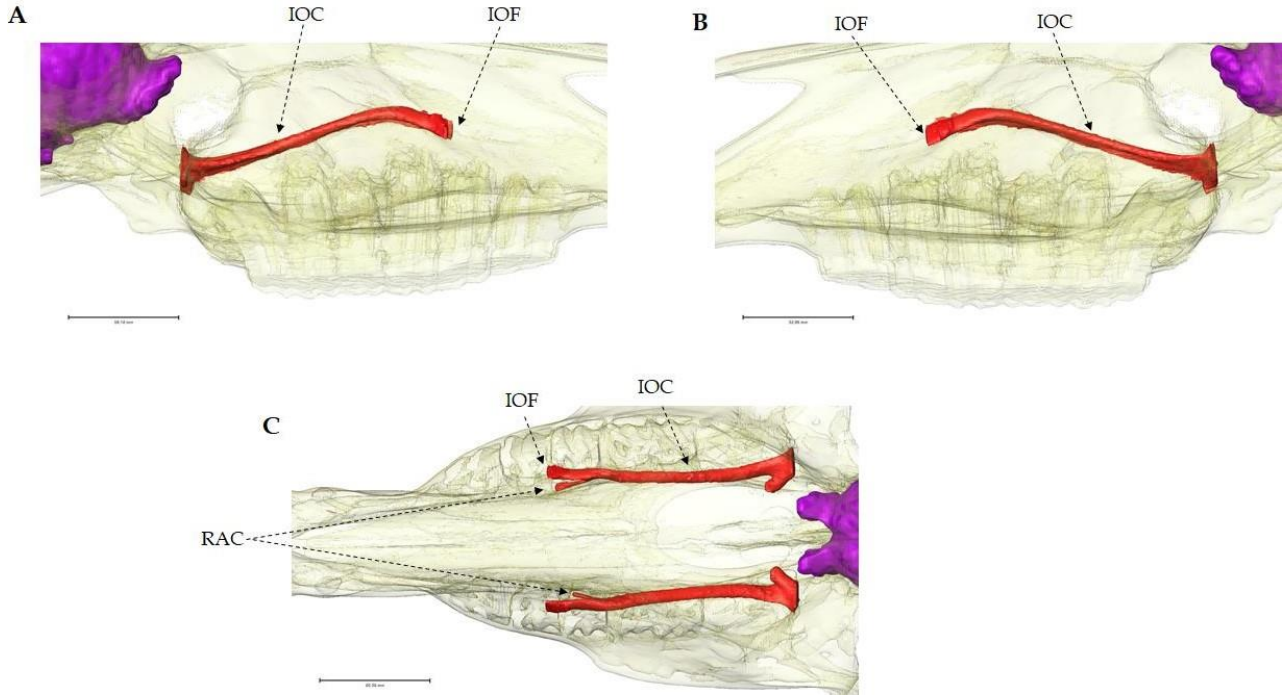


Figure 41. The infraorbital canal Equus zebra*; A; right lateral view (scale: 60.39 mm), B; left lateral view (scale: 52.86 mm), C; dorsal view (scale: 60.39 mm), all transparent. IOC; infraorbital canal, IOF; infraorbital foramen;MAC, middle alveolar canal, RAC; rostral alveolar canal. The purple structure in all the figures is the brain.*

Rhinocerotidae

Rhinoceroses bear a canal morphology with multiple branches, being more complex compared to equids. The infraorbital canal in *Ceratotherium* (figure 42) is relatively thicker compared to that of *Diceros* (figure 43). It is thicker caudally and narrows rostrally in *Ceratotherium simum*, whereas *Diceros* bears a uniformly tubular canal. *Ceratotherium* has a MAC and RAC that are further divided into smaller single or double branches. *Diceros* exhibits a special condition, in which the canal divides into three smaller branches that terminate on the surface of the maxilla, at the level of the infraorbital foramen (figure 43). Both taxa do not appear to possess the CAC.

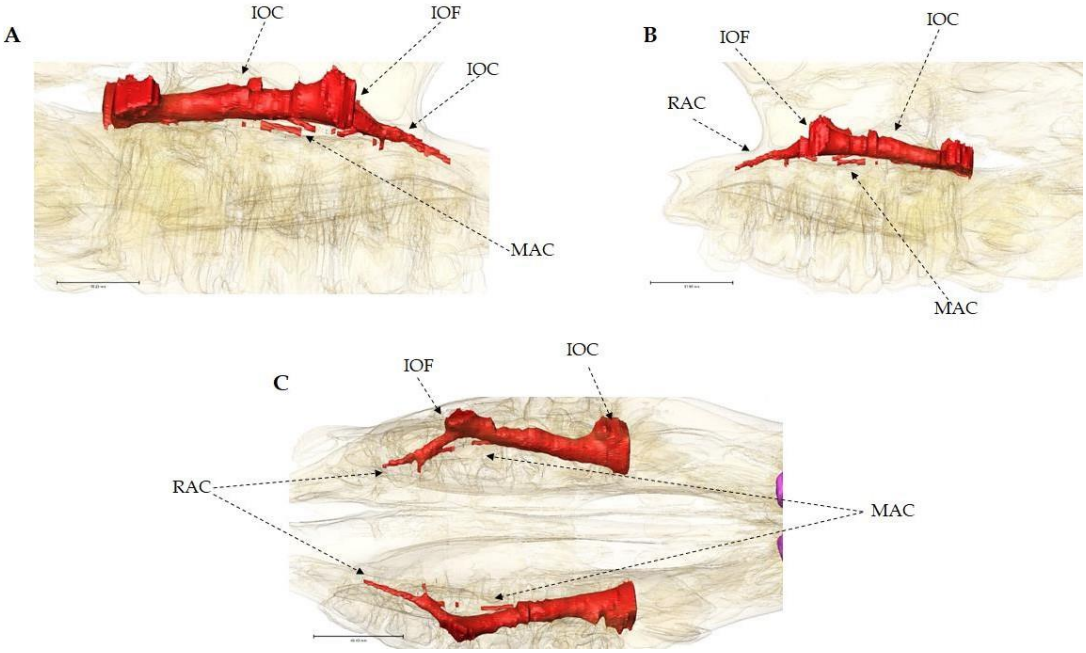


Figure 42. Infraorbital canal of Ceratotherium simum*; A; right lateral view (scale: 35.23 mm), B; left lateral view (scale: 51.88 mm), C; dorsal view (scale: 49.43 mm), all transparent. IOC; infraorbital canal, IOF; infraorbital foramen; MAC, middle alveolar canal, RAC; rostral alveolar canal.*

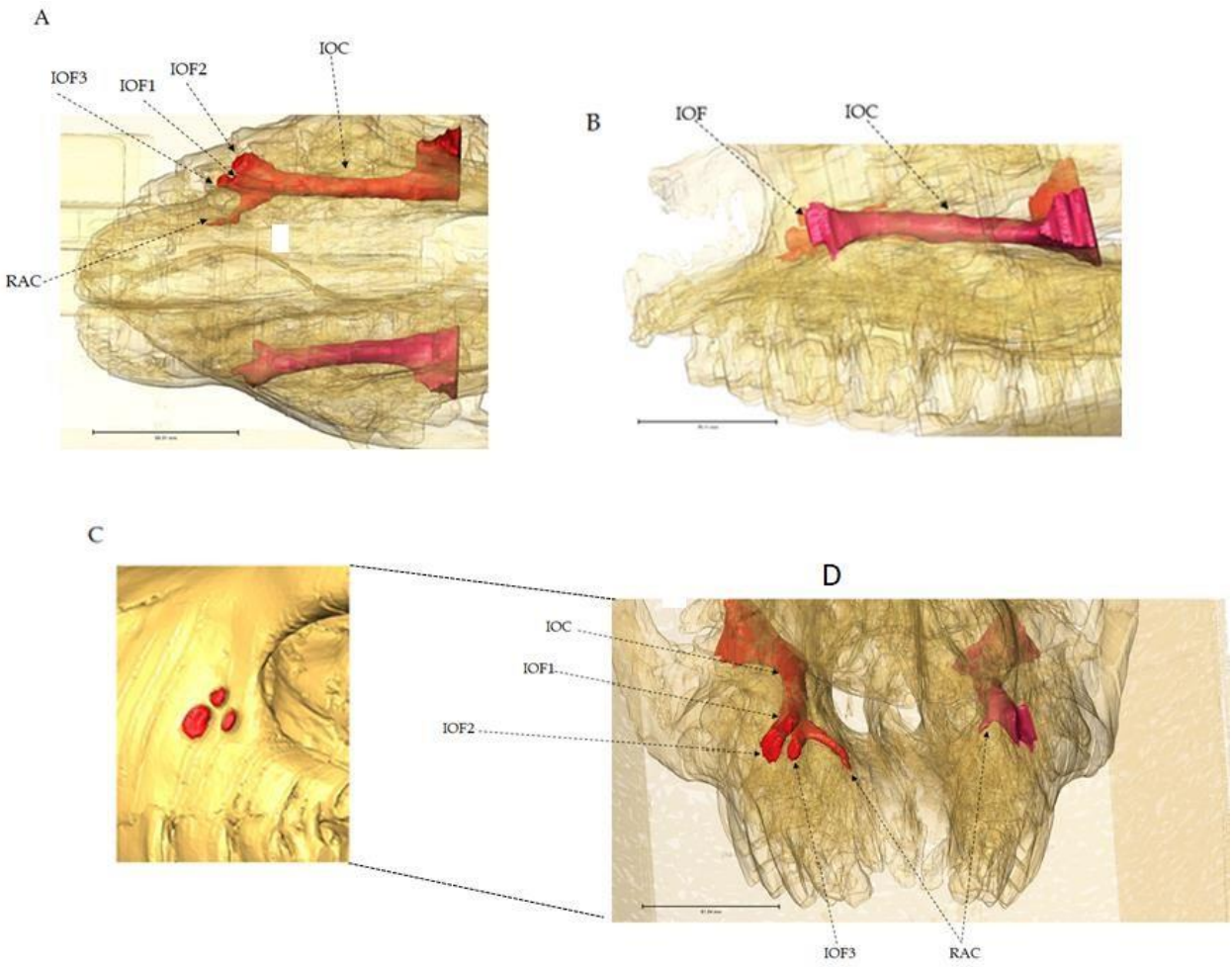


Figure 43. The infraorbital canal of Diceros bicornis*; A; dorsal view (scale: 99.31 mm), B; left lateral view (scale: 19.03 mm), C; left lateral view (scale: 20.47 mm), all transparent except for C. IOC; infraorbital canal, IOF; infraorbital foramen; MAC, middle alveolar canal, RAC; rostral alveolar canal. C; right anterior-lateral view showing the infraorbital foramen in an opaque skull, D; dorso-ventral view showing the infraorbital foramen in a transparent skull (scale: 81 mm).*

Tapiridae

Of all the proboscis-bearing taxa, the tapirs possess the most complex infraorbital canal condition, having more branches (especially *T. indicus*, figure 44). The gross infraorbital canal in tapirs is thicker caudally than rostrally, and narrows and increases in complexity rostrally as the number of branches increases. The infraorbital canal in *T. indicus* is much thicker than that of *T. terrestris* (figure 45), and bears more branches. Its overall shape is conical and broader caudally, and then

narrows rostrally. *Tapirus terrestris* bears a relatively simple canal morphology, with fewer branches. It possesses a thick, short RAC, with a uniform tubular shape compared to *T. indicus* (figure 45). Both taxa do not appear to possess the MAC and CAC branches.

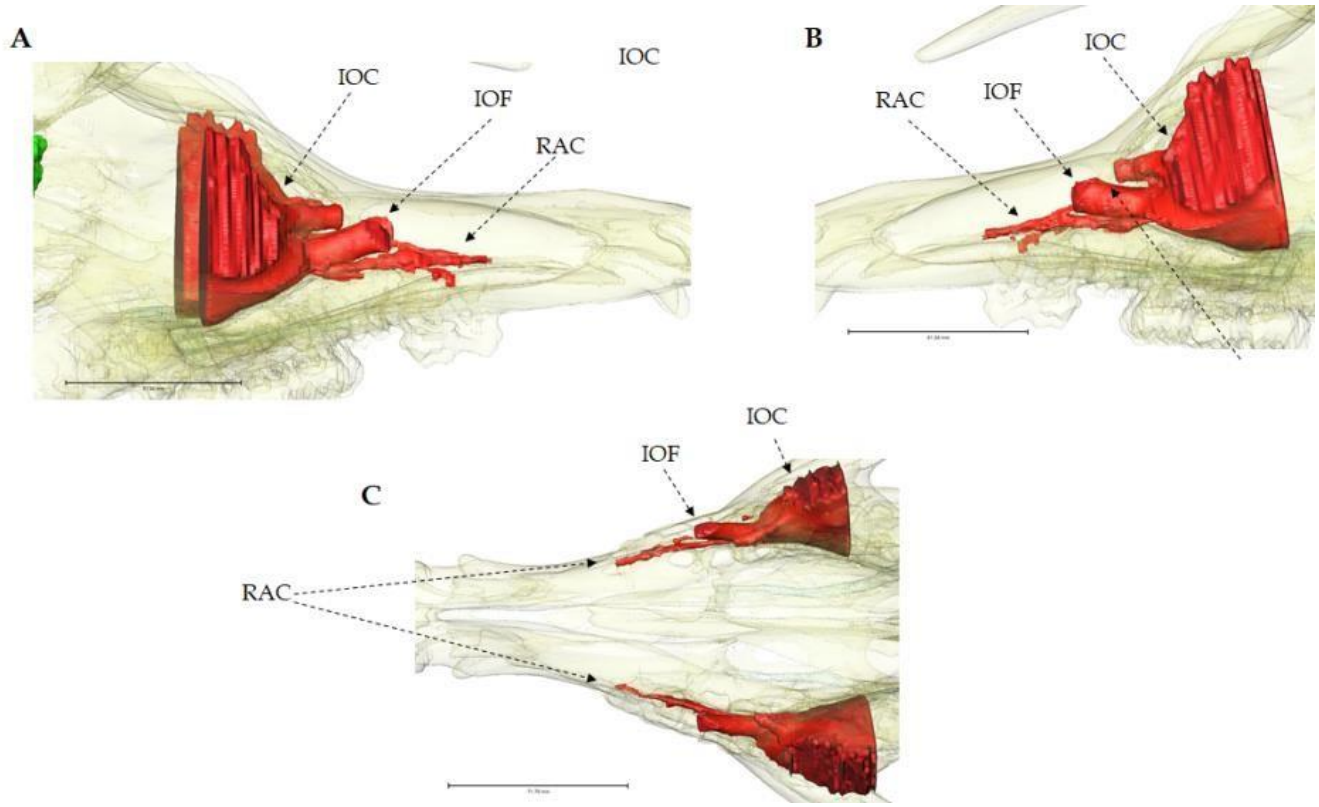


Figure 44. The infraorbital canal in Tapirus indicus*; A; right lateral view (scale: 14.41 mm), B; dorsal view (scale: 19.03 mm), C; left lateral view (scale: 20.47 mm), all transparent. IOC; infraorbital canal, IOF; infraorbital canal; MAC, middle alveolar canal, RAC; rostral alveolar canal.*

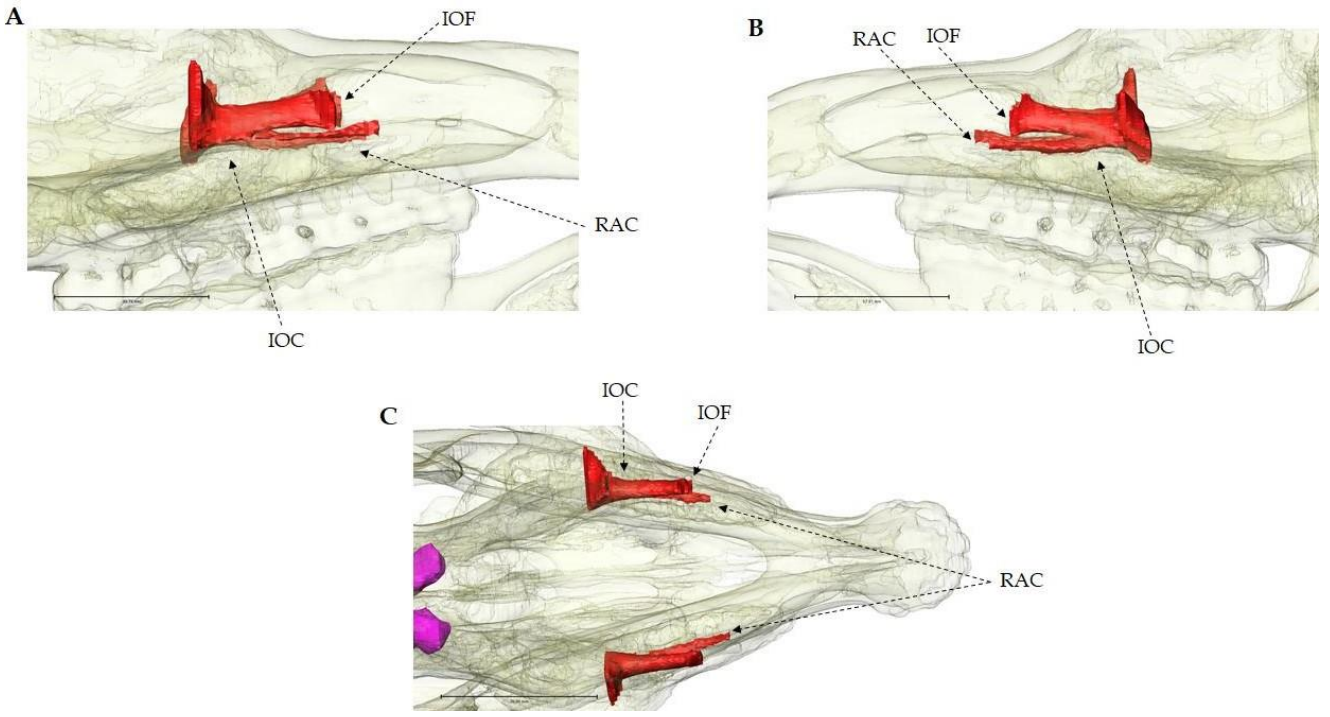


Figure 45. The infraorbital canal in Tapirus terrestris*; A; right lateral view (scale: 14.41 mm), B; dorsal view (scale: 19.03 mm), C; left lateral view (scale: 20.47 mm), all transparent. IOC; infraorbital canal, IOF; infraorbital foramen; MAC, middle alveolar canal, RAC; rostral alveolar canal. The purple structure in C is the brain.*

II - Statistics

The three proposed osteological proxies (i.e. volume of the infraorbital canal, surface area of the infraorbital foramen, and degree of narial retraction) were quantified and simple linear regressions were generated on the "all taxa" sample (Table 3). The first generated model (model 1, SL/Hl vs Surface area IOF) has the most significant P–value of the three models tested on the "all taxa" sample (P–value = 9.8E-05); however, its r^2 is low = 0.339. The degree of narial retraction is the second most significant model with a P-value = 0.018. Interestingly, while its P-value is significant, its r^2 is very low (0.141). The third generated model (model 3, Sl/Hl vs Volume IOC) has a non-significant P-value = 0.57 and a low r^2 = 0.094. Overall, these generated models are only weakly predictive, and thus application to the fossil samples was not attempted.

Simple linear regressions were generated and tested on taxa that possess a trunk or proboscis-like snouts (Table 4). The 4th generated model (model 4, SL/Hl vs Surface area IOF) was found to be the most significant, with a P-value = 1.73E-05. The r^2 was the highest of all the generated models, with a value = 0.98 (best correlated, figure 46). The 5th model (Narial retraction) was again found to be significant with a P-value = 0.006 although its r^2 value was very low = 0.233. The last generated model (narial retraction, model 6, Volume IOF) is non-significant with a P-value = 0.182. The r^2 was very low = 0.25, but higher than that of the narial retraction model for the taxa that possess proboscis-like snouts.

Only the model using IOF surface area in taxa bearing a proboscis-like snout proved to be both significant and has a high determination quotient. It was thus applied to the proboscidean fossils because it has the best predictive power (highest r^2 and most significant P-value). The estimated ratio of the Snout length to Head length for the proboscidean fossil taxa are shown below (Table 5). The estimated ratios were obtained from model 3, and they are as follows: *Numidotherium koholense* = 0.8477; *Deinotherium bozasi* = 0.98; *Mammut americanum* = 1.622; *G. indet* (KNM-WS12874) = 0.69; G. indet (KNM-WS12660) = 0.78; *Anancus kenyansis* = 0.8; *Elephas recki* = 0.98; *Loxodonta africana* (KNM-Juvenile 1) = 0.76; *Loxodonta africana* (KNM-Juvenile 2) = 0.86; *Loxodonta* sp. = 1.13. The estimated snout lengths are as follows: *Numidotherium koholense* = 31.36 cm; *Deinotherium bozasi* = 113 cm; *Mammut americanum* = 158.47 cm; *G. indet* (KNM-WS12874) = 62 cm; G. indet (KNM-WS12660) = 70 cm; *Anancus kenyansis* = 56 cm; *Elephasrecki* = 76.88 cm; *Loxodonta africana* (KNM-Juvenile 1) = 55 cm; *Loxodonta africana* (KNM- Juvenile 2) = 62.12 cm; *Loxodonta* sp. = 81.144 cm.

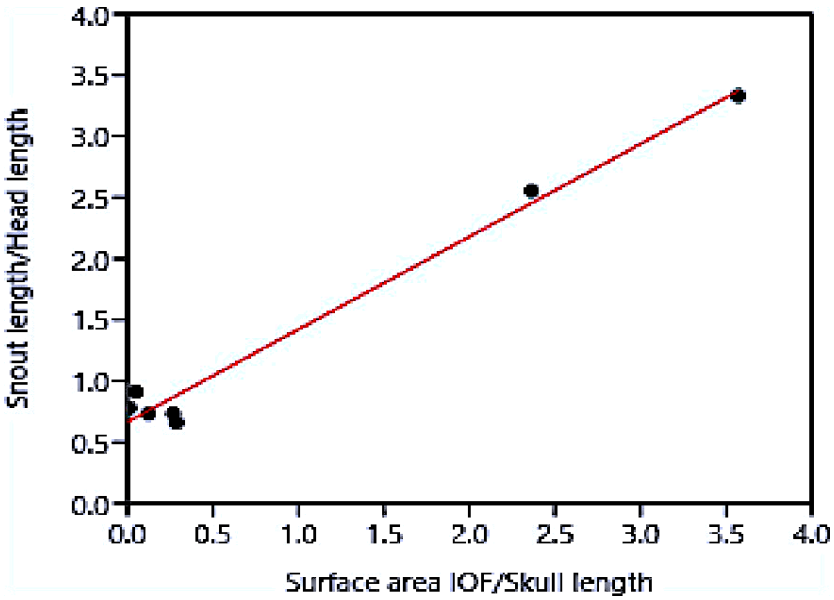


Figure 46. The Snout length/Head length (pictures) vs Surface area of the infraorbital foramen/ Skull length (CT scan) in proboscis-bearing taxa, n = 8.

Table 3. Summary of the statistics results in all taxa, n = 43.

Regression Model	Slope	standard error a/b	r^2	r	P(slope)	Intercept b
1) Snout length/Head length (image) vs Surfacearea of IOF/ Skull length (CT scan)	0.963	0.221 / 0.21	0.339	0.582	9.98E-05	-0.132
2) Snout length/Head length vs Narial retraction	0.003	0.001/0.122	0.141	0.376	0.018	0.563
3) Snout length/Head length vs Average IOCVolume	2.44E-05	1.24E-05/ 0.097	0.094	0.306	0.057	0.689

Table 4. Summary of the statistics results in the taxa bearing a proboscis-like snout, n = 8.

Regression Model	Slope	standard error a/b	r^2	R	P(slope)	Intercept b
4) Snout length/Head length (image) vs Surface area of IOF/ Skull length (CT scan)	0.003019	0.0012229/ 0.12191	0.98089	0.9904	1.73E-05	0.66446
5 Snout length/Head length vs Narial retraction	3.75E-08	0.0046737/ 0.67225	0.23255	0.48223	0.005753	0.71657

6) Snout length/Head length vs Average IOC Volume	7.87E-05	5.07E-05/ 0.32494	0.25	0.57004	0.182	0.8265

Table 5. Fossil application results

Regression Model	**Estimated Snout length/Skull length,** ***Numidotherium koholense***	**Estimated Snout length/Skull length,** ***Deinotherium bozasi***
4) Snout length/Head length (image) vs Surface area of IOF/ Skull length (CT scan)	0.8477	0.98
Estimated length of the trunk in cm	31.36	113

Regression Model	**Estimated Snout length/Skull length,** ***Mammut americanum***	**Estimated Snout length/Skull length,** **Gomphotheriidae indet (KNM-WS12874)**
4) Snout length/Head length (image) vs Surface area of IOF/ Skull length (CT scan)	1.622	0.69
Estimated length of the trunk in cm	158.47	62

Regression Model	**Estimated Snout length/Skull length,** ***Gomphotheriidae*** **indet (KNM-WS12660)**	**Estimated Snout length/Skull length,** ***Anancus kenyansis***

4) Snout length/Head length (image) vs Surface area of IOF/ Skull **length (CT scan)**	0.774	0.8
Estimated length of the trunk in cm	70	56

Regression Model	**Estimated Snout length/Skull length,** ***Elephas recki***	**Estimated Snout length/Skull length,** ***Loxodonta* sp.**
4) Snout length/Head length (image) vs Surface area of IOF/ Skull **length (CT scan)**	0.98	1.127
Estimated length of the trunk in cm	76.88	81.144

Discussion

The general morphology of the infraorbital canal in the taxa studied here is consistent with the general mammalian pattern described by Benoit *et al.,* (2016). The morphology of the canal in afrotherians is relatively short, and the interspecific variation amongst these taxa ranges from short and conical, to short and cylindrical. In contrast to the afrotherians, the artiodactyls possess a thin, elongated and tubular infraorbital canal (i.e. Bovidae). The results show that Hippopotamidae possesses the most voluminous (relative to head size) and complex canal morphology (many branches) within the Ruminanta, followed by Giraffidae, Suoidea and Tylopoda. The gross morphology of the canal in Perissodactyla varies greatly between taxa. The overall shape of the infraorbital canal in equids is similar to that in bovids, but the morphoogy becomes more complex, in terms of the number of branches, in the Rhinocerotidae and Tapiridae.

The comparative description of these mammalian taxa reveals that there is a strong taxonomic and phylogenetic signal in the morphological complexity of the infraorbital canal. The internal branching morphology appears to increase in complexity in the taxa with an enlarged and mobile upper lip. The infraorbital canal morphology appears to vary across taxa, and there are notable differences between the infraorbital canal of the proboscis-bearing taxa when compared to those without. The taxa that possess a true proboscis and those that bear proboscis-like structure have a larger, cylindrical canal, with a more spherical infraorbital foramen (i.e. elephants, saigas, elephant shrew's, dik-dik and tapirs). In addition, the canal of these taxa has fewer branches in comparison with taxa that have a short proboscis and fleshy mobile upper lip since those taxa with a mobile upper lip (e.g. Rhinocerotidae, Hippopotamidae) have a highly ramified canal. It appears that there is a trade-off between the volume and length of the canal, such that the canal is long in taxa that

have a narrow canal, whereas taxa with a large canal, such as *Mammut americanum* and *Loxodonta africana*, have a shorter canal. The taxa that have a mobile upper lip such as rhinoceroses and hippopotami have more branches (especially the RAC), or multiple infraorbital foramina in comparison to species with a proboscis-like structure, which tend to have a simpler, more cylindrical and shorter canal. Noticeably, tapirs have a relatively voluminous canal, but more complex than that of elephants (many branches), and appear thus intermediate in this respect.

These qualitative observations are consistent with the literature that hypothesized that a large dimensions of the infraorbital canal and foramen are expected to be associated with the presence of a proboscis-like structure or mobile upper lip (Adam & Berta, 2002; Galton *et al*., 2006; Shoshani, 1998; Troxell, 1921; and Wall, 1980). The statistical results also support this observation, as there is a significant correlation between the length of the snout and the surface area of the infraorbital canal (table 3). This correlation is even more significant and the determination quotient higher when considering taxa with a proboscis or proboscis-like snouts alone (table 4).

Many authors, who have attempted to study, infer and reconstruct the presence of the trunk in extinct taxa, used the degree of narial retraction (Adams *et al*., 2019; Blanco *et al*., 2021; Burmeister, 1864; Osborn, 1898; Scott, 1910; Sharp & Trusler, 2016; Shoshani & Tassy, 2005; Troxell, 1921; and Wall, 1980) to support their reconstructions. The statistical results provided above (tables 3 and 4) challenge this long-standing view, as the regression lines between snout length and narial retraction are found to be statistically significant, but the coefficients of determination are very low (tables 3 and 4). This implies that the dispersion around the regression lines is too low, both in all taxa and taxa bearing a trunk-like structure only, to enable a reliable prediction of the length of the snout. This result contradicts more than a century of untested assumptions (e.g. Burmeister, 1864; Osborn, 1898; Scott, 1910; and Wall, 1980).

It was found that the length of the snout is strongly correlated to the surface area of the infraorbital foramen. Compared to the other two proposed proxies, this proxy shows the best p-values and determination quotient, particularly if considering the analysis performed with taxa bearing proboscis-like structures only.

Using the equation of this regression line, the estimated snout length for *Numidotherium* is 31 cm, which is short relative to estimated shoulder height and within the tapir average range (29 - 42 cm). *Numidotherium* has a body mass and an estimated shoulder height = 90 - 100 cm, which are both similar to that of tapirs. This finding supports the literature that proposes a tapir-like proboscis for *Numidotherium* (Larramendi, 2016; Shoshani, 1998; Shoshani & Tassy, 2005; and Sukumar, 2003). Contrary to what the literature above has stated (Harris, 1975, Markorv *et al.*, 2001, Svistun, 1974, Tassy, 1998; and Tarabukin, 1974), *Deinotherium* was estimated to possess a trunk-length of 113 cm. This trunk condition is longer than that of tapirs, but not in the range of extant elephants (167 - 243 cm). This finding supports the reconstruction proposed by Abel (1922), with a more elephantine length for the trunk.

Note: I disagree with the sentence above. Using Larramendi's figure, I estimate that the trunk length of a 360 cm tall *Deinotherium bozasi* (Larramendi, 2016 pp: 556) would have had a 130 cm trunk according to the usual "tapir-like hypothesis". As such, a 113 cm long trunk is in fact quite short, and perfectly in line with Markhov's hypothesis.

Mammut was estimated to possess a snout length of 158.47 cm, which is almost within the range of extant elephants, and closer to that of *Deinotherium* than to the estimated gomphothere length. The estimated shoulder height for *M. americanum* is 289 cm (Larramendi, 2016 pp: 571) and this estimated trunk length is quit long as it makes up more than half the limb length (and almost within the elephantine range). *M. pacificus* has an estimated shoulder height of (182 – 244 cm)

(Yeagar, 1989) and this trunk length is almost as long as the lower boundary of this limb length range.

The gomphotheres have estimated shoulder height 230 - 320 cm (Larramendi, 2016) and an estimated snout length of 62 – 70 cm. When using the shoulder height 230 cm, both estimated snout lengths do not make up half the limb length. *Anancus* has an estimated shoulder height = 310 – 350 cm (Larramendi, 2016) and the estimated trunk length is very short (the ratio of limb to trunk length is higher than that of tapirs and *Numidotherium*). *Elephas recki* has an estimated shoulder height = 540 cm (Larramendi, 2016), and the estimated trunk length is also very short compared to shoulder height (possesses the highest limb to trunk length ratio, of all the fossils in the study). These findings support the proposed snout lengths for basal elephantiforms such as *Palaeomastodon* (shoulder height = 220 cm; Larramendi, 2016), and challenge that of more derived taxa (i.e. gomphotheres, usually more elephantine) (Andrews, 1904; Nabavizadeh, 2015; Nabavizadeh & Reidenberg, 2019; Osborn, 1936, 1942; and Sanders *et al*., 2010).

Results show that this model has strong predictive power, and its findings are consistent with the previous qualitative estimates for Plesielephantiformes. However, this model challenges the qualitative estimates for the trunk lengths of elephantiforms, especially that of *Anancus* and *Elephas recki*. Based on the findings of this study, we now have a quantitative metric protocol that can be used to infer the presence, and estimate the dimensions of the trunk in fossil taxa (i.e. Model 4). We now know that ‘Plesielephatiforms’ such as *Numidotherium* possessed a snout length much shorter than that of tapirs, but longer than a mobile upper lip for a similar overall body shape and size. The most derived “plesielephantiforms”, the deinotheres, had a tapir-like trunk. The estimated trunk length of gomphotheres does not make half the limb length, however, still longer than that

of tapirs. The estimated snout lengths for *Anancus* and *Elephas recki* are very short compared when compared to their shoulder heights (shortet than that of tapirs and *Numidotherium*).

The trunk did not originate as a single event at the root of the proboscidean tree, but is the result of a long evolution that spanned the proboscidean phylogenetic tree for at least 60 million years between the last common ancestor of Proboscidea and that of Sirenia. More proboscidean fossils are needed to investigate this research question, such as *Eritherium*, *Phosphatherium*, *Daouitherium* and *Moeritherium* for us to gain insight as to when exactly the trunk originated and elongated. For the gomphotheres, the actual head lengths must be used instead of the average skull length for the family in order to increase the reliability of these results. In addition, more extant taxa such as proboscis monkeys and elephant seals are needed to increase the sample size of the taxa who possess proboscis-like snouts, and strengthen these regression models.

Conclusion

This research aimed to investigate the evolutionary origins of the trunk in Proboscidea, quantify and test proxies that have been hypothesized to be associated with the presence of the trunk in a statistical framework, and to create a quantitative protocol that can be used to reconstruct the evolution of the trunk in the fossils record. The results indicate that there is a significant and strong correlation between the surface area of the infraorbital foramen with the dimensions of the snout (in taxa with proboscis-like structures, particularly). The results also challenge the longstanding hypothesis that narial retraction is a reliable proxy for reconstructing the presence of a trunk. It can be concluded that there is a strong taxonomic and phylogenetic signal in the condition and morphology of the infraorbital canal.

Acknowledgements

I thank the DSI-NRF Centre of Excellence in Palaeosciences (CoE-Pal) and The Palaeontological Scientific Trust (PAST), Johannesburg South Africa, for financial support, my supervisors Dr. Julien Benoit and Prof. Paul Manger for academic support, the Evolutionary Studies Institute (ESI) at the University of the Witwatersrand and the National Museum of Nairobi, Kenya.

References

Abel, O. (1922). Lebensbilder aus der Tierwelt der Vorzeit. *Jena*.

Abraha, M., Berhe, S., Ghirmai, T., Libsekal, Y., Marchant, G. H., Sanders, J. W., ... Zinner, D. (2007). A Proboscidean From the Late Oligocene of Eritrea,a ‘‘Missing link’’ Between Early Elephantiformes and Elephantimorpha, and Biogeographic Implications. *Proceedings of the National Academy of Sciences*, Vol. 103, 46: 17296–17301.

Adaci, M., Bensalah, M., Hartenberger, J. L., Jaegar, J. J., Mahboubi, M., Marivaux, L., … Tafforeau. (2007). Early Tertiary Mammals From North Africa Reinforce the Molecular Afrotheria Clade. *Proceedings of the Royal Society of Britain*, 274: 1159–166.

Adam, P. J., and Berta, A. (2002). Evolution of Prey Capture Strategies and Diet in the Pinnipedimorpha (Mammalia, Carnivora). *Oryctos*, 4: 83–107.

Adams, J. W., Evans, A. R., Fitzgerald, G. M., Richards, H. L. and Wells, R.T. (2019). The Extraordinary Osteology and Functional Morphology of the Limbs in Palorchestidae, a Family ofStrange Extinct Marsupial Giants. *Public Library of Scince ONE,* 14 (9): e0221824.

Alberdi, M.T., Donato, M., Ortiz-Jaureguizar, E., Prado, J.L., and Posadas, P. (2011). Paleo-Biogeography of Trilophodont Gompotheres (Mammalia: Proboscidea). Areconstruction Applying DIVA (Dispersion-Vicariance Analysis). *Revision of Mexican Ciencias Geology.* Vol. 28, 2: 235e245.

Amaghzaz, M., Bouya, B., Cappetta, H., Gheerbrant, E., Iarochène, M., and Sudre, J. (2002). A New Large Mammal From the Ypresian of Morocco: Evidence of Surprising Diversity of EarlyProboscideans. *Acta Palaeontologica Polonica*, 47: 493–506.

Amaghzaz, M., Bourdon, E., Bouya, B., Cappetta, H., Gheerbrant, E., Iarochène, M., …Sudre,

J. (2003). Les Localités à Mammifères des Carrières de Grand Daoui, Bassin des Ouled Abdoun, Maroc, Yprésien: Premier état des lieux. *Bulletin de la Société Géologiquede France*, 174: 279–293.

Amaghzaz, M., Bouya, B., Gheerbrant, E., Iarochène, M., Tassy, P. and Sudre, J. (2005). Nouvelles Données sur *Phosphatherium escuilliei* (Mammalia, Proboscidea) de l'Éocène inférieur du Maroc, Apports à la Phylogénie des Proboscidea et des Ongulés Lophodontes. *Geodiversitas* 27: 239–333.

Ameur, R., Crochet, J. Y., Jaeger, J. J., and Mahboubi, M., (1984). El Kohol (Saharan Atlas, Algeria): A New Eocene Mammal Locality in Northwestern Africa. *Palaeontographica Africa*, 192: 15–49.

Andrews C. W. (1904IV). On the Evolution of the Proboscidea. *Philosophical Transition of the Royal Society of London*, B196**:** 99–118.

Benoit, J. Manger, P. R. and Rubidge, B. S. (2016). Paleoneurological Clues to the Evolution of Defining Mammalian Soft Tissue Traits. Cenozoic. *Scientific Reports*, 6: 25604.

Benoit, J., Legendre, J. L., Manger, P., Mararescul, V., Obada, T. and Tabuce, R. (2019). Brain Evolution in Proboscidea (Mammalia, Afrotheria) Across the Cenozoic. *Scientific Reports*, 9: 9323.

Benoit, J., Cousteur, S., Farke, A., Legendre, J. L., A., Mennecart, B., Merigeaud, S., …Neenan, J. M. (2020). A Test of the Lateral Semi-circular Canal Correlation to the Head Posture, Diet and Other Biological Traits in "Ungulate" Mammals. *Scientific Reports*, 10: 19602.

Bennett, C. N., Chiminba, C. T. and Medger, K. (2012). Seosonal Reproduction in the Eastern Rock Elephant–Shrew: Influenced by Rainfall and Ambient Temperature? *Journal of Zoology*, 288: 283-293.

Berenbrink, M., Burns, J. M., Campbell, L. K., Cossins, A. R., Mirceta, S. and Signore, A. V.

(2013). Evolution of Mammalian Diving Capacity Traced by Myoglobin Net Surface Charge. *Science*, 340: 1234192.

Blanco, E. R., Jone, W. W., Rinderknecht, A. and Yorio, L. (2021). *Macrauchenia patachonica* Owen, 1838: Limb Bones Morphology, Locomotory Biomechanics, and Paleobiological Inferences. *Geobios*, 30 (30): 30.

Boas, J. E. V., and Paulli, S. (1908). The Elephant's Head. Studies in the Comparative Anatomy of the Organs of the Head of the Indian Elephant and Other Mammals. *Part I. Gustav Fischer, Jena*.

Branstrator, J., W. and Woodman, N. (2008). The Overmyer Mastodont (*Mammut ameticanum*) from Fulton County, Indiana. The American Midland Naturalist, Vol. 159 (1): 125-146.

Brunet, M., Hautier, L., Lihoreau, F., Mackaye, H. T., Tassy, P. and Vignaud, P. (2009). New Material of *Anancus kenyansis* (Proboscidea, Mammalia) From Toros-Menalla (Late Miocene, Chad): Contribution to the Systematics of African Anancines. *Journal of African Earth Sciences*,53: 171–176.

Bryden, M. M. and Ling, J. K. (1992). *Mirounga leonina*. *Mammalian Species*, 391: 1–8.

Burckle, L. H., Denton, G. H., Partridge, C. T. and Vrba, E. S. (1995). Paleoclimate and Evolution, with Emphasis on Human Origins, *Yale University Press, New Haven, CT*.

Burmeister, H. (1864). Descripción de la *Macrauchenia patachonica*. *Anales del Museo Público de Buenos Aires*, 1: 32–66.

Cawthra, C. H., Dixon, G. M., Helm, C. W., Lockley, G. M., Moolman, L., Stear, W., …Vyncka, C. D. J. (2021). Morphology of Pleistocene Elephant Tracks on South Africa's Cape South Coast and Probable Elephant Trunk-drag Impressions. *Quaternary Research*, 1–15.

Clifford, A. B. and Witmer, L. M. (2002b). Not All Noses are Hoses: An Appraisal of

Proboscis Evolution in Mammals. Annual Meeting of the Society of Vertebrate Paleontology, Norman, Oklahoma. *Journal of Vertebrate Paleontol*ogy, 22 (Supplimentary to 3): 66A.

Clifford A. B, and Witmer, L. M. (2004a). Case Studies in Novel Narial anatomy: 3 Sturcture and Function of the Nasal Cavity of saiga (Artiodactyla: Bovidae: Saiga tatarica). Journal of Zoology, Vol. 264 (3): 217-230.

Clifford A. B, and Witmer, L. M. (2004b). Case studies in Novel Narial Anatomy: 2. The Enigmatic Nose of Moose (Artiodactyla: Cervidae: *Alces alces*). *Journal of Zoology* 262: 339-60.

Court, N. (1994). Limb Posture and Gait in *Numidotherium koholense* a Primitive Proboscidean From the Eocene of Algeria. *Zoological Journal of the Linnean Society*, 111: 297-338.

Crumpton, N. and Thompson, R. S. (2013). The Holes of Moles: Osteological Correlates of the Trigeminal Nerve in Talpidae. *Journal of Mammal Evolution*, 20: 213–225.

Cuvier, G. (1796). Sur le Squelette d'une Très-grande Espèce de Quadrupède Inconnu Jusqu'à pPésent, Trouvé au Paraguay, et Déposé au Cabinet D'histoire Naturelle de Madrid. *Magasin Encyclopédique*,1: 303–310.

Dechaseaux, C. (1958). L'encephale d'*Elephas meridionalis*. *Annales de Paleontologie*, 54: 269–278.

Delmer, C. (2005). Les Premières Phases de Différenciation des Proboscidiens (Tethytheria, Mammalia): Le Rôle du Barytherium Grave de Libye. Unpublished PhD Dissertation, *Muséum National d'Histoire Naturelle*, Paris, 470 pp.

Delmer, C. (2005b). Phylogenetic Relationships Between Paleogene Probosci− Deans: New Data and Impact on Tethytherian Systematics. *Journal of Vertebrate Paleontology,* Supplement

25: 50A.

Delmer, C. (2005c). Early Proboscideans Phylogeny and Systematics: The Role of *Barytherium* Grave (Proboscidea; Mammalia). Abstracts of the Plenary Symposium, Poster and Oral Papers Presented at IMC9, *IX International Mammalogical Congress*, 25–26. Sapporo Hokkaido, Japan.

Dierefield, E. S. and Milewski, A. V. (2013). Structural Composition of the Proboscis Between Tapirs, and Other Extant and Extinct Vertebrates. *Intergrative Zoology*, 8: 84–94.

Domning, D. P., McKenna. C. M. and Ray, C. E. (1986). Two New Oligocene Desmostylians and a Dis? Cussion of Tethytherian Systematics. *Smithsonian Contribution to Paleobiology*. 59:1-56.

Eisenberg, F. J. and Shoshani. (1982). *Elephas maximus*. The American *Society of Mammalogists*, 182: 1-8.

Fairfield, H. O. (1934). Evolution and Geographic Distribution of Proboscidea: Moeritheres, Deinotheres and Mastodonts. *Journal of Mammalogy*, Vol. 15: 177-184.

Fisher, C. D. (2018). Palaeobiology of Pleistocene Proboscideans. *Annual review of the Earth and Planetary Sciences.*

Frey R, and Hofmann R. R. (1996). Skull, Proboscis Musculature and Preorbital Gland in the saiga Antelope and Guenther's Dik-dik (Mammalia, Bovidae). *Zoologischer Anzeiger*, 235: 183–99.

Galimberti F., Miller E. H. and Sanvito, S. (2007). Having a Big Nose: Structure, Ontogeny, and Function of the Elephant Seal Proboscis. *Canadian Journal of Zoology*, 85, 207–20.

Galton, M. O., Knoll, F. and Lopez-Antananzas, R. (2006). Paleoneurological Evidence Against a Proboscis in the Sauropod Dinosaur Diplodocus. *Geobios*, 29: 215-221.

Gheerbrant, E. and Tassy, P. (2009). Origin and Evolution Proboscideans. *C. R., Paleontology,*

Vol. 8.

Giannini, N. P. and Moyano, R. S. (2018). Cranial Characters Associated With the Proboscis Postnatal-Development in Tapirus (Perissodactyla: Tapiridae) and Comparisons With Other Extantand Fossil Hoofed Mammals. *Zoologischer Anzeiger,* 277: 143-147.

Gohlich, B. U. (1999). Order Proboscidea. *The Miocene Land Mammals of Europe*, 157-168.

Gromova, V. (1954). *Boltnye Nosorogi* (Amynodontidae) Mongolii. Trudi Paleontology Institution, Akad. Nauk SSSR, 55: 85-189 (in Russian). Hatcher, J. B. 1896. Recent and Fossil Tapirs. *American Journal of Sci*ences, 4th series 1: 161-180.

Guillermo, A. E. and Spencer, G. L. (2010). Fossil Proboscidea from the Upper Cenozoic of Central America: Taxonomy, Evolutionary and Palaeogeographic Significance. *Revista Geológica de América Central,* 42: 9-42.

Hammer, O. (1992 – 2021). Paleontological Statistical. *Natural History Meseum.* Harris, J. M.

Harris, J, M. (1975). Evolution of Feeding Mechanisms in the Family, Deinotheridae (Mammalia: Proboscidea). *Journal of Linnean Society.,* 36: 331-362.

Harris, J. M. (1978). Deinotherioidea and Barytherioidea; pp. 315–332 in Maglio, J. V. and Cooke, B. H. S. (eds.), *Evolution of African Mammals*. Harvard University Press, Cambridge.

Harzhauser, M., Piller, W. E. and Steininger. F. F. (2002). Circum- Mediterranean Oligo-Miocene Biogeographic Evolution: The Gastropods' Point of View. *Palaeogeography, Palaeoclimatology, Palaeoecology* 183:103–133 in Hillis, D. (1995). Approaches for Accessing Phylogenetic Accuracy. *Systematic Biology*, 44(1): 3-16.

Hautier, L., Jaeger, J. J., Mahboubi, M. Noubhani, A. and Tabuce, R. (2008). Dental and Cranial Variability of Numidotherium Koholense (Mammalia, Proboscidea) From El Kohol, Eocene, Algeria. Geobios, 41 (4): 515-531.

Illiger, C. D. (1811). Prodromus Systematis Mammalium et Avium Additis Terminis. *Zoographicis Uttriusque Classis*, Salfeld.

Janis, C. M. (1989). A Climatic Explanation for Patterns of Evolutionary Diversity in Ungulate Mammals. *Palaeontology*, Vol. 32, part 3: 463–481.

Jaroon Duangkrayom, Wang Shi-Qi, Wen He, Xiang-Wen Yang Yu Li, and Shan-Qin Chen. (2017).A New Species of Gomphotherium (Proboscidea, Mammalia) From China and the Evolution of Gomphotherium in Eurasia. *Journal of Vertebrate Paleontology*, DOI: 10.1080/02724634.2017.1318284.

Kappelman, J., Rasmussen, D. T. and Sanders, J. W. (2004). New Large-Bodied Mammals From the Late Oligocene Site of Chilaga, Ethiopia. *Acta Palaeontologica Polonica*, 49(3): 365-392.

Kupsky, J. W., Marchant, G. H. and Shoshani, J. (2006). Elephant Brain Part I: Gross Morphology, Functions, Comparative anatomy and Evolution. Brain Research Bulletin, Vol. 70: 124-157.

Kingdon, J. (1997). The Kingdon Field Guide to African Mammals. *Academic Press, London*.

Lambert, D. W. and Holling, C. S. (1998) Causes of Ecosystem Transformation at the End of the Pleistocene: Evidence From Mammal Body-Mass Distributions. *Ecosystems*, 1998:157–175.

Larramendi, A. (2016). Shoulder Height, Body Mass, and Shape of Proboscideans. *Acta Palaeontologica Polonica*, 61 (3): 537–574.

Linnaeus, C. (1758). Systema Naturae per Regna tria Naturae, Secundum Classis, Ordines, Genera, Species cum Characteribus, Differentiis, Synonymis, Locis, Tenth Edition, Vol. 1. *Laurentii Salvii, Stockholm,* pp. 824.

Liu, A. C. G. S., Seiffert, E. R. and Simon, E. L. (2008). Stable Isotope Evidence for an

Amphibious Phase in Early Proboscidean Evolution. *Proceedings of the National Academy of Sciences* , Vol. 105, 15: 5786–5791.

Lydekker, R. (1903). The Burmese gaur, or Pyoung. *Zoologist*, Vol. 7: 264–266.

Markov, G. N., Simeonovski V. and Spassov N. (2001). A Reconstruction of the Facial Morphology and Feeding Behavior of the Deinotheres. In: Cavarretta G., Giola P., Mussi M., Palombo M. R., Editions. The World of Elephants. *Proceedings of the First International Congress*; 16–20 (September 2001), Rome, Italy, pp. 652–5.

Matsumoto, H. (1923). A Contribution to the Knowledge of *Moeritherium*. *Bulletin of the AmericanMuseum of Natural History*, 48: 97–140.

Muchlinski, M. N. (2008). The Infraorbital Foramen, Infraorbital Nerve, and Maxillary Mechanoreception: Implications of Interpreting the Paleoecology of Fossil Mammals Based on Infraorbital Foramen Size. *Anatomical Rec*ord, 291: 1221-1226.

Nabavizadeh, A. (2015). Proboscidean Jaw Mechanics and the Evolution of the Proboscis and Feeding Apparatus in Extant Elephants. *The Federation of American Societies for Experimental Biology Journal*, 29: 867-10.

Nabavizadeh, A. and Reidenberg, J. S. (2019). Anatomy of the Proboscideal Nerve in the Proboscis of the African Elephant (*Loxodonta africana*). *The Federation of American Societites for Experimental Biology*, 33: lb148-lb148.

Osborn, F. H. (1898). The Extinct Rhinoceroses. *Memoirs American Museum of Natural His*tory, 1:75-164.

Osborn, F. H. (1909). The Feeding Habits of Moeritherium and Palaeomastodon. *Nature*, 81:139–140.

Osborn, F. H. (1936). Proboscidea, Vol. 2. *Amereican Museum of Natural History Press,* New York.

Osborn, F. H. (1942). Evolution and Geographic Distribution of the Proboscidea: Moeritheres, Deinotheres and Mastodonts. *Journal of Mammalogy,* 15: 177–184.

Palombo, M. R. and Giovinazzo, C. (2005). *Elephas falconeri* From Spinagallo Cave (South-Eastern Sicily, Hyblean Plateau, Siracusa): Brain to Body Weight Comparison. *Monografies de la SocietatD'Historia Natural de les Balears*, 12: 255-264A.

Sanders, J. W. (2010). Proboscidea. In: Harrison, T. (Ed.), Paleontology and Geology of Laetoli: Human Evolution in Context, Fossil Hominins and the Associated Fauna, Vol. 2. *Springer, Dordrecht*, pp. 233-262.

Scott, B. W. (1910). *Litopterna* of the Santa Cruz Beds. *Part 1 of Reports of the Princeton UniversityExpeditions to Patagonia*, Vol. 7: 1896-1899.

Sharp, A. C. and Trusler, P. W. (2016). Description of New Cranial Material of *Propalorchestes* (Marsupialia: Palorchestidae) From the Middle Miocene Camfield Beds, Northern Territory, Australia. *Memoirs of Museum Victoria*, 74: 291–324.

Shoshani, J. (1996). Skeletal and Other Basic Anatomical Features of Elephants. In The Proboscidea: Evolution and Palaeoecology of Elephants and Their Relatives: 9-20. Shoshani, J. and Tassy, P. (Eds). *Oxford University Press,* New York.

Shoshani, J. (1998). Understanding Proboscidean Evolution: A Formidable Task. *Elsevier Science*, Vol. 13, 12: 169–5347.

Sanders, J. W., Shoshani, J. and Tassy, P. (2001a). Elephants and Other Proboscideans: A Summaryof Recent Findings and New Taxonomic Suggestions: pp. 676–679 in Cavarretta, G., Gioia, P., Mussi, M., and Palombo, M. R. (Editions), *Proceedings of the First International*

Congress of la Terra degli Elefanti: The World of Elephants. Consiglio Nazionale delle Ricerche, Rome. A Shoshani, J., and Tassy, P. (1996). The Proboscidea, Evolution and Palaeoecology of Elephants andTheir Relatives, *Oxford University Press*, New York.

Shoshani, J. and Tassy, P. (2005). Advances in Proboscidean Taxonomy & Classification, Anatomy & Physiology, and Ecology & Behaviour. *Quaternary international*, 5-20: 126-128.

Simons, E. L. (1968). Early Cenozoic Mammalian Faunas. Fayum Province, Egypt: Part I. AfricanOligocene Mammals: Introduction, History of Study, and Faunal Succession. *Peabody Museum ofNatural History, Yale University Bulletin*, 28: 1–21.

Sternberg, C. M. (1939). Were There Proboscis-bearing Dinosaurs? Discussion of Cranial Protuberances in the Hadrosauridae. *Annals and Magazine of Natural History* 3: 556–560.

Sukumar, R. (2003). The Living Elephants: Evolutionary Ecology, Behavior and Conservation. *Oxford University Press*.

Svistun, I. V. (1974). Deinotheres of Ukraine. *Kiev: Naukova Dumka*. (In Russian).

Tassy, P. (1985). La place des Mastodontes Mioce`nes de l'ancien Monde dans laPhyloge´nie des Proboscidea (Mammalia): Hypothe`ses et Conjectures. 861 p., Unpublished Dissertation these, *UPMC*, Paris.

Tassy, P. (1998). Et la trompe vint aux éléphants. *La Rechèrche* 305.

Tassy, P. (2013). L'anatomie cranio-mandibulaire de Gomphotherium angustidens (Cuvier, 1817) (Proboscidea, Mammalia): Donne´es issues du gisement d'En Pe´jouan (Mioce`ne moyen du Gers, France). *Geodiversitas*, 35(2): 377–445.

Tarabukin, A. B. (1974). New Data on the Systematics, Phylogeny and Ecology of Suborder Deinotherioidea Osborn (1921). In *Mammals of the Late Cenozoic From*

Southwestern USSR: 77-90. Kishinev: Shtiintsa. (In Russian). Todd, N. 2006. Trends in Proboscidean Diversity in the African Cenozoic. *Journal of MammalianEvolution*, Vol. 13, No 1*:* 1064-7554.

Troxell, E. L. (1921). New Amynodonts in the Marsh Collection. *American. Journal of Sci*ences, 5th series 2: 21-34.

Bezuidenhout, A. J.., Seegers, C. D and Van der Merwe, J. N. (1995). The Skull and Mandible of the African Elephant (*Loxodonta africana*). *Onderstepoort Journal of Veterinary Research*, 62: 245- 260. Vrba, E. S. (1993). Turnover-Pulses, the Red Queen, and Related Topics. *American. Journal of Sci*ences, 293 - A: 418–452.c

Wall, P. W. (1980). Cranial Evidence for a Proboscis in Cadurcodon and a Review of Snout Structure in the Family Amynodontidae (Perissodactyla, Rhinocerotoidea). *Journal of Paleontology*, 54: 968–977.

Wilfarth, M. (1938). Gab es rüsseltragende Dinosaurier? *Zeitschrift der Deutschen GeologischenGesellschaft*, 90: 88–100.

Wilfarth, M. (1939). Die Nasenbasis der Lambeosaurinae. *Zentralblatt für Mineralogie, Geologieund Paläontologie Abteilung B* 1: 24 – 39.

Wilfarth, M. (1940). Der Atemrüssel der Hadrosauriden. W. Knapp,

Hall.

Wilfarth, M. (1948). Rüsseltragende Dinosaurier. *Orion* 2: 525–5 32.

Wilfarth, M. (1949). Die Lebensweise der Dinosaurier. E. Schweizerbart'sche, Stuttgart.

Sampson, S.D., Solounias, N. and Witmer, L. M. (1999). The Proboscis of Tapirs (Mammalia: Perissodactyla): A Case Study in Novel Narial Anatomy. *Journal of Zoology*, 249: 249–267.

Yeager, C. P. (1989). Feeding Ecology of Proboscis Monkeys. *International Journal of*

Primatology, Vol. 10, 6.

Supplementary table 1. CT scan measurements. AV, average volume IOC (cm^3)/Log (body mass); SA, surface area IOF (cm^2); NR, narial retraction (cm); SL/HL, snout length/head length (CT scan); parameters are the CT scanning parameters.

Species	**Order**	**Sub-order**	**Specimen no.**	**AV**	**SA**	**NR**	**SL/HL**	**Parameters**
Orycteropus afer	Afrotheria	Tubulidentata	Aixis	486.484	59.664	28.5	0.611722	0.283203 x 0.283202 x 1
Procavia capensis	Afrotheria	Paenungulata	UN76	40.858	8.591	5.2	0.2681	0.046 x 0,046 x 0.046
Macroscelides proboscideus	Afrotheria	Paenungulata	AMNH161535	3.2819	1.4675	2.39	0.9139	0.022 x 0,022 x 0.055
Loxodonta Africana	Afrotheria	Paenungulata	Loxoafricana	12481	1708.063	271.79	2.55263	0.976562 x 0.976562 x 0.6
Loxodonta Africana	Afrotheria	Paenungulata	Not specified	15526.7	2653.379	124.54	3.330268	1.26953 x 1.26953 x 1.00125
Camelus bactrianus	Artiodactyla	Tylopoda	ZA849	4301.45	217.4796	125.81	0.3471	0.408854 x 0.408854 x 1.5
Camelus dromedaries	Artiodactyla	Tylopoda	MS198	2811.36	245.253	157	0.347973	0.73 x 0.7 x1.6
Bos Taurus	Artiodactyla	Ruminantia	ZA1342	1421.67	156.48	70.88	0.64112	0.599609 x 0.599609 x 1.6
Capra aegagrus	Artiodactyla	Ruminantia	AZ1624	711.771	62.505	35.26	0.9784	0.264323 x 0.264323 x 1.5
Connochaetes taurinus	Artiodactyla	Ruminantia	322700	2070.5	149.357	50.74	0.47108	0.802734 x 0.802734 x 1.6
Kobus ellipsiprymnus	Artiodactyla	Ruminantia	AZ2938	1641.11	65.41	187	0.7744	0.286459 x 0.286459 x 1.5
Kobus leche	Artiodactyla	Ruminantia	TM35471	716.958	66.32	53.88	0.73651	0.334635 x 0.334635 x 1.5
Madoqua kirkii	Artiodactyla	Ruminantia	YPM3985	106.021	13.98	29.19	0.73228	0.234375 x 0.234375 x 0.31
Raphicerus campestris	Artiodactyla	Ruminantia	BP610	121.79	9.067	27.79	0.51785	0.139323 x 0.139323 x 0.33
Syncerus caffer	Artiodactyla	Ruminantia	Buffalo	2559	122.68	35.4	0.667081	0.976601 x 0.976599 x 1.6
Redunca fulvorufula	Artiodactyla	Ruminantia	YPM3979	283.8	49.117	41.09	0.736287	0.388672 x 0.388672 x 0.31

Saiga tatarica	Artiodactyla	Ruminantia	YPM1510	697.919	62	98.56	0.734237	0.442919 x 0.442919 x 0.5
Tragelaphus strepsiceros	Artiodactyla	Ruminantia	AZ2107	1015.07	81.82	127	0.656173	0.273438 x 0.273438 x 1.5
Tragulus javanicus	Artiodactyla	Ruminantia	Beauval	22.433	318.75	6.7	0.644489	0.337891 x 0.337891 x0.4
Alces alces	Artiodactyla	Ruminantia	Male	6800.68	213.449	232.91	0.797571	0.498047 x 0.498047 x 0.7
Cervus alaphus	Artiodactyla	Ruminantia	male_3864	811	74.245	72.95	0.691996	0.976564 x 0.976563 x 0.2
Dama dama	Artiodactyla	Ruminantia	Male	653.265	37.64	46.84	0.796415	0.573438 x 0.800003 x 0.573437
Cervus alaphus	Artiodactyla	Ruminantia	Red deer	1911.19	115.604	77.1	0.647481	0.683594 x 0.683594 x 1.6
Okapia johnstoni	Artiodactyla	Ruminantia	AZ3275	1022.76	556.499	146.33	0.651319	0.488281 x 0.48281 x 1
Giraffa Camelopardalis	Artiodactyla	Ruminantia	TM22257	1400.71	55.833	95.64	0.741161	0.488282 x 0.488282 x 1
Potamochoerus porcus	Artiodactyla	Suoidea	TM3460	3419.16	184.1484	58.21	0.89976	0.85 x 0.85 x 1.6
Sus scrofa	Artiodactyla	Suoidea	TM13210	1166.7	83.395	8.81	0.547997	0.402344 x 0.402344 x 0.65
Sus scrofa domesticus	Artiodactyla	Suoidea	ZA906	2027.49	100.024	110.02	0.805623	0.333984 x 0.333985 x 1.6
Phacochoerus africanus	Artiodactyla	Suoidea	AZ2621	3419.16	67.265	-3.59	0.899756	0.402344 x 0.402344 x 0.65
Choeropsis liberiensis	Artiodactyla	Hippopotamidae	AZ939	1175.94	112.231	39.24	0.489299	0.390625 x 0.390625 x 0.75
Hippopotamus amphibious	Artiodactyla	Hippopotamidae	Clean	34656.7	995.851	48.15	0.545558	0.976562 x 0.976562 x 1
Equus asinus	Artiodactyla	Equidae	AZ422	2507.04	465.403	62.71	0.742761	0.351562 x 0.351562 x 1.5
Equus burchelli quagga	Artiodactyla	Equidae	BP147	3041.2	141.431	70.3	0.661844	0.738 x 0.738 x 1.6
Equus caballus	Perissodactyla	Equidae	AZ1969	2886.89	196.36	51.11	0.768461	0.390625 x 0.390625 x 1.5
Equus zebra	Perissodactyla	Equidae	BP147	2235.26	79.05	69.07	0.6901	0.390625 x 0.390625 x 0.15

Ceratotherium simum	Perissodactyla	Rhinocerotidae	AZ1247	5577.9	807.84	-12.75	0.586415	0.585938 x 0.585938 x 1.6
Diceros bicornis	Perissodactyla	Rhinocerotidae	ZA1204	16264.3	570.233	-26.87	0.686874	0.611979 x 0.611979 x 2.76351
Tapirus indicus	Perissodactyla	Tapiridae	MS195	17898.4	118.161	103.71	0.660191	0.632815 x 0.632811 x 1.6
Tapirus terrestris	Perissodactyla	Tapiridae	WLSM122	3075.39	465.403	184.7	0.780268	0.339844 x 0.339844 x 1.5
Mammut americanum	Afrotheria	Paenungulata	ANSPVP13307	72.17	12.3465			0.0275076 x 0.0331422 x 0.0256272
Numidotherium koholense	Afrotheria	Paenungulata	UOK5	2330.5	109.4425	159.94		0.24 x 0.24 x 0.24

Supplementary table 2. Measurements on the photos. Sl/Hl Is the ratio of snout length to head length (Photos).

Species	**Image no.**	**Snout Length**	**Head length (Photos)**	**Sl/Hl**
Addax nasomaculatus	3866	1158.792	1470.49	**0.788031**
Aepyceros melampus	4078	1150.562	1378.238	**0.834806**
Alcelaphus buselaphus	3528	927.694	1048.645	**0.88466**
Alces alces	9995	1149.309	1441.012	**0.797571**
Vicugna pacos	3820	894.232	1325	**0.674892**
Ammotragus lervia	2121	1073.813	1269.362	**0.845947**
Oryx leucoryx	2788	921.478	1310.896	**0.702938**
Potamochoerus porcus	892	396.319	623.403	**0.635735**
Axis axis	1067	734.267	1071.549	**0.685239**
Bison bison	360	1145.114	1309.541	**0.874439**

Bos tauras	3639	1675.934	2614.08	**0.641118**
Diceros bicornis	3703	1334.879	1943.413	**0.686874**
Connochaetes gnou	4706	388.675	524.047	**0.74168**
Antilope cervicapra	1260	590.223	828.914	**0.712044**
Damaliscus pygargus	1446	1009.54	1201.974	**0.839902**
Damaliscus dorcas	1516	558.875	657.034	**0.850603**
Damaliscus dorcas	1516	558.875	657.034	**0.850603**
Connochaetes taurinus	4140	577.994	1226.955	**0.47108**
Tragelaphus eurycerus	1034	1201.388	1754.25	**0.684844**
Bubalus bubalis	1400	632.874	784.145	**0.807088**
Camelus bactrianus	1486	760.523	2191.226	**0.347076**
Camelus dromedarius	487	307.333	883.209	**0.347973**
Capra caucasica	2851	1144.357	1651.069	**0.693101**
Catagonus wagneri	3022	1645.298	1757.736	**0.936032**
Cephalophus natalensis	4009	1003.651	1583.568	**0.633791**
Dama dama	3622	1280.727	1641.392	**0.780269**
cervicus dama	2010	1773.894	2154.141	**0.823481**
Sus domesticus	2194	500.308	2089.043	**0.239491**
Equus africanus asinus	646	1099.135	1332.116	**0.825105**

Taurotragus oryx	4388	1527.005	1953.578	**0.781645**
Loxodonta africanas	951	454.332	471.223	**0.964155**
Equus przewalkii	2842	1865.768	1414.486	**1.319043**
Equus caballus	1538	1186.835	1541.968	**0.769688**
Gau bos gaurus	3600	984.318	1524.778	**0.645548**
Oryx gazelle	1300	1264.634	1441.562	**0.877266**
Giraffa camelopardalis	1073	1539.523	2844.943	**0.541144**
Capra hircus	666	964.852	986.152	**0.978401**
Guanaco Lama guanicoe	3208	761.527	1502.35	**0.506891**
Alcelaphus buselaphus	1737	1073.396	952.773	**1.126602**
Hipopotamus ambhibius	1417	1357.35	1228.684	**1.104719**
Aepyceros melampus	861	844.595	1,261,403	**0.00067**
Axis porcinus	3728	808.709	1,261,403	**0.000641**
Ibex capra ibex	744	556.166	746.957	**0.744576**
Antidorcas marsupialis	2283	626.102	928.828	**0.674077**
Antilocapra americana	610	1413.264	1269.748	**1.113027**
Antilope cervicapra	1268	744.218	1162.515	**0.640179**
Axis kuhlii	2627	777.92	1312.081	**0.59289**
Axis porcinus	2788	1115.968	642.028	**1.738192**

Babyrousa babirussa	2187	1414.01	1907.83	**0.741161**
Babyrousa celebensis	6494	1244.85	2046.352	**0.608326**
Bison bison	1781	663.21	1001.569	**0.662171**
Bison bonasus		1113.885	1731.704	**0.643231**
Bos frontalis gaurus	8817	954.075	1627.494	**0.586223**
Bos grunniensis	2813	1734.343	1678.26	**1.033417**
Bos javanicus	2419	1412.869	2190.748	**0.644925**
Bos taurus	1550	687.805	1229.18	**0.559564**
Boselaphus tragocamelus	6333	1808.629	2588.233	**0.698789**
Bubalus bubalis	1397	1164.139	1789.942	**0.650378**
Bubalus depressicornis	1016	1070.424	1588.1	**0.674028**
Budorcas taxicolor	2843	1219.12	1572.5	**0.775275**
Camelus bactrianus	1473	631.028	1359.4	**0.464196**
Camelus dromedarius	487	455.724	883.31	**0.515928**
Capra caucasica	3747	1068.61	1486.41	**0.71892**
Capra falconeri	2749	459.7	675	**0.681037**
Capra hircus	3164	866	1342	**0.645306**
Capra ibex	8400	587.9	752.97	**0.780775**
Capra nubiana	1997	1077.931	1371.167	**0.786141**

Capreolus capreolus	8644	611.882	1012.792	**0.604154**
Cephalophus natalensis	643	1103.087	1735.743	**0.635513**
Cephalophus niger	1045	1055.761	1610.55	**0.655528**
Cephalophus sylvicultor	125	1207.238	1861.596	**0.648496**
Ceratotherium simum	3227	703.434	1107.776	**0.634997**
Cervus (Przewalskium) albirostris	4468	760.392	1127.298	**0.674526**
Cervus elaphus	8936	783.063	1131.601	**0.691996**
Cervus Nippon	7236	857.244	1488.484	**0.575918**
Choeropsis liberiensis	856	839.657	1716.042	**0.489299**
Connochaetes gnu	2897	764.924	927.053	**0.825114**
Connochaetes taurinus	5958	1512.024	1820.533	**0.830539**
Dama dama	1435	1400.303	1758.258	**0.796415**
Damaliscus pygargus (Bontebok Damaliscus pygargus dorcas)	1916	1154.497	1395.835	**0.827101**
Diceros bicornis	601	1090.235	2023.877	**0.538686**
Elaphodus cephalophus	8085	922.304	1385.013	**0.665917**
Elaphurus davidianus	2490	1297.804	1669.003	**0.777592**
Elephas maximus	8707	1270.838	497.855	**2.552627**
Equus asinus (Equus asinus africanus)	36	832.531	1120.86	**0.742761**
Equus quagga	845	818.511	1236.713	**0.661844**

Equus caballus	1589	751.51	978.018	**0.768401**
Equus grevyi	1567	1418.401	1934.942	**0.733046**
Equus hemionus (Kulani)	8113	1078.349	1531.493	**0.704116**
Equus zebra	2706	881.918	1278.056	**0.690046**
Gazella dama	9437	1080.033	1309.705	**0.824638**
Gazella spekei	709	559.771	826.803	**0.677031**
Giraffa camelopardalis	1073	2258.305	2917.271	**0.774116**
Hemitragus jemlahicus	5281	1062.593	1353.835	**0.784876**
Heterohyrax brucei	5594	921.151	1963.477	**0.469143**
Hippopotamus amphibius	1682	842.568	1544.414	**0.545558**
Hippotragus equinus	5458	930	1098.41	**0.846678**
Hippotragus niger	658	195.492	1448.997	**0.134915**
Hydropotes inermis	338	998.112	1567.046	**0.636939**
Kobus ellipsiprymnus	945	1104.261	1340.366	**0.82385**
Kobus leche	218	891.601	1210.573	**0.736512**
Kobus megaceros	3952	1273.047	1665.505	**0.764361**
Lama guanicoe	1888	1168.461	1896.551	**0.616098**
Lama lama	9152	1029.713	1652.366	**0.623175**
Litocranius walleri	87	978.294	1597.961	**0.612214**

Loxodonta africana	2662	2016.164	605.406	**3.330268**
Macrosclides proboscideus	7694	949.082	1038.555	**0.913849**
Madoqua kirkii	27	900	1227.363	**0.733279**
Moschus moschiferus	2531	1030.953	1058.388	**0.974079**
Muntiacus reevesi	1296	980.261	1027.262	**0.954246**
Naemorhedus goral	3111	944.957	1409.298	**0.670516**
Naemorhedus griseus	2739	1612.561	2092.796	**0.770529**
Nanger soemmeringii	547	2124.72	1579.231	**1.345414**
Odocoileus virginianus	379	1407.892	1732.411	**0.812678**
Okapia johnstoni	2255	1362.119	2091.325	**0.651319**
Oreamnos americanus	2839	1449.668	1900.779	**0.76267**
Oreotragus oreotragus	299	982.261	1536.762	**0.639176**
Orycteropus afer	5217	697.266	1139.842	**0.611722**
Oryx beisa	5998	1371.602	1861.596	**0.736788**
Oryx dammah	1876	1414.894	1904.421	**0.742952**
Oryx gazella	2027	1092.016	1425.553	**0.76603**
Oryx leucoryx	2941	1000.292	1364.891	**0.732873**
Ovibos moschatus	8220	925.246	1194.136	**0.774825**
Ovis ammon	3102	1138.167	1588.811	**0.716364**

Ovis aries	3299	1289.372	1703.715	**0.7568**
Ovis orientalis	2688	575.781	756.309	**0.761304**
Panolia eldii	5024	592.422	956.13	**0.619604**
Phacochoerus africanus	4900	1339.99	1489.282	**0.899756**
Philantomba monticola	4900	1226.483	1960.173	**0.625701**
Potamochoerus porcus	6968	1371.364	1660.44	**0.825904**
Procavia capensis	989	278.234	1037.913	**0.268071**
Pseudois nayaur	4444	2085.041	2764.62	**0.754187**
Pudu puda	32192	988.617	1847.737	**0.535042**
Rangifer tarandus	2340	1281.924	1607.507	**0.797461**
Raphicerus campestris	3812	702.026	1355.655	**0.51785**
Redunca arundinum	9262	1473.608	2162.707	**0.681372**
Redunca fulvorufula	8688	530.754	670.82	**0.791202**
Rhinoceros unicornis	7040	681.812	1305.355	**0.522319**
Rucervus duvauceli	1903	1612.762	2599.171	**0.620491**
Rupicapra rupicapra	8473	459.304	622.267	**0.738114**
Rusa alfredi	388	831.947	1324.628	**0.628061**
Rusa timorensis	5385	951.298	1357.062	**0.700998**
Rusa unicolor	7355	1658.889	2298.07	**0.721862**

Saiga tatarica	21641	160.897	219.135	**0.734237**
Sus barbatus	1985	1279.07	1587.678	**0.805623**
Sus cebifrons	6080	1022.362	1205.388	**0.84816**
Sus scrofa	2198	689.67	1258.528	**0.547997**
Syncerus caffer	9492	1244.317	1865.316	**0.667081**
Tapirus bairdii	1550	1203.749	484.85	**2.482725**
Tapirus indicus	3580	1670.102	2140.42	**0.780268**
Tapirus terrestris	1644	1608.855	2436.953	**0.660191**
Taurotragus derbianus	1678	1539.792	1960.311	**0.785484**
Taurotragus oryx	1942	1175.173	1491.914	**0.787695**
Tayassu pecari	1956	1245.184	1797.248	**0.692828**
Tragelaphus angasii	1120	875.342	1354.38	**0.646305**
Tragelaphus eurycerus	3519	1550.661	2388.226	**0.649294**
Tragelaphus imberbis	6674	822	1242.464	**0.661589**
Tragelaphus scriptus	9599	1280.012	2062.412	**0.620638**
Tragelaphus spekei	5493	432.042	697.266	**0.619623**
Tragelaphus strepsiceros	1881	1346.409	1859.806	**0.723951**
Tragulus javanicus	7254	1366.17	1891.866	**0.722128**
Tragulus nigricans	6944	1133.158	1999.045	**0.56685**

Vicugna pacos	706	1541.44	2591.312	**0.594849**
Vicugna vicugna	3515	628.856	1104.848	**0.569179**